

# Relating extratropical atmospheric heat transport to cyclone life cycle characteristics and numbers in Southern Hemispheric winter

Jan Zibell<sup>1</sup>, Alejandro Hermoso<sup>2</sup>, Aaron Donohoe<sup>3,4</sup>, and Sebastian Schemm<sup>1,5</sup>

<sup>1</sup>Institute for Atmospheric and Climate Science, ETH Zurich, Zurich, Switzerland

<sup>2</sup>Climate and Environmental Physics and Oeschger Centre for Climate Change Research, University of Bern, Bern, Switzerland

<sup>3</sup>Department of Atmospheric Sciences, University of Washington, Seattle, WA, US

<sup>4</sup>Applied Physics Laboratory, University of Washington, Seattle, WA, USA

<sup>5</sup>Department of Applied Mathematics and Theoretical Physics, Centre for Mathematical Sciences, University of Cambridge, Cambridge, UK

**Correspondence:** Jan Zibell (jan.zibell@env.ethz.ch)

## Abstract.

~~Extratropical cyclones, which develop and propagate in regions known as storm tracks, account for the majority of~~  
Outside the tropics, extratropical cyclones account for most of the poleward atmospheric heat transport (AHT) ~~outside the~~  
~~tropics. This allows the intensity and position of the zonal mean storm track to be constrained by the hemispheric-wide radiative~~  
5 ~~budget, and extreme heat transport events are known to occur in their vicinity.~~ Yet, ~~the zonal-mean nature of this approach~~  
~~masks the contribution of individual cyclones, which can locally constitute extreme eddy AHT. In this study, we adopt it~~  
remains unclear how individual cyclones contribute to heat transport over the course of their lifetime and whether the seasonal  
heat transport — viewed from a zonally integrated standpoint — is determined by their number. This study adopts a cyclone-  
centered perspective to quantify in detail the relationship between poleward AHT heat transport and the life cycle characteristics  
10 of extratropical cyclones in Southern Hemispheric winter. Specifically, ~~we combine~~ objectively identified surface cyclone tracks  
derived from ERA5 data (1981–2021) are combined with a moist static energy (MSE) framework ~~that features involving~~  
an eddy-mean decomposition of the ~~circulation. The~~ heat transport.

It is found that the local transient eddy MSE flux maximizes during the cyclone intensification phase and is largest in the  
warm sector with a secondary maximum in the cold sector. ~~Importantly, a~~ A considerable fraction of the flux in the warm-sector  
15 is located well equatorward of the cyclone ~~center~~ and thus outside the cyclonic region identified by the tracking algorithm. This  
leads to a latitudinal shift between maxima in cyclone frequency and transient eddy MSE fluxes. To bridge the gap between  
zonally integrated AHT heat transport and contributions from individual cyclones, local vertically integrated transient eddy  
MSE flux events are attributed to cyclones based on spatial overlap ~~criteria. When integrating zonally and over the cyclone with~~  
the identified cyclone area. Accumulated over their entire lifetime, the ~~most intense cyclones (and not the ones intensifying~~  
20 ~~most rapidly)~~ generally cyclones that become most intense generally are the ones that exhibit the largest zonally integrated  
cyclone-attributed ~~eddy MSE fluxes~~ heat transport. Despite a disproportionate contribution of the most intense cyclones to  
the cyclone-attributed transient eddy MSE fluxes ~~by the most intense cyclones on the seasonal scale~~, the relationship between

the seasonal number of intense cyclones and the ~~poleward-seasonal mean poleward transient~~ eddy MSE flux is sensitive to ~~the choice details~~ of the eddy-mean decomposition. This result indicates that low wavenumber background flows mask the influence of cyclone characteristics in the vertical, zonal, and seasonal integral. Notably ~~however,~~ at 50° S the relationship between the overall cyclone number and total ~~AHT~~ heat transport shows a peak ~~at 50 S, which resembles the dominance of synoptic waves at this latitude in terms of AHT while the relevance of planetary waves increases poleward.~~ Further research on the interplay between synoptic and planetary MSE fluxes in the vicinity of cyclones is needed to understand to which extent the cyclone number ~~, which is projected to decrease under warming, could~~ may be constrained by the global energy budget imbalance.

## 1 Introduction

~~Extratropical cyclones shape weather variability in the midlatitudes. In the Southern Hemisphere (SH), several extreme weather events have been linked to surface cyclones and their accompanying fronts such as South African cold spells (Chikoo et al., 2024) or flood events in Australia (Callaghan and Power, 2014). More generally, most extreme precipitation events in the extratropics can be related to extratropical cyclones (Pfahl and Wernli, 2012). Thus, understanding how the number and intensity of cyclones varies from year to year and will change under global warming is relevant for both immediate and long-term adaptation measures.~~

It is well known that extratropical cyclones intensify in regions of large baroclinicity, i.e., ~~where horizontal temperature gradients are large~~ and static stability is relatively low (e.g. Eady, 1949) — for instance near a land-sea contrast ~~or,~~ sea ice edge — ~~and static stability is relatively low (e.g. Eady, 1949). These regions are also commonly referred to as storm tracks,~~ or the Gulf Stream sector. In addition, individual storms can be strengthened by the release of latent heat during condensation ~~within~~ (e.g. Booth et al., 2013; Büeler and Pfahl, 2017), which takes place in the ascent regions ~~(e.g. Booth et al., 2013; Büeler and Pfahl, 2017)~~. ~~The circulation response to latent heating is non-linear and has been a matter of investigation for multiple decades (see the comprehensive review by Pfahl and Wernli, 2015). Recent progress includes recognizing that latent heat release within a warm conveyor belt~~ along the fronts or within the cyclone center (e.g., Attinger et al., 2019; Rüdüsühli et al., 2020). The growth of an individual extratropical cyclone can therefore be understood as baroclinic growth modulated by diabatic heat release and an associated poleward heat transport. The mean baroclinicity, which is the ascending moist airstream in the warm sector of a cyclone, can be linked to the amplification of the upper-level anticyclonic circulation downstream (Pomroy and Thorpe, 2000; Grams et al., 2011; Schemm et al., 2013; Steinfeld et al., 2020) and thereby the formation and maintenance of atmospheric blocking (Pfahl et al., 2015). The corresponding stationary flow can — depending on moisture availability — lead to further enhanced poleward moisture transport. One outstanding example where this self-amplifying poleward latent heat flux mechanism was identified is the March 2022 Antarctic heatwave: The extremely anomalous amount of moisture transported across the coastline into the continent led to the largest surface temperature anomaly (3.9) over the instrumental record (Blanchard-Wrigglesworth et al., 2023; Wille et al., 2024). Overall, cyclones in fact a measure for the growth potential of extratropical cyclones (Lindzen and Farrell, 1980), thereby helps to explain why extratropical cyclones develop in localized geographic regions (called storm tracks). However, while it helps to explain the

growth rates of cyclones, it does not explain the exact number of storms in a season or how changes in cyclone number and intensity relate to each other. A small number of intense cyclones, for example, may erode as much baroclinicity as many weak cyclones (Sinclair and Catto, 2022).

60 Within the warm sectors of cyclones, not only sensible heat is transported poleward but also the fraction of latent heat that is not immediately condensed. Thereby, cyclones account for the dominant fraction of the poleward latent heat fluxes into Antarctica (Tsukernik and Lynch, 2013) and, more generally, throughout the SH extratropics (Sinclair and Dacre, 2019), throughout the Southern Hemispheric (SH) extratropics (Sinclair and Dacre, 2019) and into Antarctica (Tsukernik and Lynch, 2013)

65 Poleward This poleward latent heat fluxes make a vital contribution to the global meridional atmospheric heat transport (AHT), which moderates the equator-to-pole temperature gradient. Since Earth receives more solar energy in the tropics than at the poles and this equator-to-pole contrast in absorbed solar radiation is only partly compensated by gradients in emitted thermal radiation, the atmosphere and ocean must collectively transport energy poleward to counteract the net radiative energy imbalance (Peixoto and Oort, 1992). AHT is, which counteracts the radiative imbalance between the equator and the pole (Peixoto and Oort, 1992). Atmospheric heat transport is conveniently described by the flux of moist static energy (MSE), which is. Traditionally, the MSE framework is a zonal mean framework. MSE is the sum of latent and dry heat. The MSE flux can be related to and potential energy. MSE flux occurs on different time-scales and length-scales such that total AHT is commonly separated heat transport is commonly decomposed into eddy and background flux contributions, which are typically assessed in the zonal mean (e.g. Priestley, 1949; Barpanda and Shaw, 2017). In midlatitudes, high-frequency synoptic-scale eddies are the largest contributors to AHT in both hemispheres (e.g. Armour et al., 2019; Stoll et al., 2023). Adding to that are low-frequency stationary waves and the mean overturning circulation; the latter corresponding to (e.g., Priestley, 1949; Barpanda and Shaw, 2017). The mean flow corresponds to the overturning circulation, which in the midlatitudes is the Ferrell cell transporting heat equatorward in the midlatitudes.

80 Different flow decompositions and definitions of storm tracks have led to various insights on their dynamics: Defining storm tracks using the zonal mean high-frequency that transports heat equatorward. Furthermore, low-frequency planetary-scale waves are associated with considerable poleward MSE flux especially in the Northern Hemisphere (NH, Barpanda and Shaw, 2017; Stoll et al.). The largest share of midlatitude MSE flux is, however, related to transient synoptic-scale eddies (e.g. Peixoto and Oort, 1992; Armour et al.). In these frameworks, storm track activity is typically assessed in the zonal integral by defining the storm track latitude as the maximum in transient eddy MSE flux, for instance, allows seasonal and climatological changes in storm track intensity and latitude (Barpanda and Shaw, 2017; Shaw et al., 2018). This framework allows changes in the storm track latitude and intensity to be decomposed into changes in the hemispheric scale heat budget, i.e., the background heat transport, the heat storage, and energy input by radiative and turbulent fluxes. On the seasonal scale, for instance, the storm track response to radiative forcing in the NH is delayed by the stationary background circulation (Barpanda and Shaw, 2017). Alternatively, the zonally integrated heat transport can also be decomposed into contributions by different wavenumbers, which have been linked to the occurrence of weather regimes (Lembo et al., 2022). Although these existing approaches connect the zonally integrated atmospheric heat transport to be related to large scale energetic constraints on total AHT alongside information about the AHT

by the stationary circulation (Barpanda and Shaw, 2017; Shaw et al., 2018). Moreover, decomposing AHT by spatial scale has enabled a link between zonal mean MSE flux extremes and localized weather patterns (Lembo et al., 2022). These studies are examples for what can be classified as a kind of ‘top-down’ approach to connect the zonal mean AHT to local weather phenomena. Conversely, the corresponding ‘bottom-up’ approach that investigates how local eddy MSE flux extremes impact the contributions of cyclones to the zonally integrated AHT has also been studied extensively. On the one hand, heat transport have not been systematically quantified.

Local (extreme) eddy-transient MSE fluxes have been linked to the warm- and cold-sectors of midlatitude cyclones (Messori and Czaja, 2015; Messori et al., 2017), which. These MSE flux peaks typically form banded structures which, in some cases, follow the frontal zones near surface cyclones (Geen et al., 2016; Messori et al., 2017). These events majorly contribute to the zonal-mean-eddy-zonally integrated transient MSE flux (Messori and Czaja, 2013). In addition, days with enhanced zonal-mean eddy-zonally integrated transient MSE fluxes have a disproportionate impact on the seasonal integral (Messori and Czaja, 2015) suggesting that local extreme events may significantly contribute to climatological zonal-mean-zonally integrated flux. On the other hand, it was found that local flux extremes arise from a combination of synoptic and planetary signals (Messori and Czaja, 2014). This indicates that eddy-transient MSE fluxes in the vicinity of a cyclone might not solely be determined by its life cycle characteristics but also contain contributions from low-frequency background flows. Despite the advances from both ‘top-down’ and ‘bottom-up’ approaches these advances, a systematic quantification how individual cyclones contribute to AHT over their life cycle and how the cyclone number and intensity over a season are related to eddy MSE flux (and thereby more generally the total AHT) analysis of when during the cyclone life cycle MSE fluxes maximize has not been performed thus far. Consequently, it remains unclear which life cycle characteristic most strongly modulates the instantaneous zonally integrated transient MSE flux and how much individual cyclones contribute to the seasonally integrated flux (Messori and Czaja, 2015) depending on their characteristics.

Further motivation for this study arises from the conception that the atmospheric energy budget might impose a constraint on the number of extratropical cyclones. In

This study is further motivated by the modeled decrease in cyclone numbers under global warming. Most studies that investigate cyclone numbers within coupled climate simulations agree that the cyclone number in SH winter decreases in a warmer climate, for instance, eddy latent heat fluxes in the warm sectors of cyclones increase — even if the circulation in the eddy were unchanged — simply due to the (König et al., 1993; Geng and Sugi, 2003; Lambert and Fyfe, 2006; Grieger et al., 2014; Chang whereas Chang et al. (2012) identified no robust decrease apart from the Atlantic sector. This response to warming is also underpinned by highly idealized atmosphere-only experiments (Sinclair et al., 2020; Schemm et al., 2022). A plausible explanation for this reduction could be that, as individual cyclones transport more latent heat because of the Clausius-Clapeyron relationship (Geen et al., 2016). Assuming for simplicity that the equator-to-pole gradient in net radiative imbalance (and the ocean heat transport) were unchanged (Boer and Sargent, 1985), this would require total AHT to be unchanged as well. Given that high-frequency eddy MSE fluxes remain the dominant component of extratropical AHT (especially in SH winter, Donohoe et al., 2020) the required total AHT could be achieved by fewer cyclones each transporting more latent heat (Zhang and Wang, 1997). Apart from few exceptions (Chang et al., 2012), there is agreement based on various warming scenarios, models, and approaches

to cyclone counting that the SH cyclone number decreases in a warmer climate (König et al., 1993; Geng and Sugi, 2003; Lambert and Fry  
- Highly idealized atmosphere-only experiments underpin this response to warming (Sinclair et al., 2020; Schemm et al., 2022)  
- However, the relationship between the extratropical cyclone number and AHT is complicated by the fact that the eddy, fewer  
cyclones account for same heat transport as in a present-day climate (Zhang and Wang, 1997). Yet, the total heat transport does  
130 not remain constant (as had been suggested by Boer, 1995) but exhibits a latitude-dependent response (Donohoe et al., 2020)  
Moreover, the change in MSE transported by individual cyclones likely also depends on the cyclone characteristics such  
as the spatial extent. On the one hand, the Rossby radius of deformation — an estimate for typical eddy size — is expected  
to respond to changes in static stability and tropopause height (Gill, 1982). On the other hand, strongly diabatically-driven  
cyclones become smaller under warming (Booth et al., 2013). intensity or spatial extent, which are projected to change as well  
135 (Dai and Nie, 2022; Priestley and Catto, 2022). Thus, how the partitioning of the total eddy MSE fluxes heat transport onto  
extratropical cyclones is affected by changes under warming is non-trivial. Further complexity arises from possible changes  
in ocean heat uptake and transport in the Southern Ocean which may buffer the atmospheric response to changes in radiative  
forcing and enhanced atmospheric latent heat storage.

Addressing the storm track response to climate forcing therefore necessitates a more profound understanding of the rela-  
140 tionship between zonal mean AHT zonally integrated heat transport and cyclone number and intensity under current present  
climate conditions.

In this study, we aim to bridge the gap between the synoptic-scale cyclone and zonal mean AHT zonally integrated heat  
transport perspectives by investigating 41 years of reanalysis data. We make the assumption that the MSE flux related to  
cyclones is described by the transient eddy component of a flux decomposition, and hereafter refer to this simply as the  
145 transient MSE flux. Firstly, the spatio-temporal relationship between meridional eddy transient MSE fluxes and extratropical  
cyclones is explored. Building on that, we inspect the contribution of a cyclone to the zonally integrated, meridional eddy  
transient MSE flux — in other words its energy transport footprint — by introducing a feature-based approach to attribute  
eddy transient MSE fluxes to individual cyclones. While trends in AHT heat transport (and its sub-components) have been  
investigated in previous studies (Rydsaa et al., 2021; Clark et al., 2022; Simmons, 2022; Franzke and Harnik, 2023; Cox et al.,  
150 2024a; Kang et al., 2024), we examine the inter-annual variability of the seasonal cyclone number along with seasonal eddy  
transient MSE fluxes. We focus on the SH storm track during the winter months June, July, and August (JJA). In contrast  
to the NH, the SH storm track is nearly circumpolar and therefore more zonally symmetric, which simplifies linking zonally  
integrated fluxes to cyclone characteristics. Moreover, winter is the season during which cyclone activity is maximum. The  
specific research questions thus are:

- 155
- How does the eddy local transient MSE flux evolve in the vicinity of surface cyclones in the SH during their life  
cycle during the life cycle of extratropical cyclones?
  - Are different cyclone characteristics, in particular intensification rate and intensity, reflected differently in the zonally  
integrated energy flux, and if so, how? How much of the zonally integrated heat transport can be attributed to cyclones.

and how do their contributions differ according to their key life cycle characteristics such as intensification rate, intensity, and lifetime?

160

- On a seasonal scale, how is the number of cyclones related to eddy transient MSE flux, and more generally the total AHT atmospheric heat transport?

~~We focus on the SH storm track during the winter months June, July, and August (JJA). In contrast to~~ The aim behind the last of the above research questions is to diagnose the existence of a relationship between atmospheric heat transport and the Northern Hemisphere (NH), the SH storm track is nearly circumpolar and therefore more zonally symmetric, which simplifies linking zonal mean fluxes to cyclone characteristics. Moreover, winter is the season during which cyclone activity is maximum cyclone number. The methods applied in this study are detailed in Sect. 2. The evolution of eddy transient MSE fluxes along cyclone life cycles, including spatial composites, is presented in Sect. 3. How cyclone characteristics influence the energy transport footprint of a cyclone in the zonal integral is shown and discussed in Sect. 4. The seasonal relationship between (eddy AHT transient heat transport) and extratropical cyclone number is examined in Sect. 5. Finally, the results are summarized and put into discussed in a broader context in Sect. 6.

165

170

## 2 Methods

### 2.1 Reanalysis data

~~This study discusses extratropical dynamics during the winter season in the~~ All computations of this study are based on the ERA5 reanalysis data set (Hersbach et al., 2020), which corresponds to JJA in the SH. The analyses are based on (Hersbach et al., 2020) using six-hourly data of the years 1981 to 2021–2021 during the winter season (DJF, i.e., December, January, February, in the NH and JJA in the SH). All variables are obtained at  $0.5^\circ \times 0.5^\circ$  ~~resolution and MSE fluxes are computed at 28 of the 37 available pressure levels spanning 1–1000. This vertical coarsening has minimal impact on the monthly closure of the energy budget (see Sect. 2.3, Eq. 1).~~ horizontal grid resolution.

175

180

### 2.2 Cyclone tracking

#### Automated cyclone tracking

Extratropical cyclones are identified using the cyclone tracking algorithm developed by Wernli and Schwerz (2006) and refined to improve the handling of splitting and merging events by Sprenger et al. (2017). Local minima of sea level pressure (SLP) are identified and followed over time. The ~~spatial extent of each of these identified cyclones is then defined using a cyclone mask is defined by the outermost closed SLP contour approach. The outermost SLP contour around a SLP minimum which is. Thereby, the outermost closed contour must be~~ shorter than 7500 km ~~encircles the cyclone area. Flagging grid cells within this area thus yields a cyclone mask.~~ The lifetime of a track is defined as the ~~length of each track while intensity (and intensification) are defined by the center SLP (and its change)~~ number of time steps of a track starting at genesis and including lysis. The maximum

185

intensity is defined as the minimum SLP along a track and the growth rate as the change in SLP between two consecutive time steps. While cyclones are tracked using hourly SLP input, only six-hourly time steps are considered in the analysis to match the temporal resolution of the calculated MSE fluxes. ~~Tracks~~

### Track postprocessing

We focus on well-defined cyclone tracks with a clear growth phase in this study. Thus tracks are excluded tracks that are shorter than 24 h, ~~weaker than and with lowest central SLP above 990 hPa, and intensify equatorward of 30~~ are discarded, to remove spurious tracks in and around topography and thermal lows. Furthermore, we ~~exclude tracks that do not intensify based on filter out tracks for which~~ the maximum SLP tendency reduction over 24 h normalized with  $\frac{\sin 60^\circ \text{S}}{\sin \phi}$  with the cyclone center at latitude is smaller than zero (Sanders and Gyakum, 1980),  $\phi$  (Sanders and Gyakum, 1980). Thus, we filter out tracks that intensify less than here represents the latitude of the cyclone center averaged over 24 h. This alternative threshold for the intensification rate would also be referred to as 0 Bergeron. As a reference, 1 Bergeron corresponds to a deepening rate of 24 hPa  $\text{d}^{-1}$  at 60° S. These criteria are applied to discard thermal lows that originate and disappear with the daily cycle, tropical cyclones that do not undergo extratropical transition, and cyclones that remain very weak. For comparability of different MSE flux decomposition methods, a track is not included in a composite if the considered stage falls onto a leap day. Lastly, we discard tracks that do not intensify poleward of 30° S, i.e., tropical cyclones without an extratropical transition.

### Cyclone-centered composites

To investigate the transient MSE fluxes associated with cyclones, cyclone-centered composites are computed at different stages of the cyclone life cycle (e.g. time of maximum intensification). MSE fluxes are regridded such that the cyclone center is located at (0,0) in cyclone-centered coordinates. Bilinear interpolation is used for all fields except precipitation, where conservative remapping is employed. As we aim to investigate meridional fluxes, the resulting fields are *not* rotated along the direction of propagation to preserve the distinction between meridional and zonal winds and fluxes.

## 2.3 MSE fluxes

~~A simplified version of the vertically integrated and zonally averaged atmospheric energy balance reads~~

$$\partial_t \langle [h] \rangle + \partial_y \langle [vm] \rangle = [F_{\text{TOA}} - F_{\text{S}}]$$

~~(Neelin and Held, 1987; Barpanda and Shaw, 2017).~~

### Zonal mean budget

To quantify atmospheric heat transport, we use the MSE framework. MSE is defined as  $m = h + \Phi$  where the first contribution is the thermal energy of the atmosphere  $h = c_p T + Lq$  corresponds to the thermal energy within the atmospheric column and  $m = c_p T + Lq + \Phi$  the MSE with where  $c_p$  being is the specific heat capacity of air,  $L$  is the latent heat of evaporation,  $T$  and is

temperature,  $q$  air temperature and denotes specific humidity, respectively, and  $\Phi$  the geopotential.  $v$  denotes meridional wind is geopotential. In the vertical integral and zonal average, the local atmospheric heat budget (as derived, for instance, in Trenberth, 1991) is written as

$$\partial_t \langle [h] \rangle = [F_{\text{TOA}} - F_{\text{S}}] - \partial_y \langle [vm] \rangle, \quad (1)$$

where  $F_{\text{TOA}}$  and  $F_{\text{S}}$  represent the net energy flux at the top of atmosphere (TOA) and surface, respectively, and  $v$  denotes meridional wind (Neelin and Held, 1987; Barpanda and Shaw, 2017).  $F_{\text{TOA}}$  is comprised of only radiative fluxes whereas  $F_{\text{S}}$  includes both radiative fluxes at the surface and turbulent fluxes. The temporal change in  $h$  is thus determined by the convergence of atmospheric heat flux and the net energy input at the surface and TOA.

The meridional divergence is computed as  $\partial_y(\cdot) \equiv \partial_\phi \{ \cos \phi(\cdot) \} / (a \cos \phi)$  and the meridional divergence and  $\langle \cdot \rangle \equiv \frac{1}{g} \int_{\bar{p}_S}^0 (\cdot) dp$  the mass-weighted vertical integration from the vertical integral is mass-weighted ( $\langle \cdot \rangle \equiv \frac{1}{g} \int_0^{\bar{p}_S} (\cdot) dp$ ). The integral is computed from the TOA to the climatological mean surface pressure  $\bar{p}_S$  to the TOA (Boer and Sargent, 1985). Note that this  $\bar{p}_S$  (Boer and Sargent, 1985). This formulation neglects kinetic energy and latent heat related to the liquid-ice transition (Mayer et al., 2024) and defines the energy tendency fluxes relative to a fixed mass of atmosphere following Cox et al. (2024b). MSE fluxes are computed at 28 of the 37 available pressure levels spanning 1–1000 hPa<sup>1</sup>.

### Eddy-mean decomposition

We further decompose the MSE flux into eddy and mean components. Transient eddies are defined as deviations from a background mean state and are traditionally thought to be related to synoptic weather systems (e.g. Kaspi and Schneider, 2013; Barpanda and Schneider, 2024). One established approach defines eddies from the background state using monthly means, such that the monthly mean flux reads

$$[\overline{vm}] = \text{TE}[\overline{v'm'}] + \text{SE}[\overline{v^*m^*}] + \text{MOC}[\overline{v}][\overline{m}] \quad (2)$$

with dashes and asterisks signifying anomalies from the monthly  $\bar{\cdot}$  and zonal averages  $[\cdot]$ , respectively (Priestley, 1949; Peixoto and Oort, 1992). Here we adopt the interpretation of the Following Barpanda and Shaw (2017), the first two terms on the right-hand side from Barpanda and Shaw (2017): the terms denoted with TE and SE represent right hand side represent fluxes by transient and (temporally) stationary eddies, respectively, whereas the third term corresponds to the meridional overturning circulation (MOC). Note that vertical averages of  $m$  and  $v$  are subtracted before computing the MOC (Marshall et al., 2014).

To investigate the total MSE flux, we perform a correction to account for mass conservation — MSE fluxes associated with a net mass flux are noisy and do not correlate strongly with the corresponding mass changes of the polar cap (Cardinale et al., 2021). This study focuses on the TE fluxes which are thought to be related to synoptic weather systems (e.g. Kaspi and Schneider, 2013; Barpanda and Schneider, 2024). Hereafter, we will refer to the TE fluxes calculated in this framework with  $v'm'_{\text{TE}}$ . The NH DJF and SH JJA climatologies of vertically integrated  $v'm'_{\text{TE}}$  are shown in Fig. 1. Throughout this study, fluxes in each hemisphere are defined positive if

<sup>1</sup>The exact levels used are 1, 3, 5, 10, 30, 50, 100, 150, 200, 250, 300, 350, 400, 450, 500, 550, 600, 650, 700, 750, 800, 850, 875, 900, 925, 950, 975, and 1000 hPa. Note that we ensured that the sub-selection of vertical levels has minimal impact on the monthly closure of the energy budget.

poleward. Climatologically, the maximum fluxes (shading in Fig. 1a) are located equatorward of the storm tracks (surface cyclone frequency in black contours). Zonally integrating (eddy) AHT involves a multiplication with a cosine of latitude and we present the cosine latitude weighted cyclone frequency in Fig. 1b to account for the changing area per grid cell and remain consistent with the definition of AHT. Seasonally averaged fluxes (purple lines in Fig. 1b) in the SH amount to 6 with the difference between the weakest and the strongest season being roughly 1 at 45°S which is not guaranteed in ERA5 (e.g., Mayer et al., 2021). In the zonal mean, mass conservation corresponds to  $\langle [v] \rangle = 0$  when calculating heat transport with respect to a time-independent atmospheric mass. We thus adopt the approach introduced by Marshall et al. (2014) and subtract vertical averages of  $[m]$  and  $[v]$  before computing the overturning circulation. Thereby, the MSE flux that is related to a net mass flux, which can be unrealistically large (Cox et al., 2023), is removed.

Climatologies of TE MSE fluxes and cyclone frequencies during winter. (a) Vertically integrated and seasonally averaged TE MSE fluxes,  $\langle \overline{v'm'}_{TE} \rangle$ , (shading) are shown along with the cyclone mask frequency (black contours in steps of 5 starting at 5 with 15 and 30 highlighted in thicker contours). (b) Zonally integrated TE MSE fluxes,  $\langle [\overline{v'm'}_{TE}] \rangle$ , (purple) and zonal mean cyclone frequencies (black) for individual seasons (thin lines) and the climatology thereof (solid lines). For compactness and better comparability, MSE fluxes are shown positive poleward in this panel. Note that the cyclone frequency in (b) is multiplied with the cosine of latitude for consistency with the zonally integrated poleward energy fluxes. In both (a, b), values in the NH are for DJF and JJA in the SH, while latitudes near the equator are masked.

The above boxcar approach to monthly averaging in the ‘TE framework’ leads to somewhat unphysical

## 265 Sensitivity regarding the decomposition

Defining transient eddies as deviations from monthly mean data introduces discontinuities at the turn-end of each month. Also, the window-length of around 30 is to some extent arbitrary and arguably unrelated to the synoptic timescales of interest. Most results are based on large cyclone sample sizes such that the introduced methodological biases are assumed to average out. We use two additional MSE flux decomposition methods for to We explore the sensitivities of the results. One of the most widely used approaches in weather science to separate eddy and background signals is a decomposition into using two additional definitions of transient eddies: (i) high-pass and low-pass filtered components (e.g. Hoskins et al., 1983; Schemm and Rivière, 2019; Franzke et al., 2023). While closing the energy budget using such an approach can require computing many cross-terms (Franzke and Harnik, 2023), we simply compare  $v'm'_{TE}$  to the eddy flux signal,  $v'm'_{HP}$ , where dashes denote the high-pass (HP) components.  $v$  and  $m$  are concatenated for the entire analysis period (only ignoring leap days) and high-pass filtered with a frequency filtering (e.g. Hoskins et al., 1983; Schemm and Rivière, 2019; Franzke and Harnik, 2023) with a cut-off at frequency of 10 d and; (ii) defining eddies as anomalies from instantaneous zonal means (Cox et al., 2024b).

The third method that is used for sensitivity tests defines eddy fluxes via anomalies from zonal means *instantaneously* (Cox et al., 2024b). In contrast to the other two methods, no timescale is introduced in this decomposition method. The eddy fluxes derived from zonal anomalies (ZA) are referred to as  $v^*m^*_{ZA}$ . These local eddy fluxes depend on the flux that occurs elsewhere. This eddy flux thus depends on the atmospheric state up- and downstream at the same latitude, whereas for the

~~other methods the eddy flux. In contrast, the eddy flux in the other two methods depends on the local flux evolution in time. characteristics of the time series of the data at the same location.~~

285 Throughout the manuscript, we use superscripts to indicate anomalies: A prime ( $\cdot$ )' for deviations from a temporal mean (referred to as 'transient' anomaly), and ( $\cdot$ )\* for deviations from the zonal mean. A corresponding subscript indicates the method used for the computation of the background state. A subscript MA indicates monthly anomalies, HP refers to high-pass filtering, and ZA indicates zonal anomalies. Thus, in sensitivity tests we compare  $v'm'_{MA}$  to  $v'm'_{HP}$  and  $v^*m^*_{ZA}$ . A complete list of the used mathematical symbols is provided in Appendix A.

## 2.4 Cyclone composites

290 Going beyond the zonal mean, eddy MSE fluxes are inspected in the vicinity of cyclone centers by the use of composites. For a given set of cyclones (including all or only the deepest ones, for instance) and stages (e.g. time of maximum intensification), nearby eddy MSE fluxes are regridded such that the cyclone center is located at (0,0) in cyclone-centered longitude and latitude coordinates. Bilinear interpolation is chosen for all fields except for precipitation where conservative remapping conserves the peaks. Note that unlike other studies (e.g. Catto et al., 2010; Daere et al., 2023), the resulting fields are *not* rotated along track direction. Rotated coordinates are usually preferred to retain and highlight separate signals from warm and cold 295 fronts. However, when investigating meridional energy fluxes we chose to conserve the direction of flux within the composite. Grid points falling below climatological surface pressure (which approximates the topography) have been masked out for the composites.

## 2.4 ~~Attributing eddy Cyclone-attributed MSE fluxes to cyclones~~

~~The composite analyses based on the complete eddy MSE flux fields in Sect.~~

300 In this section it is described how local MSE fluxes are attributed to individual cyclones. Having computed cyclone masks from the SLP fields, the simplest approach is to spatially integrate the MSE fluxes over the cyclone mask at each timestep. Note, however, that climatologically the maximum transient MSE flux is located equatorward of the maximum in surface cyclone frequencies (Fig. 3.2 reveal that substantial fluxes are located further away from the cyclone center and outside of the largest closed SLP contour (which the cyclone mask is derived from). Instead of using the cyclone masks to attribute eddy MSE 305 fluxes to the cyclones, we identify and attribute to the cyclone eddy MSE fluxes (which can be outside of the mask) that are thought to be associated with the cyclone-induced circulation. There is no single correct approach to identify coherent features in atmospheric flows (see, for instance, a comparison of atmospheric river tracking algorithms in Shields et al., 2018). In this work, flux features 1a). This is similar to the relationship between surface cyclones and eddy kinetic energy (e.g., Shaw et al., 2016). Schemm et al. (2018) argue that this latitudinal offset occurs because eddy fluxes peak during the rapid growth phase of 310 extratropical cyclones, whereas cyclone detection frequencies peak in regions where cyclones have evolved into mature, slowly propagating systems. This latitudinal offset is also evident in the zonal mean (Fig. 1b): In the SH, transient MSE flux peaks at 6 PW around 45° S, while the zonally integrated cyclone frequency reaches up to 12 % near 62° S. Thus, most of the transient MSE fluxes are expected to be excluded when spatially integrating fluxes only within the (SLP-based) cyclone masks.

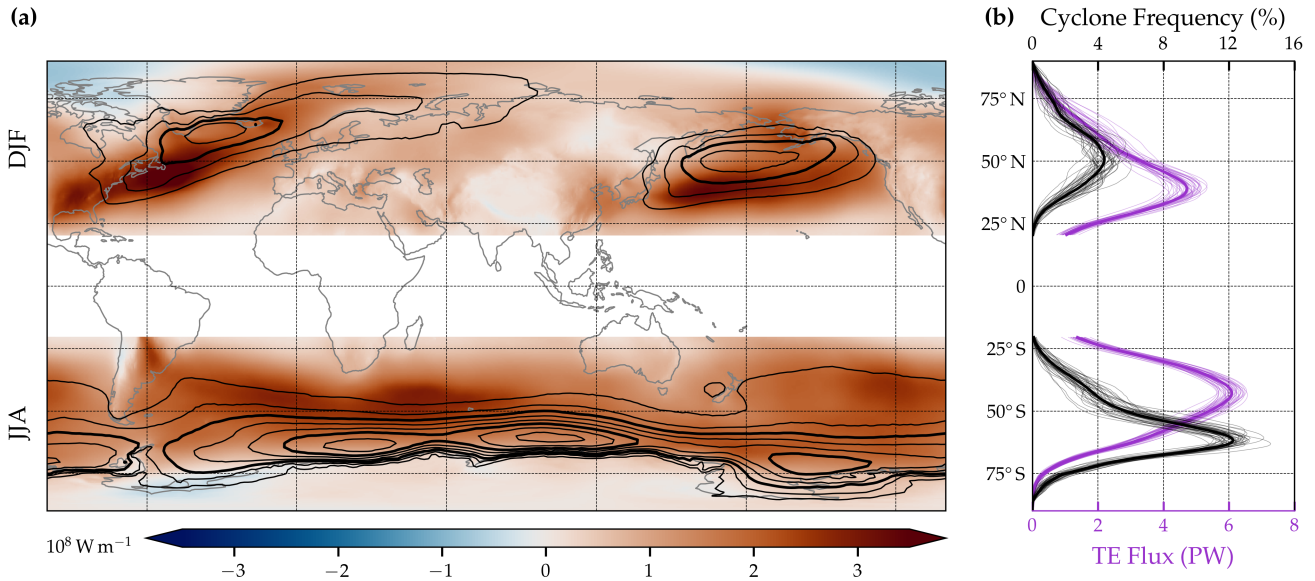


**Figure 1.** Climatologies of transient MSE fluxes and cyclone frequencies during winter for both hemispheres (DJF in the NH and JJA in the SH.) (a) Vertically integrated and seasonally averaged transient MSE fluxes,  $\langle v'm'_{MA} \rangle$ , (shading) are shown along with the cyclone mask frequency (black contours in steps of 5 % starting at 5 % with 15 % and 30 % highlighted in thicker contours). (b) Zonally integrated transient MSE fluxes,  $\langle [v'm'_{MA}] \rangle$ , (purple) and zonal mean cyclone frequencies (black) for individual seasons (thin lines) and the climatology thereof (solid lines). MSE fluxes are shown positive poleward. Note that the cyclone frequency in (b) is multiplied with the cosine of latitude for consistency.

To overcome this latitudinal gap between the two storm track metrics, a flux attribution method is introduced that identifies coherent MSE flux features and connects them to cyclones via spatial overlap criteria. Transient MSE flux features in this work are identified using a flux threshold based on a percentile which broadly resembles the spirit of the approach of Messori et al. (2017). Since especially MSE is varying greatly with season and latitude, the percentile threshold (similarly to studies tracking atmospheric rivers, the flux threshold is chosen to be latitude- and time-dependent. This is achieved by taking a percentile of to account for the high spatial and temporal variability of MSE. The percentile is drawn from all values of a latitude band at the same time step of each year (resulting in, (see Fig. B1). Thus, it is computed from 29,520 values ( $360^\circ / \Delta_{lon} \times N_{years} = 29520$  values to draw the percentile from, see gridspacing  $\times$  the number of years as illustrated in Fig. B1) at each latitude and timestep.

B2). Given a percentile rank  $p$ , features of the vertically integrated flux  $\langle v'm'_{TE} \rangle$  are identified transient flux  $\langle v'm'_{MA} \rangle$  is masked using the flux thresholds corresponding to  $p > 0.5$  for northward fluxes and  $100\% - p - p$  for southward fluxes with  $p > 50\%$ . The resulting MSE flux features that are larger than

A well-defined MSE flux feature mask is defined by adjacent grid points at which the percentile threshold is exceeded. The features are identified and labeled using TempestExtremes v2.1 (Ullrich et al., 2021). Small features ( $4.9 \times 10^4 \text{ km}^2$  (about or approximately  $1^\circ \times 1^\circ$ ) and poleward of 15 are then labeled using TempestExtremes v2.1 (Ullrich et al., 2021). Instead

of tracking, which are located predominantly in the tropics and subtropics, are discarded. The remaining features (describing both poleward and equatorward flux) are attached to cyclone tracks if they spatially overlap with the SLP-based cyclone masks (filled orange and blue patches in Fig. 2). This is done at every timestep separately as the MSE flux features are not tracked (or "stitchingstitched" in the language of the tool) the resulting flux features over time, the eddy MSE flux features that spatially overlap the SLP masks are attributed to unique cyclones at each time step over time. Non-overlapping features are considered 'other' eddy fluxes (see MSE features are labeled as 'other MSE fluxes' (orange and blue contours in Fig. B22). If a flux feature mask overlaps with multiple cyclones, the cyclone with the lowest center SLP at that time step is chosen. Choosing from Randomly selecting between the overlapping cyclones randomly instead was also tested but makes no qualitative difference, but had no qualitative effect on the results in this paper. Therefore, we think that a more sophisticated algorithm that tracks flux features which are then attributed to cyclones based on some evolution criteria would not lead to markedly different results. Note that given the percentile rank  $p$ , the ratio of grid points attributed to cyclones is not exactly  $2 \cdot (100\% - p) \cdot 2 \cdot (1 - p)$  ('northward' plus 'equatorward' areas) but less because small features are filtered out of filtering out small features and not all of the remaining are attributed to cyclones. The Due to the relative simplicity of the attribution method, sensitivity analyses boil down to the choice of  $p$  and the flux decomposition method. While the results in Sects. 4 and 5 are for  $p = 90\%$ . Two other percentile ranks  $p = 80\%$  and  $p = 95\%$  have been tested which tend to attribute broader and narrower features to the cyclones, respectively.  $p = 0.9$ ,  $p = 0.8$  and  $p = 0.95$  were also tested. The percentile generally determines the width of the attributed features. The location of these features in turn differs depending on the decomposition method (Fig. B2).

#### 345 **From local fluxes to the zonal budget**

In the zonal heat budget, the MSE flux attributed to a cyclone is simply the zonal integral of the flux within the attributed MSE flux features (orange curve in Fig. 2). To define the cyclone number at each latitude, each cyclone is counted once towards all latitude bands where its attributed MSE flux is different from zero along its lifetime (purple bars in Fig. 2). Thus, the seasonal number of cyclones at a given latitude corresponds to the cyclones that have attributed transient MSE flux at this latitude, whereas their corresponding life cycle characteristics, such as maximum intensification rate or maximum intensity, can occur at any latitude.

The seasonal sets of strongly intensifying cyclones are then determined using climatological thresholds: Cyclones are considered 'strongly' intensifying if their intensification rate lies above the 75<sup>th</sup> percentile determined from the climatological set of all cyclones passing that latitude. If the 75<sup>th</sup> percentile of cyclone intensification based on all SH JJA cyclones is, for instance,  $24 \text{ hPa d}^{-1}$ , then this threshold defines the number of strongly intensifying cyclones in every season. Thus, their number is *not* simply 25% of the seasonal number if that year has more or less strongly intensifying storms than the climatology. Choosing the 75<sup>th</sup> percentile (instead of the 90<sup>th</sup>, for instance) is found to be an adequate compromise between selecting only the strongest cyclones and including a large enough number of cyclones to counteract the event-to-event variability (see discussion in Appendix D). If the intensification rate lies within the inter-quartile range or below, cyclones are denoted 'moderately' or 'weakly' intensifying, respectively. The classification of cyclones as 'strong', 'moderate', and 'weak' works analogously for intensity.

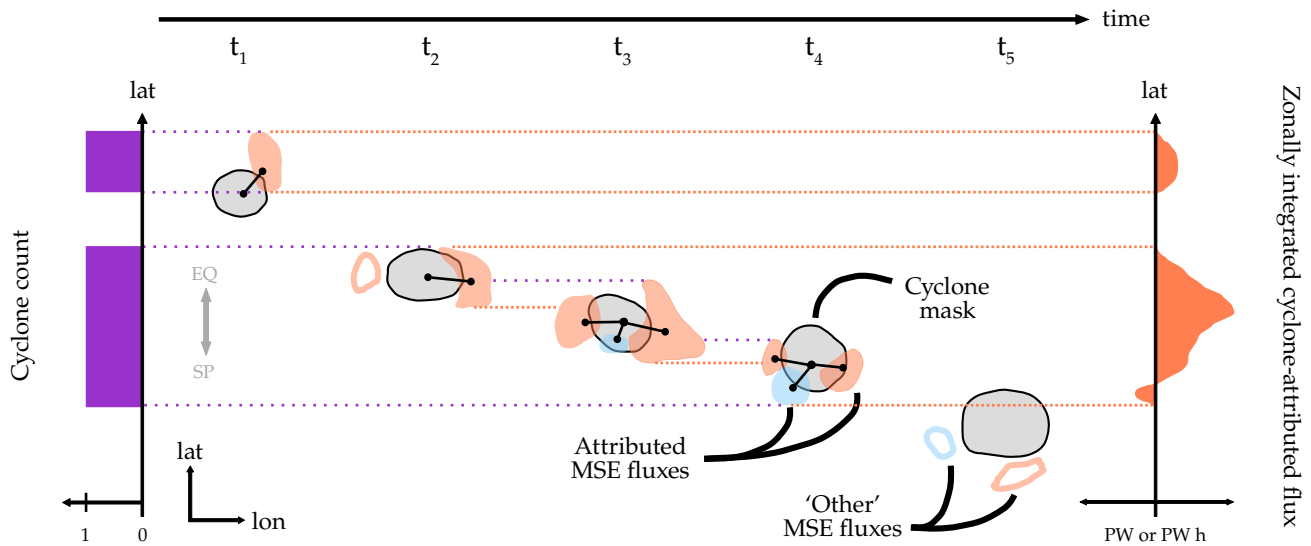


**Figure 2.** The attribution of transient MSE flux to surface cyclones exemplified for a cyclone that lasts for five six-hourly time steps. The cyclone mask is indicated with grey patches and the attributed poleward and equatorward transient MSE flux features with orange and blue shading, respectively. Other MSE fluxes that are not spatially overlapping are shown with orange and blue contours. In the zonal integral, cyclone-attributed transient MSE fluxes are expressed in PW h if accumulated or in PW if averaged over the cyclone lifetime (orange curve). The latitudinal extent used for counting is then determined by the latitudes at which the attributed fluxes along its lifetime are non-zero. At any latitude band, a cyclone is therefore counted either once or zero times (purple bars). A grey arrow serves orientational purposes.

365 These methods enable us to study the relationship between various extratropical cyclone life cycle characteristics and MSE fluxes. They also allow us to analyze the fractional contribution of cyclone-related MSE flux to the zonally integrated poleward heat transport and the relationship between cyclone number and intensity and zonally integrated atmospheric heat transport. By defining the number of cyclones as where they contribute to MSE flux we can study the linkage between cyclone numbers and heat transport in a consistent way.

### 3 Eddy MSE fluxes along extratropical cyclones

#### 3 Transient MSE fluxes along extratropical cyclones

370 This first result section starts addressing the relationship between TE MSE fluxes and extratropical cyclones by investigating the evolution of  $v'm'_{TE}$  along the typical cyclone life cycle. The adopted cyclone-centered perspective allows for a better understanding of how  $v'm'_{TE}$  co-locates with cyclone centers, changes along cyclone life cycle, and relates to cyclone intensification. The life cycle analyses and cyclone-centered composites complement and expand on previous research aggregating eddy MSE flux events based on flux magnitude. Special attention is paid to the partitioning into dry and moist flux components in the warm

and cold sectors across different latitudes. As indicated, the following results are based on calculating eddy MSE fluxes using the TE framework — from anomalies defined as departures from the monthly mean. 4 and 5. First, it is investigated how the local transient MSE fluxes ( $v'm'_{MA}$ ) evolve along the extratropical cyclone life cycle and where they maximize relative to the cyclone center.

### 3.1 Eddy Temporal evolution of transient MSE flux along during the cyclone life cycle of extratropical cyclones

To obtain an impression of the evolution of a variable along the compare extratropical cyclones life cycles of different durations the transient MSE flux is interpolated to a normalized cyclone life cycle, it has proven helpful to consider normalized cyclone tracks (e.g. Rudeva and Gulev, 2007; Schemm et al., 2018): For the first analysis, tracks (e.g. Rudeva and Gulev, 2007; Schemm et al., 2018). Following previous studies, cyclone tracks are split into a deepening an intensification and a weakening phase. All tracks that feature more and tracks with less than two time steps in both of these phases are then normalized for both periods genesis, mature stage and mature stage, lysis separately. Any quantity can be interpolated onto the resulting, uniform x-axis using cubic spline interpolation (Fritsch and Carlson, 1980; Schemm et al., 2018).

This approach is applied to the maximum each phase are removed from the analysis. The maximum transient MSE flux at 850 hPa  $v'm'_{TE}$  within a  $7.5^\circ$  radius from around the cyclone center. Considering all is interpolated to the normalized life cycle using cubic spline interpolation (Fritsch and Carlson, 1980; Schemm et al., 2018).

Considering all SH cyclones, the maximum  $v'm'_{TE}$  features a peak  $v'm'_{MA}$  peaks before mature stage and declines afterwards (black line in Fig. 3).<sup>2</sup> The peak flux during intensification phase is, on average, around 50 % larger than towards the end of the deepening phase. The maximum TE MSE flux peaking before mature stage is during the weakening phase. This evolution is broadly consistent with the baroclinic life cycle whereby, in which transient eddy heat flux peaks while baroclinicity is being eroded and as baroclinicity is eroded, before intensification terminates (Novak et al., 2015). Certainly, computing the maximum flux within a fixed radius from the center introduces the possibility of capturing the signal of another cyclone at a different stage. Thus, for larger radii fluxes before and after mature stage increase uniformly (not shown). Moreover, both lifetime and latitude of this large set of SH cyclones span broad ranges. This motivates studying cyclone subsets as done throughout the remainder of the section.

Maximum near-cyclone TE MSE flux,  $v'm'_{TE}$ , at 850 for all (black) and the 10 most strongly intensifying cyclones (blue) along the normalized cyclone life cycle. The search radius is 7.5. Median and interquartile range are shown in solid lines and shading, respectively. Genesis and lysis correspond to the first and last time steps of the track, respectively, while the mature stage is defined as the time of minimum central SLP. For track normalization, a cubic spline fit is performed for each track and the resulting distribution. The number of all SH cyclones is included in the upper right.

With fluxes peaking during the intensification phase, it is natural to ask whether the magnitude of the intensification rate plays a role for the magnitude of the nearby fluxes. Indeed, the above TE MSE flux contrast before and after mature stage is even larger when considering the subset of the Using larger attribution radii does not qualitatively affect this result, but it

<sup>2</sup>This is verified by centering the tracks onto the stage of peak intensification or mature stage without performing the spline interpolation and using different radii (not shown).

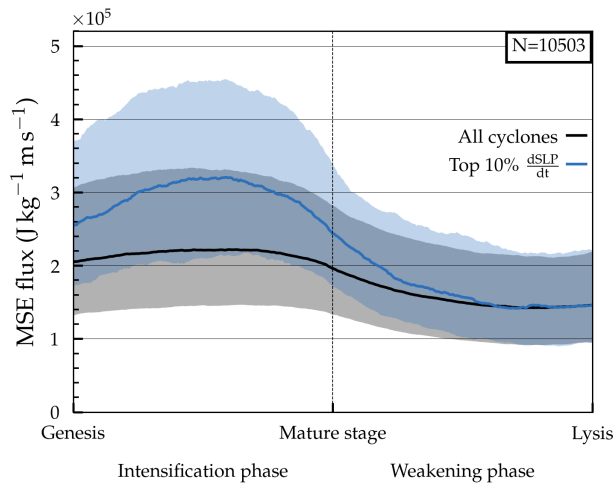


**Figure 3.** Maximum near-cyclone transient MSE flux,  $v'm'_{MA}$ , at 850 hPa for all (black) and the 10 % most strongly intensifying cyclones (blue) along the normalized cyclone life cycle. The search radius is  $7.5^\circ$ . Median and interquartile range are shown in solid lines and shading, respectively. Genesis and lysis correspond to the first and last time steps of the track, respectively, while the mature stage is defined as the time of minimum central SLP. The number of all SH cyclones is included in the upper right.

increases the proportion of flux attributed to a cyclone that, upon visual inspection, would be attributed to a nearby cyclone. For the 10 % most strongly intensifying cyclones (blue line in Fig. 3). The peak of MSE flux during genesis is exaggerated with a median flux of this subset is roughly 50 % larger during the intensification phase compared to all SH cyclones, but levels off after mature stage to comparable values of all SH tracks towards lysis. The difference of median flux during intensification and deepening amounts to a factor of around two. As above, near-cyclone  $v'm'_{TE}$  has been weakening again when mature stage is reached. Therefore, the following analyses will focus solely on the deepening all cyclones (blue line in Fig. 3). In turn, similar flux values are observed during the weakening phase. This highlights the close relationship between transient MSE flux and the intensity of baroclinic growth. The following spatial analyses will thus focus entirely on the intensification phase.

### 3.2 Spatial relation of eddy transient MSE fluxes and cyclones

Next, cyclone-centered composites are inspected to study how fluxes are distributed. The spatial distribution of MSE fluxes around the cyclone center and occur spatially along the cyclone life cycle is studied using cyclone-centered composites. Recall that in the SH, cyclonic flow is clockwise and that poleward flux is chosen positive in this study. Also note that. Also, both the poleward transport of (temporally) anomalously warm and moist and anomalously warm moist as well as the equatorward transport of anomalously cool and dry air both have result in a positive poleward MSE and, thus, both. Thus the warm and cold sectors show both show up as positive MSE fluxes in the composites.

Composites of all SH cyclones indicate poleward  $v'm'_{TE}$  downstream. The composite based on all cyclones indicates a maximum in poleward  $v'm'_{MA}$  at the 850 hPa level in the warm sector of the cyclone center during genesis and peak intensification at 850 all three key stages the cyclone life cycle (Fig. 4a,c). The MSE flux is generally larger on the equatorward side of the cyclone center. This is consistent with previous findings that heat transport is bound by the frontal zones (compare, for instance, with the 990 which in the SH frequently extend to 20–40° b). Note that the signal at the genesis stage in Fig. 4a is partly due to secondary cyclogenesis along the cold front leading to cyclones ‘inheriting’ fluxes from previous, still intensifying ones, which is well equatorward of the cyclone centers (Schemm et al., 2015; Rudeva et al., 2019). Closer inspection of the peak at genesis indicates that, in some cases, the flux is associated with a cold front accompanying a mature cyclone further downstream. This suggests that some cases are secondary cyclogenesis events, when a cyclone grows on the pre-existing front of a mature system (Schemm and Sprenger, 2015). During mature stage, this signal the location of the maximum poleward flux is located further downstream and accompanied with an emerging negative (equatorward) in the warm sector relative to its position at genesis, when it is located closer to the cold front. In addition, a negative flux upstream of the cyclone center at ( $r_{lon} = -1^\circ$ ,  $r_{lat} = 0^\circ$ ) in the composite coordinates. Further upstream, a positive signal related to the cold sector only stands out towards in the local coordinates (light blue patch in Fig. 4c). While the warm sector features a local flux peak during all life cycle stages, the cold sector displays a well-marked positive flux signal in the composites only at the mature stage (Fig. 4c). From vertical-

In vertical west-to-east cross-sections across  $= 0$ , i.e. the latitudinal band through the center, it becomes clear that the signal of the warm sector through the cyclone center, the pronounced warm sector flux extends up to roughly 300 hPa during all considered stages with a peak stages and reaches its maximum at around 900 hPa (Fig. 4d-f). This generally agrees with the vertical extent when centering around 850 MSE flux extremes (Messori and Czaja, 2015). Thus, the signal in the warm sector signal is the footprint of the ascending warm and moist airstream known as warm conveyor belt. Likewise, the flux in the cold sector at mature stage maximizes at that level, which was also identified by centering around 850 MSE flux extremes instead of cyclone centers (Messori and Czaja, 2015). The aforementioned negative signal located upstream of flux located near the cyclone center extends up to around 700 hPa, while around 500 hPa a second negative signal downstream of the center appears (Fig. 4f). A significance test supports that these fluxes that we relate to cyclonic flow features are. All of the flux signals discussed here are significantly different from climatology (see Sect. Appendix C, Fig. C1).

Composite To better understand the negative flux anomalies, consideration is given to composite mean meridional winds (grey lines in Fig. 4d-f). Overall, the wind anomalies tilt westward with height during genesis and intensification but intensification and become more barotropic at mature stage.<sup>2</sup> Conceptually, this vertical velocity tilt matches the characteristic of the most unstable, fastest-growing perturbation in the Eady model (Eady, 1949). Likewise, the more barotropic flow at mature stage represents the end of baroclinic growth. Temperature anomalies (which dominate MSE anomalies), in turn, are expected to tilt eastward with height (Eady, 1949), which was confirmed for the composite MSE anomalies (not shown). The which agrees with baroclinic theory (Eady, 1949; Thorncroft et al., 1993). For the mature stage, the wind field suggests that the mid-level negative flux signal during mature stage at at the 500 hPa level results from cold air moving poleward (Fig. 4f). Furthermore, and that

<sup>2</sup>While  $v'$  is shown in Fig. 4, this is also the case for the full meridional wind  $v$  (Fig. C1).

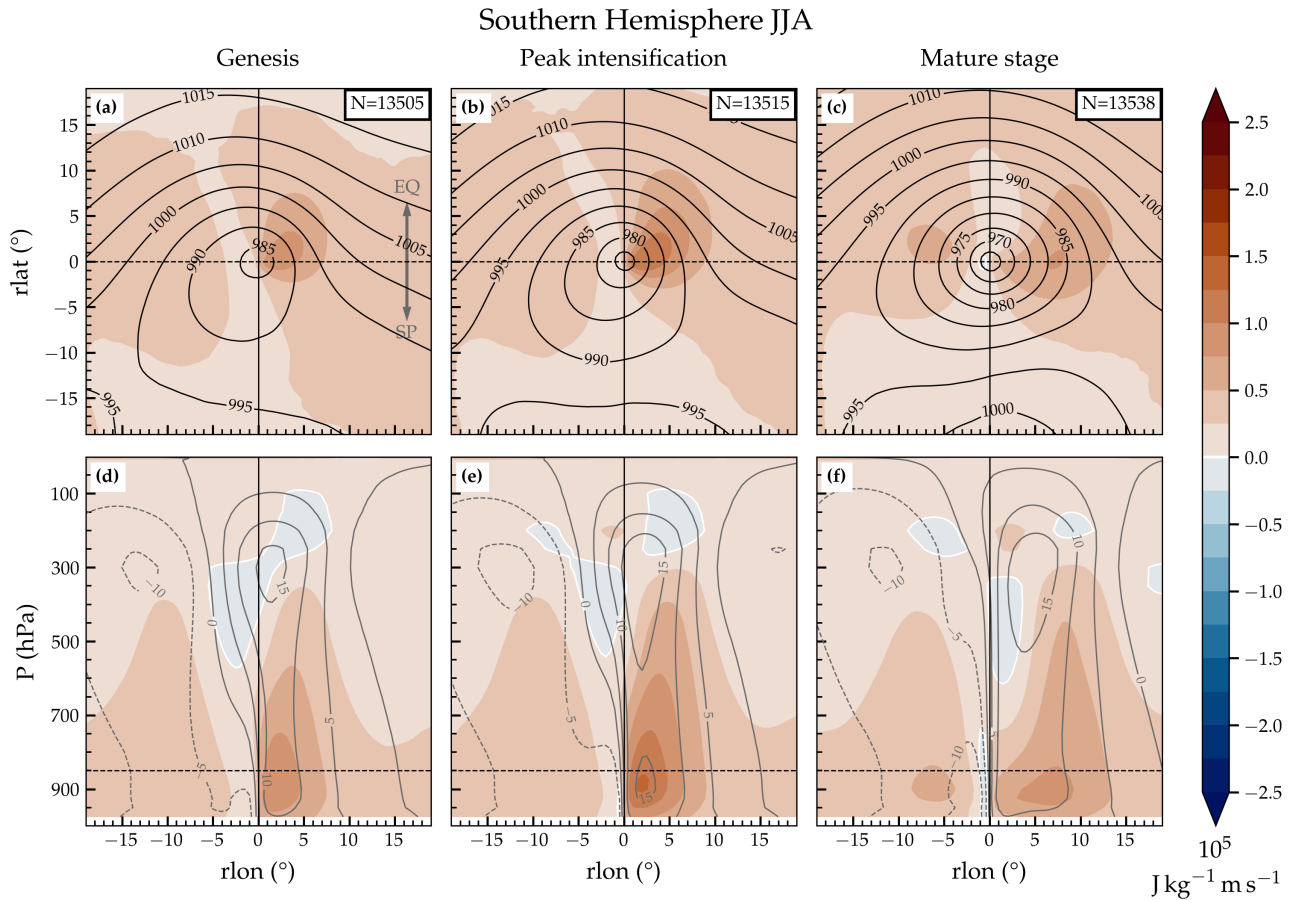


**Figure 4.** Cyclone-centered meridional **TE-transient** MSE flux,  $v'm'_{TE}v'm'_{MA}$ , composited for different stages along the cyclone life cycle. Horizontal maps are shown for fluxes (colors) at 850 hPa for (a) genesis, (b) time of peak intensification, and (c) mature stage. Black contours indicate composite mean SLP in hPa. Similarly in panels (d)–(f), height-longitude the west-to-east cross-sections through  $r_{lat} = 0$  are shown in panels (d)–(f) for correspond to the same stages as in (a)–(c) above. Grey lines depict meridional wind velocities ( $v'$ ) in  $\text{m s}^{-1}$  (positive poleward). Horizontal dashed black lines represent the intersection of the corresponding vertical and horizontal panels. Furthermore, the number of cyclones in the composites are included in the upper right in panels (a)–(c). A grey arrow is included for better orientation indicating directions of equator (EQ) and South Pole (SP).

455 the low-level equatorward flux at mature stage can be related to represents warm and moist air flowing equatorward along the bent-back extension of the warm front (Shapiro and Keyser, 1990). This-The latter signal does not emerge when centering on flux extremes but highlights the importance and value of the cyclone life cycle perspective.

The composite analysis confirms the previous findings based on normalized tracks that meridional **TE-transient** MSE fluxes near cyclones are, on average, largest during the intensification phase. Likewise, from a spatial composite perspective, the flux  
 460 of the 10 % most strongly intensifying cyclones is roughly 50 % larger in the cold sector, but and up to 80 % larger in the warm

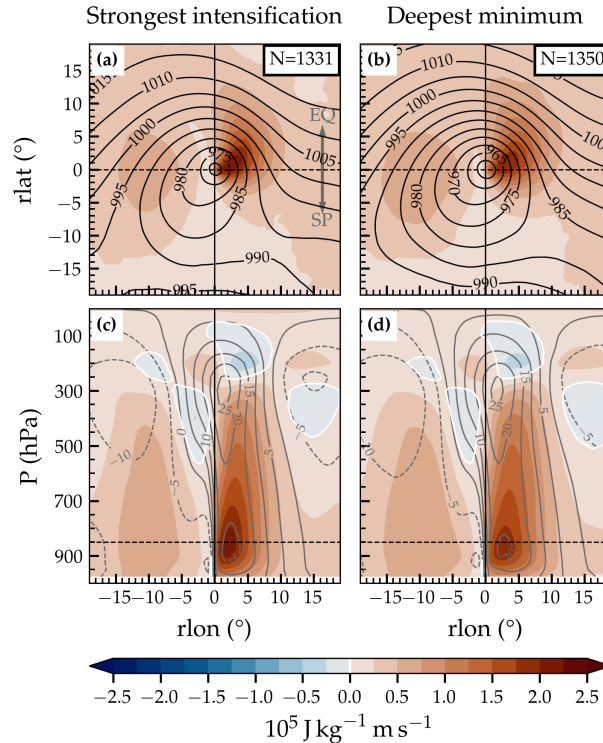


**Figure 5.** Cyclone-centered  $\overline{TE}$ -transient MSE flux at 850 hPa composited during time of peak intensification for (a) the 10% most strongly intensifying cyclones and (b) the 10% deepest cyclones at mature stage. Black contours indicate composite mean SLP in hPa. As in Fig. 4, horizontal maps are complemented with height-longitude cross-sections in panels (c, d) show the corresponding west-to-east cross-sections. Grey lines depict meridional wind velocities ( $v'$ ) in  $\text{m s}^{-1}$  (positive poleward). Horizontal dashed black lines represent the intersection of the corresponding vertical and horizontal panels. Furthermore, the number numbers of cyclones in the composites are included in the upper right in panels (a, c). A grey arrow is included for better orientation indicating directions of equator (EQ) and South Pole (SP).

sector close to the cyclone center as compared to all SH cyclones (compare, for instance, compared to all cyclones (cf. Fig. 5a to Fig. 4b at 850 hPa). Differing percentage increases between the along-track evolution and composite map perspectives likely arise from applying a fixed radius to search for a maximum in the former method and varying lifetimes being aggregated (as discussed above). Strongly intensifying cyclones feature negative fluxes at 300 hPa downstream of the center, which can be related to the anticyclonic return flow of the warm conveyor belt and which are less prominent in the composites of all SH cyclone-all SH cyclones (compare Fig. 5c and Fig. 4e).

We want to note that selecting for the tracks with deepest SLP. These conclusions remain unchanged when cyclones with the deepest SLP values are considered instead of those deepening most strongly does not qualitatively impact the above conclusions. Both that deepen most strongly. The corresponding warm and cold sector signals are slightly fluxes are more horizontally and vertically extended with and the warm sector peak is slightly reduced (at peak intensification, Fig. 5b, d). This points toward

deep cyclones not necessarily being the ones intensifying most strongly but being larger in size confirms the findings of earlier studies which argue that, while very deep cyclones cover typically wider areas, they are not necessarily the cyclones that intensify most rapidly (Rudeva and Gulev, 2007).

475 While these results suggest that near cyclones,  $v'm'_{TE}$  is largest. The asymmetry in the MSE flux between the cold and warm sectors is strongly related to the presence of moisture in the warm sector, for some cyclones fluxes may also be large in cold sectors. Previous research has shown that poleward transport. However, MSE flux extremes can be both related to warm air moving poleward as well as equatorward cold air advection. Both of these 'flavors' of poleward heat transport can be associated with  $v'm'_{TE}$  of comparable magnitude (Messori and Czaja, 2015). Furthermore, banded structures of the latter account for around related to both warm and cold sectors (Messori and Czaja, 2015) and in the seasonal mean, cold air  
480 advection contributes up to 40% of to the total poleward heat transport across a wide range of latitudes (Messori et al., 2017). Thus, the lack of a signal upstream of the cyclone center that is comparable to the one found in the warm sector might be surprising.

We expect this warm-cold sector flux contrast in our composites to arise for several reasons. Firstly, a simple geometrical explanation for this contrast can be seen when assuming the wind field in geostrophic balance with the SLP contours ( $v = (f\rho_A)^{-1} dp/dx$  with  $f$  the Coriolis parameter,  $\rho_A$  air density,  $p$  pressure, and  $x$  longitude). When inspecting the latitude of  
485 the cyclone center (dashed horizontal line) in Fig. 4b, for instance, one can see that the contours of SLP are almost perfectly meridionally oriented downstream of the center but contain an additional zonal component upstream (in other words the upstream SLP contours resemble a bottom-left to top-right tilt on the panel). Therefore,  $v$  is larger in the warm sector and, thus,  $v'm'_{TE}$  would be expected to be larger in Messori et al. (2017). In the composites, the warm sector flux stands out more  
490 strongly, which could be related to the fact that compositing by the cyclone center implies a tendency to centering next to the warm sector. Since the warm sector even if the winds in both sectors were advecting the same magnitude MSE gradient. This is an important caveat of focusing only on meridional TE MSE fluxes.

Secondly, in particular during the intensification phase fronts are located relatively close to the cyclone center (Schemm et al., 2018) and only detach when an occlusion forms at a later stage of the life cycle (Shapiro and Keyser, 1990). The warm sector is  
495 spatially bound by the warm and cold fronts and narrows towards mature stage and lysis narrows during the life cycle as the cold front catches up with the warm front. Compositing by the cyclone center implies a tendency to centering next to the warm sector especially during the intensification phase. Conversely, the upstream extent of the cold sector is generally not limited by frontal zones and hence can be more smeared out in the composite.

Thirdly, moisture causes the warm sector eddy MSE fluxes to be greater than those in the cold, the fluxes in the warm sector  
500 At low levels such as 850, latent heat in the warm sector adds to MSE while cold sectors are much drier (Messori and Czaja, 2015; Geen et al. In addition to its mere presence, if calculated as anomalies from a mean of a sample (such as monthly mean or zonal mean), positive specific humidity anomalies are even larger than negative ones because the spatiotemporal are spatially more constrained than in the broader cold sector (Shapiro and Keyser, 1990).

### 3.3 Latitudinal variations of dry and latent heat flux contribution to the MSE flux

505 The contribution of latent heat flux to the MSE flux varies with latitude, which results from the latitudinal distribution of specific humidity is skewed — due to the non-linear Clausius-Clapeyron relationship, specific humidity increases exponentially with the temperature in a warm sector under constant relative humidity — and has a lower bound.

### 3.4 Latitudinal variations of dry and latent eddy heat fluxes

Of course, specific humidity,  $q$ , and thereby the contribution of latent heat flux to MSE flux is highly dependent on temperature and therefore also latitude. In the following, the above set of To explore the dependency of the relative contributions by dry and latent energy on latitude, the top 10 % most strongly intensifying cyclones of cyclones with the strongest intensification are sorted into  $10^\circ$  latitude bands according to the cyclone center latitude at time of their centre latitude at peak intensification.

Downstream of the cyclone center, both  $v'm'_{TE}$  and  $v'Lq'_{TE}$  decrease towards Both MSE and latent heat flux decrease for cyclones closer to the pole (Fig. 6). Unlike  $v'm'_{TE}$ ,  $v'Lq'_{TE}$  The maximum of  $v'Lq'_{MA}$ , which is confined to the warm sector downstream of the center which is in line with the arguments above. Notably, going towards the pole the decrease in  $v'm'_{TE}$  in the cold sector is less pronounced than, largely overlaps with six-hourly accumulated precipitation (black contours in Fig. 6d,e). The relative contribution of  $v'Lq'_{MA}$  reduces for cyclones propagating closer to the pole as expected due to the Clausius-Clapeyron relationship (black contours in Fig. 6a–c). As a result, the contrast between fluxes in the warm sector such that the contrast between warm and cold sectors almost vanishes for cyclones intensifying within  $60\text{--}70^\circ\text{S}$  (Fig. 6c). This points to a explains the larger relative importance of cold air outbreaks to the energy budget towards the high heat budget towards higher latitudes (Messori et al., 2017).

Not only the magnitude of  $v'Lq'_{TE}$  but also the relative contribution to  $v'm'_{TE}$  reduces towards pole (black contours in Fig. 6a–c corresponding). Assuming, for the sake of simplicity, the temporal variance of warm-sector temperature anomalies does not depend on latitude, then a decrease of the mean temperature towards the pole implies a reduction of the variance in specific humidity (at constant relative humidity). Thus, towards the pole the anomalies in specific humidity decrease relative to temperature anomalies and thereby the percentage to  $v'm'_{TE}$ .

Six-hourly accumulated precipitation is overlaid in Fig. 6d–e with black contours. The signal is spatially prominent in the warm sector, yet its peak is spatially shifted by around 3 towards the cyclone center compared to the maximum in  $v'Lq'_{TE}$ . From a moisture budget perspective, precipitation is balanced by evaporation, column moisture storage, and the convergence of latent heat flux. A large meridional transport of latent heat per se does not have to yield a large latent heat flux convergence, which in turn does not imply a release of latent heat (and related precipitation) because the converging specific humidity could — in principle — also be completely stored within the column. Indeed, the composite maxima of vertically integrated (eddy) latent heat flux convergence and precipitation do not align either (not shown).

This latitudinal separation highlights that cyclones at lower latitudes disproportionately influence the MSE flux signals in Figs. 4 and 5 especially due to the Clausius-Clapeyron relationship. Therefore, analyses involving aggregation of eddy MSE fluxes across wide ranges of latitudes (Figs. 4 and 5 or, e.g., Messori and Czaja, 2015) should be interpreted with care.

Overall, the cyclone-centered perspectives supports and complements perspective confirms and expands on previous findings on (low-level) transient eddy MSE flux extremes (Messori and Czaja, 2015; Geen et al., 2016; Messori et al., 2017). The As the

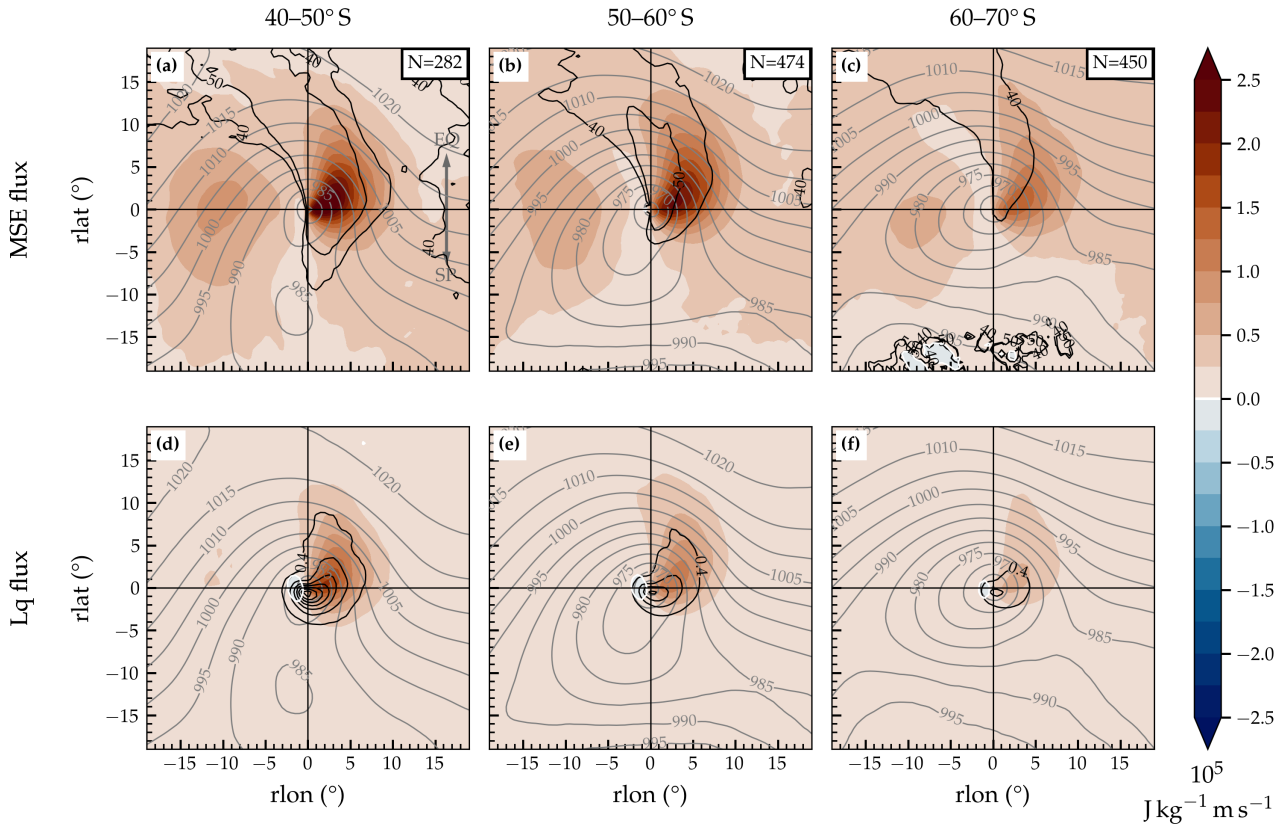


**Figure 6.** Cyclone-centered TE-transient MSE flux,  $v'm'_{TE}v'm'_{MA}$ , at 850 hPa composited during time of peak intensification for cyclones with center within (a) 40–50° S, (b) 50–60° S, and (c) 60–70° S. As Shading in (a)–(c), (d)–(f) indicates the latent heat component flux,  $v'Lq'_{TE}$ , is separately shown in panels (d)–(f) for the corresponding latitudinal ranges  $v'Lq'_{MA}$ . Regions where latent heat flux makes up for 40 % and 50 % of the MSE flux are outlined with black contours in (a)–(c). Black lines in (d)–(f) depict precipitation in steps of 0.4 mm h<sup>-1</sup>. Grey contours indicate composite mean SLP in hPa. The number of cyclones in the composites are included in the upper right in panels (a)–(c). A grey arrow is included for better orientation indicating the directions of the equator (EQ) and South Pole (SP).

540 following sections discuss vertically integrated TE MSE fluxes and discuss the influence of the cyclone characteristics on the zonally-integrated AHT. As particular focus is on the intensification rate MSE fluxes, it is worth pointing out that the previous findings regarding the horizontal structure of the eddy MSE fluxes around cyclones are also valid for transient MSE fluxes also apply to vertically integrated fluxes and different flux decompositions (see Appendix C, Fig. (and fluxes calculated using different decompositions, see Appendix C2C)).

#### 4 How do **different cyclones contribute to cyclone life cycle characteristics** shape the zonally integrated **AHTheat**

545 **flux?**

It is known that an instantaneous zonal flux extreme is partly driven by the number and intensity of ~~The aim of this section is to understand the contributions of cyclones to the zonal integrated transient MSE flux,  $\langle [v'm'_{MA}] \rangle$  and to quantify to what extent their contributions differ depending on the specific life cycle characteristics such as intensification rate, maximum intensity, and lifetime. Messori and Czaja (2015) showed that zonally integrated MSE flux extremes are driven by coexisting warm and~~  
550 ~~cold sectors (Messori and Czaja, 2015). A few of these and that a few zonal flux extremes in turn have a disproportionate impact on the seasonal mean flux throughout the extratropics (Messori and Czaja, 2015). Having studied evolution of  $v'm'_{TE}$  along the cyclone life cycle, the results of the previous section suggest that the intensification rates of cyclones could play an important role in setting instantaneous and seasonal zonal mean energy flux. The goal of this section is to explore whether and~~  
~~and how different cyclone characteristics are reflected in the vertically and zonally integrated TE. A guiding question is thus:~~  
555 ~~Do strongly intensifying cyclones shape the zonally integrated heat transport, or do the maximum intensity or lifetime matter more? To answer this question, we use the newly introduced MSE flux attribution method.~~

##### 4.1 **Contribution of cyclone-attributed MSE flux to the zonal budget**

~~The zonal integral of the seasonal mean cyclone-attributed transient MSE flux,  $\langle [v'm'_{TE}] \rangle$ .<sup>3</sup> For instance, are strongly intensifying cyclones related to higher  $\langle [v'm'_{TE}] \rangle$  than weakly intensifying ones? Answering such questions requires linking TE MSE~~  
560 ~~flux to individual cyclones. Ideally, denoted as  $\langle [v'm'_{MA}]^{cycl} \rangle$ , amounts to 1.65 PW at around 50° S (orange solid line in Fig. 7a)<sup>3</sup>. Thus, around 30 % of the overall transient MSE flux is attributed to cyclones (Fig. 7b), while the rest is attributed as non-cyclone related MSE flux. The correlation between the seasonal mean of the zonally integrated MSE flux and the chosen~~  
~~attribution method resolves the latitudinal shift between the maxima of cyclone frequency and eddy MSE flux, respectively (cyclone-attributed transient MSE flux ranges from 0.5 around 40° S to 0.75 poleward of 55° S (orange line in Fig. 4b). Thereby,~~  
565 ~~the cyclone track and zonal energy budget perspectives would become better connected. Hereafter, vertically integrated flux data are used to simplify the task.~~

##### 4.2 **Attributing eddy fluxes to cyclones**

~~How can  $\langle v'm'_{TE} \rangle$  be attributed to a cyclone? One simple approach is to use the SLP-derived cyclone masks (see 7c). Due to the presence of other dynamical features, for example anticyclones, and the degrees of freedom when attributing MSE flux to~~  
570 ~~cyclone masks, which are discussed in Sect. 2.2) to label the instantaneous TE MSE flux fields. Using that approach, the TE MSE flux captured within the 2.4, one must not expect 100 % flux coverage or perfect correlation.~~

~~Note that the transient MSE flux located within the SLP-based cyclone masks is broadly below less than 1 PW (black dashed line in Fig. 7a) and barely reaches 30. This low fraction ( $\approx 10\%$  of the overall  $\langle [v'm'_{TE}] \rangle$ ) (Fig. at 50° 7b).<sup>4</sup> The low fraction~~

<sup>3</sup>In the result sections, we use square brackets for zonal means and integrals interchangeably.

<sup>3</sup>From this section onward, the overbar in  $\langle [v'm'_{MA}]^{cycl} \rangle$  denotes the seasonal mean.

<sup>4</sup>The percentage can surpass 100 if fluxes outside of the cyclone masks are predominantly equatorward.

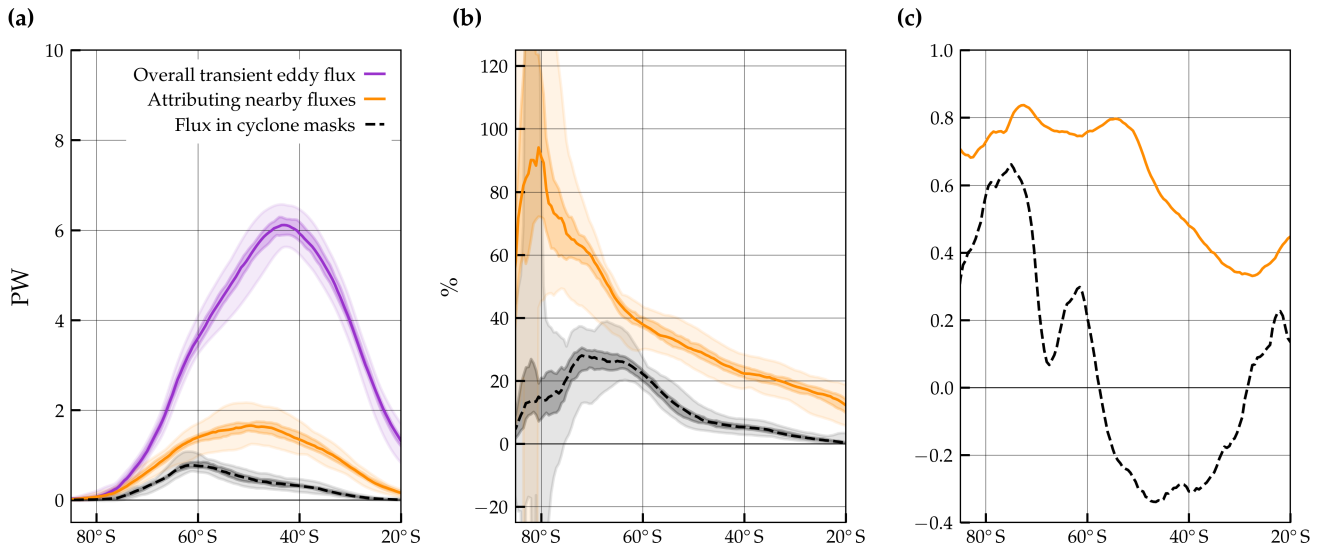


**Figure 7.** Seasonal transient MSE fluxes in SH winter: (a) the overall transient MSE fluxes,  $\langle [v'm']_{MA} \rangle$ , shown in purple are contrasted to the transient MSE fluxes within features that are attributed to cyclones,  $\langle [v'm']_{MA}^{cycl} \rangle$  (orange) and the transient MSE fluxes within cyclone masks (black, dashed). Solid and dashed lines indicate medians, light shading the full range, and darker shading the inter-quartile range of the seasonal means. (b) The percentage of the overall transient MSE flux attributed to cyclones (orange) and within the cyclone masks (black). (c) Correlations between seasonally averaged overall transient MSE fluxes and the fraction attributed to cyclones using the overlap method (orange) and with the SLP-based cyclone masks (black dashed).

of TE-MSE flux within the cyclone mask is consistent with the cyclone composites (e.g. Fig. 4b, cS, Fig. 5a): A substantial fraction of the poleward flux does not occur in close vicinity to the cyclone center but further downstream and equatorward. In the composite, this partly lies b) is consistent with large fluxes occurring at the boundary and outside of the lowest closed SLP contour which, for the sake of the argument, can be regarded as a proxy for the cyclone mask. Moreover, the correlation between seasonally averaged overall and cyclone-masked fluxes is low (and even negative) across the midlatitudes cyclone masks. Accordingly, a low to negative correlation is found between the seasonally averaged total and transient MSE fluxes within only the cyclone mask (black line in Fig. 7c) because very little of the overall TE-MSE flux occurs within the cyclone mask.

Seasonal TE-MSE fluxes in SH winter: (a) the overall TE-MSE fluxes,  $\langle [v'm']_{TE} \rangle$ , shown in purple are contrasted to the TE-MSE fluxes within cyclone masks (black, dashed) and the TE-MSE fluxes within features that are attributed to cyclones,  $\langle [v'm']_{TE}^{cycl} \rangle$  (dark orange). Solid and dashed lines indicate medians, light shading the full range, and darker shading the inter-quartile range of the seasonal means for the years considered. (b) As (a) but expressed as a percentage of the corresponding seasonally averaged overall TE-MSE flux (which is 100 by definition). (c) Correlations of seasonally averaged fluxes with overall TE-MSE fluxes.

To overcome issues related to the spatial displacement discussed above, eddy-MSE flux features are identified and attributed to nearby cyclones based on spatial overlap (see Sect. 2.4 for more details). For each cyclone, the fluxes within these attributed features are retained and yield a zonally integrated. Based on the overlap method, we find the peak of the cyclone-attributed TE-MSE flux,  $\langle [v' m'_{TE}^{cycl}] \rangle$ , as sketched out in Fig. MSE fluxes at around 50° ??. Considering all cyclones within a season, the seasonal-mean cyclone-attributed TE-MSE flux thus reads  $\langle [v' m'_{TE}^{cycl}] \rangle$ . Note that in the following, the overbar denotes the seasonal mean computed from monthly means whereas dashes still represent anomalies from monthly means as introduced in Sect. S, and therefore much closer to the MSE flux maximum near 42° 2.3. Schematic of the zonally integrated cyclone-attributed eddy-MSE flux and the derived latitudinal extent, exemplified for a surface cyclone that lasts for five six-hourly time steps. The cyclone mask is indicated with grey patches and the attributed poleward and equatorward eddy-MSE flux features with orange and blue shading, respectively. Cyclone-attributed eddy-MSE fluxes are zonally integrated and are expressed in if accumulated or in if averaged over the cyclone lifetime (orange curve). The latitudinal extent (or count) of this cyclone is then determined by the latitudes at which the attributed fluxes along its lifetime are non-zero. At any latitude band, a cyclone is therefore counted either once or zero times (purple bars). A grey arrow serves orientational purposes. Using this attribution method, the percentage of captured TE-MSE flux is increased by 15–20 (Fig. 7b) — relative to only counting TE-MSE S, while the fluxes within the cyclone mask. Additionally, the correlation of seasonal means between the total cyclone-attributed flux ranges from 0.5 around 40 SLP-based cyclone masks much further poleward (62° S to 0.75 poleward of 55 S (dark orange line in Fig. 7e). A priori, one should not expect a 100 flux coverage or perfect correlation due to the presence of other dynamical features such as anticyclones. Additionally, the cyclone attribution method improves the meridional offset between the maxima in the overall and cyclone-attributed flux. The maxima in the TE-MSE flux within cyclone masks occurs around 20 poleward of the overall TE-MSE flux  $\langle [v' m'_{TE}] \rangle$ . In contrast, the fluxes that are attributed to cyclones,  $\langle [v' m'_{TE}^{cycl}] \rangle$  (dark orange), peak around 10 further equatorward of the ones within the SLP masks and thus more closely to the peak of  $\langle [v' m'_{TE}] \rangle$  (purple distribution in in). This is consistent with the fact that transient MSE flux peaks equatorward of the cyclone center along the trailing fronts. By bridging the latitudinal gap between the surface cyclone tracks and transient MSE fluxes (see also Fig. 7a). The remaining latitudinal discrepancy may partly arise due to the SLP-based tracking method not detecting cyclones further equatorward (Sinclair, 1994). Overall, with the composite results of Sect. 1b), the overlap method is a comprehensive solution to connecting the two storm track metrics. Qualitatively, the results are robust relative to the choice of the percentile and flux decomposition method (see Appendix 3.2 in mind the latitudinal shift of the zonally integrated flux (D, Fig. 7a) suggests that the attribution method is more useful for studying the effect of cyclones on zonally integrated AHT than simply the cyclone masks because adjacent warm and cold sectors are captured. Thereby, this method is a comprehensive solution to connect the surface cyclone and MSE flux frameworks. D1).

## 4.2 Cyclone characteristics in the zonal integral

### 4.2 Relevance of cyclone life cycle characteristics for the zonally integrated heat transport

620 ~~Attributing  $\langle v'm'_{TE} \rangle$  to individual cyclones allows for studying the influence~~ Next, we address how life cycle characteristics influence the contribution of individual cyclones to the zonally integrated MSE flux. The contribution of a cyclone characteristic on the zonally integrated transport. For the seasonal timescale, the accumulated ~~is defined as the attributed MSE flux~~ along the lifetime is informative while the averaged flux per time step is more useful when studying instantaneous energy transport. Findings from Sect. 3 suggest that the duration and magnitude of cyclone intensification are important for both timescales track

625 ~~over the cyclone lifetime. We compare the accumulated MSE flux of 200 strongest and weakest cyclones (as done in Catto et al., 2010; Sinc~~

~~Accumulated over their lifetime, the~~ At  $50^\circ$  S, the lifetime-accumulated transient MSE flux of the 200 SH cyclones (Catto et al., 2010; Sinc

~~cyclones~~ that intensify most strongly are, on average, associated with poleward TE MSE transport of around ~~corresponds to~~ 20 PW h at  $50^\circ$  S (blue solid line in Fig. 8a). In turn, the ~~accumulated flux of the~~ 200 cyclones with the lowest intensification

630 rates ~~amounts to on average accumulate~~ only a few PW h, ~~which peaks further poleward at~~ around  $65^\circ$  S (red solid line in Fig. 8a). ~~Given the large variability of cyclones, we advocate for interpreting these lines as the flux built up by many cyclones with a similar characteristic instead of a representation of ‘the average cyclone’ (see discussion in Sect. ?? below). In that sense, cyclones~~ Thus, cyclones intensifying strongly accumulate 3–20 times the zonally integrated ~~TE transient~~ MSE flux of weakly intensifying cyclones (solid purple line in Fig. 8b). ~~This difference~~

635 ~~The ratio found for strongest intensification~~ is similar for the ~~longest-lived cyclones lifetime~~ (dashed line in Fig. 8b). Cyclone intensity ~~emerges as an equally important also emerges to be a clear~~ differentiator for accumulated transport, ~~although the fluxes are differently distributed across latitude~~. The fluxes of the most intense cyclones are located further poleward compared to the ~~weakest cyclones~~ (dotted lines in Fig. 8a). This can be ~~partly~~ explained by SLP climatologically decreasing towards the pole. The corresponding ratio in Fig. 8b (dotted line) ~~is thus less informative thus increases towards the pole~~.

640 ~~Do strongly intensifying~~ To investigate whether strongly intensifying and intense cyclones only transport more ~~heat~~ because they possibly exist longer ~~? By dividing the accumulated flux by the cyclone lifetime, one obtains the averaged instantaneous flux. The averaged~~ we also compare lifetime average MSE fluxes by normalizing accumulated fluxes by cyclone lifetime. Strongly intensifying cyclones are associated with a lifetime-averaged flux of 0.2 PW ~~peaking near  $50^\circ$  S (solid lines in Fig. 8c), whereas the least intensifying cyclones transport roughly 10 times less at this latitude (Fig. 8d). In turn, the lifetime-averaged~~

645 fluxes attributed to the most long- and short-lived cyclones become more comparable (dashed lines in Fig. 8c) ~~which manifests, which results~~ in a ratio around 2–two (Fig. 8d). ~~In contrast, strongly intensifying cyclones retain much higher instantaneous flux compared to the weakly intensifying ones with the ratio remaining between 2–12 depending on the latitude. Interestingly, the mean flux computed from all cyclones (black long-dashed line in Fig. 8c) is larger than~~

650 ~~of both longest and shortest cyclones. This could be explained by S. Thus, strongly intensifying (or intense) cyclones contribute more the zonal mean MSE fluxes because the attributed instantaneous fluxes are greater and not because these cyclones are more long-lived cyclones having a long weakening phase without large fluxes, while short systems are not the ones intensifying very strongly. In conclusion, the attributed fluxes are larger for strongly intensifying cyclones than for weakly intensifying ones not because they exist longer but because near-cyclone fluxes are larger at individual time steps.~~

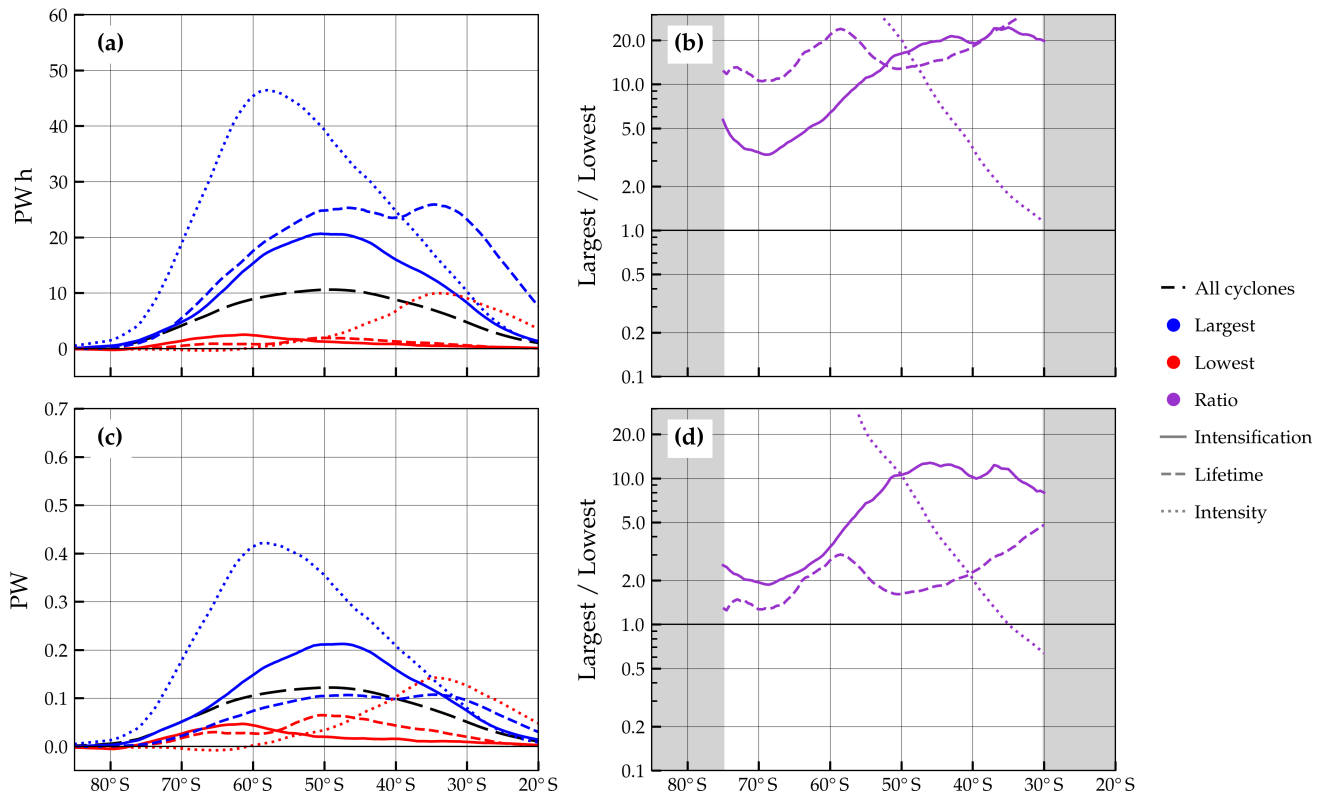


**Figure 8.** (a) Average zonally and vertically integrated  $\overline{\langle [v'm'_{TE}]_{cycl} \rangle \langle [v'm'_{MA}]_{cycl} \rangle}$  of similar grouped by characteristic. Instantaneous vertically integrated fluxes are integrated temporally over the lifetime of each cyclone and integrated longitudinally at each latitude. The accumulated flux is expressed in (unit PW h which should allow for a comparison of instantaneous fluxes in and cyclone lifetimes in hours). For each characteristic, the flux of the 200 cyclones with the largest values of that characteristic is shown in blue and the lowest 200 ones in red, respectively. Solid, dashed, and dotted lines indicate intensification rate, lifetime, and intensity, respectively. For example, the least most intense cyclones (which are the ones with the highest mature stage center SLP) are shown by the red blue dotted line. (b) Dividing the flux of the 200 largest cyclones by the flux of the 200 lowest cyclones yields the ratio for each characteristic with the same line-styles as in (a). (c, d) As in (a, b), respectively, but for the average flux per time step in PW. In panels (a, c), the average fluxes computed from all SH JJA cyclones (from which the other subsets are chosen) are shown with black long dash lines. For latitudes where the absolute fluxes are consistently low, the The ratio in panels (b, d) is masked out at latitudes where the absolute fluxes are close to zero.

655

The above analysis is repeated with the initial subset of cyclones intensifying within The average cyclone-attributed MSE flux of all SH cyclones, calculated at  $50-60^\circ$  S. This should provide a 'fairer' comparison of intense vs. weak cyclones in light of the poleward climatological SLP decrease. Furthermore, the minimum lifetime is set to three days to avoid comparing 30, is 0.12 tracks to seven-day tracks. Overall, a very similar picture emerges as compared to the analysis on all SH cyclones.

Again, the most intense, most strongly intensifying, and the longest cyclones are linked to high accumulated ( $\langle v' m'_{TE}^{cycl} \rangle$ ) (Fig. 660 PW (black dashed line in Fig. ??a) with ratios between 4–20 within 50–608c). During each winter season, around 340 unique cyclones are identified. These have an average lifetime of 3.4 days, such that 12.5 cyclones are present at an instant on average<sup>4</sup>. The estimated 1.5 S (PW that they contribute altogether matches the seasonal mean flux shown in Fig. ??b). Lifetime remains a smaller differentiator when considering the instantaneous timescale (7a).

An intriguing side result is that the lifetime-averaged cyclone-related MSE flux is larger when computed using all cyclones 665 than when using only the longest or shortest life cycles (black line in Fig. ??e,d) than the other two characteristics (8c). This could be explained by the fact that long-lived cyclones have a long weakening phase without large fluxes, whereas short systems do not intensify very strongly.

Note A key finding is that the intense cyclones are linked to a  $\approx 50$  higher averaged flux than contribute more flux to the zonal integral than the cyclones that intensify most rapidly, despite comparable near-cyclone fluxes in the strongly intensifying 670 ones (blue dotted vs. solid lines in Fig. ??e). The previous composites (Fig. 5) indicate that the magnitude of the fluxes is similar during the intensification phase for these two sets of cyclones.<sup>5</sup> The difference can be at least partly explained by the deepest cyclones covering a roughly 20. One explanation is that the most intense cyclones cover a larger area than those that intensify the most strongly intensifying ones, which agrees with the size of the cyclone being more tightly. Earlier studies suggest that cyclone size is more closely related to the intensity than to the intensification rate (Rudeva and Gulev, 2007). The larger size 675 of the cyclone mask and a slightly larger areal extent of the warm-sector fluxes also manifest in the composites (although those are only snapshots of the full life cycle, Fig. 5a,e). Consequently, there is more cyclone-attributed flux located further downstream of the cyclone center (not shown). Using a constant radius to define cyclone masks and attribute fluxes would lead to differences solely due to variations of the spatial extent not being accounted for — unjustly when acknowledging the diversity of cyclones, or purposefully if one were to study the influence of mask size on the results. Repeating the above analyses for the 680 cyclones of largest poleward propagation speed reveals lifetime-averaged fluxes comparable to those of the-, and as a result a larger contribution to the zonal integral by the most intense cyclones at some latitudes (not shown). Yet, poleward propagation speed is not the characteristic for which the cyclone-attributed eddy MSE fluxes are consistently the largest. Previous research suggests that either this is different for total moisture flux or that more fluxes are attributed to rapidly poleward-propagating cyclones (compared to others) when using a constant radius (Sinclair and Dacre, 2019).

To summarize, A comprehensive sensitivity analysis ensures the robustness of the findings presented above. The results are neither sensitive to measuring the intensification rate of cyclones does modulate both instantaneous and accumulated zonally integrated eddy MSE transports. Strongly intensifying cyclones, on average, transport more eddy MSE flux poleward than weakly intensifying ones. This matches with what one could conjecture from the previous cyclone life cycle results. Importantly, the fluxes attributed to intense cyclones are even larger on both time-scales than those of the strongly intensifying 690 ones. This analysis thus shows that not only in Bergeron instead of six-hourly changes in SLP along a track (Sanders and Gyakum, 1980), nor to defining intensity using SLP anomalies from local climatology rather than absolute SLP values (Cornér et al., 2025)

<sup>4</sup> 340 cyclones / 92 d  $\times$  3.4 d.

<sup>5</sup> Note that the sets of cyclones are not identical.

695 The only noteworthy difference is, as expected, that the latitudinal offset between the peaks of the attributed fluxes of the intensification rate but also the spatial extent (related to the intensity) are important determinants of the energy footprint of a cyclone in the zonal picture. Before moving on to addressing how the number of such cyclones relates to (eddy) AHT on a seasonal scale, we present some important considerations on the adopted flux attribution approach. These influence how the role of the cyclone number for AHT is examined.

(a)–(d) As in Fig. 8 but restricted to the subset of cyclones which reach their peak intensification within 50–60°S (dashed vertical lines) and have a minimum lifetime of 3 days.

### 4.3 On the challenges of flux attribution and limits to its interpretation

700 The chaotic nature of the atmosphere can be seen as it featuring various kinds of eddies (e.g. Barnes and Hartmann, 2012). Likewise, but from a traditionally and methodologically complementary perspective, it can also be acknowledged by appreciating the various types of surface cyclones (e.g. Troup and Stretten, 1972). In this light, attributing column-integrated eddy MSE flux to surface cyclones to improve our understanding of atmospheric dynamics might seem like a bold endeavor. We briefly discuss methodological sensitivities of the above results and put forward limits of their interpretability.

705 Individual cyclones can be associated with a lifetime-accumulated poleward energy flux beyond 100 across a latitude band of the order of 10° deepest and weakest cyclones is reduced when using SLP anomalies. When using absolute SLP, this offset is also reduced when sub-selecting cyclones intensifying only within 50–60° (Fig. D2a). Additionally, the sample mean is much more extended in latitude than are individual events. This prompts the above framing that the averages depicted in Figs. 8 and ?? are not representative of individual cyclones. Instead, the above sample means are proposed to be interpreted as the accumulated fluxes due to several cyclones with similar characteristic.

710 Importantly, studying individual cyclones using these methods is not advisable because depending on the exact method the attributed fluxes can be vastly different for the same cyclone (Fig. B2). Firstly, changing the percentile used for identifying flux features affects their areal extent and therefore their overlap with cyclones. Secondly, different flux decompositions filter out different kinds of stationary flows. An instantaneous anomaly from the zonal mean (which is how eddy flux is defined in the ZA framework, see Sect. 2.3), for instance, might contribute to stationary eddy (and not transient eddy) flux in the TE framework if the anomaly is persistent enough. In this section, it is assumed that the biases arising from the two arguments average out for large enough cyclone numbers and in regions without systematic (climatological) temporal flow stationarity (S. As a result, the fluxes attributed to the most intense cyclones remain  $\approx$  the SH midlatitudes. The influence of different decomposition methods is further addressed in Sect. 5.0 ??.

720 Due to the relative simplicity of the attribution method, the sensitivity analysis of the above results boils down to 1) the choice of percentile for defining flux features and 2) the flux decomposition method. Qualitatively, the increase in attributed flux and increase in correlation (Fig. 9) higher compared to those of the most strongly intensifying ones. Excluding tracks shorter than 37e are robust to the choice of both percentile and flux decomposition method (Fig. D1). Choosing lower percentiles moves the peak of the attributed fluxes towards the equator because larger masks (warm sectors extending further equatorward than the cyclone mask) are more often attached (Fig. D1a,d,g,j). The cause of the relatively reduced correlation around 60°S

for the ZA framework (Fig. D1i) is not clear but might be related to the presence of planetary waves. A repetition with an upper integral bound of 500 d further ensures that weak, short-lived tracks do not distort the picture. Thus, the large ratio between intense and weak cyclones (dotted line in Fig. D1i) suggests this signal arising from lower levels (and not stratospheric dynamics). Regarding the lifetime-averaged fluxes, the general conclusions on the roles of cyclone intensity, intensification rate, and lifetime remain valid for both cyclone samples (Figs 8) is not an artifact of the poleward climatological SLP decrease. Qualitatively, the results are also not sensitive to the parameter choices of the applied decomposition method or flux attribution threshold (the interested reader is referred to Appendix Fig. ??, and ??). Intensity and intensification rate consistently are more important differentiators than lifetime, albeit the ratio of lifetime varying between 1 and 2 (Figs. D3).

In summary, against expectations based on the composite analysis presented in Sect. D3 and ??). Therefore, our discussion does not put emphasis on the exact factor of how much more eddy MSE flux is 3, the fluxes attributed to intense cyclones contribute more strongly to the zonal integral compared to those attributed to the largest versus lowest cyclones of each characteristic.

Lastly, when measuring most rapidly intensifying cyclones. Thus, not only the intensification rate in instead of a simple finite SLP difference over time (Sanders and Gyakum, 1980), for all SH cyclones one observes a similar behavior as for the intensity: the more strongly intensifying cyclones (and their attributed fluxes) are located further equatorward than their counterparts (not shown). Within the more restrictive sample using the 10 latitude band, the attributed fluxes are slightly larger while the ratio is not substantially affected by the choice of intensification metric (not shown), but also the spatial extend of cyclones, which is typically large for the most intense cyclones, is an important determinant of the zonally integrated poleward energy transport associated with extratropical cyclones.

## 5 Linking The relationship between the seasonal cyclone characteristics mean transient MSE flux and AHT seasonal cyclone numbers

Finally, we investigate the relationship between extratropical cyclones and the zonally and vertically integrated TE transient MSE flux,  $\langle \overline{[v'm']_{TE}} \rangle \langle \overline{[v'm']_{MA}} \rangle$ , on a seasonal scale. Given that large TE transient MSE fluxes can be attributed to strongly intensifying and intense cyclones, we examine in this section it is examined how the seasonal number of these storms (or the overall cyclone number) relates to the seasonal mean zonally integrated eddy transient MSE flux and, ultimately, the total AHT. We focus atmospheric heat transport. The seasonally averaged transient MSE flux attributed to cyclones is denoted with  $\langle \overline{[v'm']_{MA}^{cycl}} \rangle$  as above. In the following, focus is laid on the latitude of 50° S which corresponds to the peak of the cyclone-attributed eddy transient MSE fluxes (Fig. 7a) and a correlation of around 0.7 between the attributed and the overall eddy MSE fluxes (Fig. 7c). The seasonally averaged TE MSE flux attributed to cyclones is denoted with  $\langle \overline{[v'm']_{TE}^{cycl}} \rangle$  as in Sect. 4. When addressing method dependencies, eddy fluxes derived from the other flux decompositions are denoted with the corresponding subscripts and dashing conventions (consistent with The classification of cyclones as ‘strong’, ‘moderate’, and ‘weak’ follows Sect. 2.3)-2.4.

The seasonal number of cyclones is determined using the introduced flux attribution method: A cyclone is counted once towards all latitude bands where its attributed eddy MSE flux is different from zero along its lifetime (purple bars in Fig.

## 760 5.1 Seasonally averaged transient MSE fluxes and cyclone numbers

At  $50^\circ$  ??). Thus, the seasonal number of cyclones at a given latitude corresponds to the cyclones that have attributed eddy MSE flux at this latitude, whereas their corresponding life cycle characteristics, such as maximum intensification rate or maximum intensity, can occur at any latitude. Based on this, the seasonal sub-sets of strongly intensifying and intense cyclones are determined using climatological thresholds: Cyclones are considered strongly intensifying if their intensification rate lies above the 75<sup>th</sup> percentile determined from the climatological set of all cyclones passing that latitude. Note that the number of strongly intensifying cyclones for a given season is thus *not* simply 25%. Cyclones that intensify strongly account for around 43 % of the overall cyclone number of that season. If the 75<sup>th</sup> percentile of cyclone intensification based on all SH JJA cyclones is, for instance, 24, the number of cyclones above this threshold cyclone-related transient MSE flux in a season is not dependent on the corresponding number of all cyclones during that season. Choosing the 75<sup>th</sup> percentile instead of a higher one is a compromise between selecting only the strongest cyclones and including a large enough number of cyclones to counteract the event-to-event variability and method dependency discussed in Sect. ???. If the intensification rate lies within the inter-quartile range or below, cyclones are denoted moderately or weakly intensifying, respectively. The classification of cyclones as strong, moderate, and weak works analogously for intensity.

## 5.2 Seasonal eddy MSE fluxes and cyclone number

775 Strongly intensifying cyclones (above the climatological 75<sup>th</sup> percentile) account for roughly 43 of  $\langle [v'm']_{TE}^{cycl1} \rangle$  at  $50^\circ$  S (, i.e.,  $\langle [v'm']_{MA}^{cycl} \rangle$ ) (yellow box in Fig. 9). This number fraction is slightly higher for intense cyclones. For both intensity and intensification, the fluxes attributed to moderate cyclones (with the respective characteristic between the the intense cyclones ( $\approx 47$  %). For moderately intense cyclones and moderately intensifying cyclones (defined from the 25<sup>th</sup> and to 75<sup>th</sup> percentiles) are of similar magnitude ( $\approx 40$ –50 percentile), the fractional contributions lies within the 40 – 50 % range (grey boxes in Fig. 9). This is remarkable because this definition of moderate cyclones includes, on average, twice as many cyclones as the strong cyclones yet both categories are attributed a similar flux. Weak Their contribution to the seasonal mean heat transport is therefore comparable to the strong and strongly intensifying cyclones, although they are (on average) twice as numerous. In turn, weak and weakly intensifying cyclones, in turn, only account for around 10 less than 15 % of the attributed fluxes each season. Comparing the attributed fluxes of these groups of cyclones to the overall TE fluxes, the fractions reduce by a factor of three in a season.

The above results may suggest an almost linear relationship between intensification rate and transient MSE flux: In the case of a linear relationship, one would expect the cyclones above the 75<sup>th</sup> percentile to contribute approximately 44 % to the budget<sup>5</sup>. The flux indeed increases with cyclone intensification rate and intensity. However, for cyclones intensifying very rapidly the relationship is found to be non-linear, while it is rather exponential for intensity (not shown) in accordance with how much of

<sup>5</sup>This result can be conveniently confirmed using the arithmetic series.

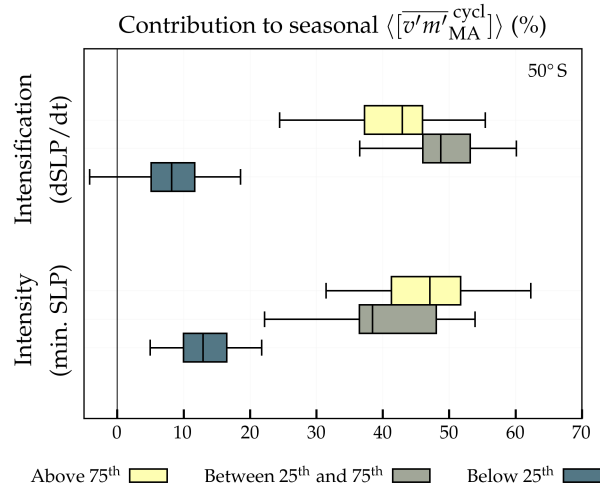


**Figure 9.** Percentage Contributions of seasonal TE MSE flux that is attributed to cyclones within three different ranges of intensification rate (top) and intensity (bottom). Percentages are shown in terms of cyclone-attributed TE to the seasonal transient MSE fluxes flux that is attributed to cyclones ( $\langle [\overline{v'm'}_{TE}^{cycl}] \rangle / \langle [\overline{v'm'}_{MA}^{cycl}] \rangle$ ). Medians are shown with solid lines within the boxes, which in turn denote the interquartile range. Whiskers indicate 1.5 times the interquartile range while values outside of this range are not shown. MSE fluxes and cyclone numbers correspond to 50°S. For each life cycle characteristic, cyclones are grouped seasonally by the 25<sup>th</sup> and 75<sup>th</sup> percentiles derived from the climatological sets of cyclones that have non-zero  $\langle [\overline{v'm'}_{TE}^{cycl}] \rangle - \langle [\overline{v'm'}_{MA}^{cycl}] \rangle$  at this latitude. The seasonal fluxes attributed to the cyclones that lie above the 75<sup>th</sup> percentile are represented in yellow, the ones between the 25<sup>th</sup> and 75<sup>th</sup> in grey, and the ones below the 25<sup>th</sup> in blue. Medians are shown with solid lines within the boxes that denote the interquartile range. Whiskers indicate 1.5 times the interquartile range while values outside of this range are not shown. MSE fluxes and cyclone numbers correspond to 50°S.

790 overall eddy MSE flux is attributed to cyclones (Fig. 7b). Thus, intense (and strongly intensifying) cyclones disproportionately  
 contribute to  $\langle [\overline{v'm'}_{TE}^{cycl}] \rangle$ . This is in line with the Eulerian perspective adopted in Messori and Czaja (2015) who found that  
 daily zonal heat fluxes above the 95<sup>th</sup> percentile account for around 13 of overall eddy MSE fluxes in SH winter. Further, the  
 intensities are not equally distributed but follow a (skewed) normal distribution for both characteristics. In sum, the identified  
 fractions mean that the strongest cyclones contribute disproportionately compared to their frequency, which agrees with the  
 795 conclusions in Messori and Czaja (2015). Yet, despite the large contribution to the zonal budget by the strong cyclones, more  
 than half of the seasonal  $\langle [\overline{v'm'}_{TE}^{cycl}] \rangle$  is unrelated to the most intense (or most strongly intensifying) cyclones, which suggests  
 that their number may not be tightly connected to the seasonal  $\langle [\overline{v'm'}_{TE}^{cycl}] \rangle$  or, more generally,  $\langle [\overline{v'm'}_{TE}^{cycl}] \rangle / \langle [\overline{v'm'}_{MA}^{cycl}] \rangle$  results  
 from moderate cyclones. This suggests that the number of strong cyclones has only a weak control on the zonally-integrated  
 seasonal mean budget of transient MSE flux that can be associated with extratropical cyclones.

800 Indeed, the seasonal zonally and vertically integrated TE transient MSE flux attributed to cyclones,  $\langle [\overline{v'm'}_{TE}^{cycl}] \rangle / \langle [\overline{v'm'}_{MA}^{cycl}] \rangle$ ,  
 is not highly correlated with either the number of strongly intensifying ( $n_{intensif}$ ) strongly intensifying or the number of intense  
 ( $n_{intense}$ ) cyclones. In other words, the number of intense or strongly intensifying cyclones does not determine (by itself) the TE

MSE flux that is attributed to all cyclones during a season. Conversely  $\langle [v'm']_{MA}^{cycl} \rangle$  is correlated with total cyclone number (Fig. 10a).

805 It was found that when omitting the flux attribution and simply correlating the total number of cyclones with the mean transient MSE flux ( $\langle [v'm']_{MA} \rangle$ ), the correlation is higher with the overall cyclone number,  $n_{all}$  (remains positive albeit weaker than the previous result based on the cyclone-attributed flux (cf. Fig. 10a-c). When considering the overall TE MSE flux ( $\langle [v'm']_{TE} \rangle$ ) instead, the relationship between the number of intense cyclones exhibits a larger correlation (a and d).  $\langle [v'm']_{MA} \rangle$  is not correlated with the number of most rapidly intensifying cyclones (Fig. 10e) but is correlated with the number of the most  
810 intense cyclones (Fig. 10f). The correlation with the overall cyclone number slightly decreases but is still visible in latter is larger compared to the case with flux attribution (c.f. Figs. 10c and f). Under the assumption that the most intense cyclones dominate the overall transient MSE flux, the decrease of the correlation from Fig. 10d. This implies f to Fig. 10c could be an indication that the attribution of TE MSE flux to cyclone masks reduces the link between the seasonal averaged attributed flux and intense cyclones (cf. method does not perfectly attribute MSE fluxes to cyclones. One possible explanation is that the  
815 attribution method attributes some fluxes of the most intense cyclones to neighboring weaker ones. This would be in line with the fact that the correlation of the cyclone-attributed fluxes with the overall cyclone number (Fig. 10a) is higher than with the intense ones (Fig. 10c and f). While this). Over a season, more cyclones with MSE fluxes attributed independently of intensity would be expected to have more attributed MSE flux overall.

While this analysis suggests that on a seasonal scale  $\langle [v'm']_{TE} \rangle \sim n_{all}$  and  $\langle [v'm']_{TE} \rangle \sim n_{intense}$ ,  $\langle [v'm']_{MA}^{cycl} \rangle$  relates to the  
820 number of all cyclones,  $n_{all}$ , and  $\langle [v'm']_{MA} \rangle$  is driven by the number of intense cyclones,  $n_{intense}$ ,<sup>6</sup> these correlations vary substantially with flux attribution percentile and flux decomposition method in both cases (Fig. E1b,h). As described in Sect. 2.3, these These analyses are also carried out defining eddy transient MSE fluxes from high-pass filtered fields (HP) and, separately, from zonal anomalies (ZA). In general, the correlations discussed above depend more strongly on the flux decomposition method than on the flux attribution percentile. For the 90% flux attribution percentile rank For the flux attributed using  
825 percentile rank  $p = 0.9$ , the correlation  $\rho(\langle [v'm']_{HP}^{cycl} \rangle, n_{all}) = 0.39$  between the cyclone-attributed fluxes and the number of all cyclones,  $\rho(\langle [v'm']_{HP}^{cycl} \rangle, n_{all})$ , equals 0.39, while  $\rho(\langle [v^*m^*]_{ZA}^{cycl} \rangle, n_{all}) = 0.70$  (Fig. E1b). Similarly, for the overall eddy MSE fluxes  $\rho(\langle [v'm']_{HP} \rangle, n_{intense}) \geq 0.65$ , the correlation between overall transient MSE fluxes and the number of intense cyclones,  $\rho(\langle [v'm']_{HP} \rangle, n_{intense})$ , is at least 0.65, whereas  $\rho(\langle [v^*m^*]_{ZA} \rangle, n_{intense}) \leq 0.27$  (Fig. E1h). Note that measuring intensification rate in and intensity based on SLP anomalies from a climatology instead does not yield a qualitatively different picture (not  
830 shown).

Relationship between seasonally averaged TE MSE flux and cyclone numbers for SH JJA at 50 S. (a) The cyclone-attributed TE MSE flux,  $\langle [v'm']_{TE}^{cycl} \rangle$ , in PW vs. the number of all cyclones with  $\langle [v'm']_{TE}^{cycl} \rangle \neq 0$  at that latitude. (b, c) as (a) but for the number of strongly intensifying cyclones and intense cyclones, respectively. (d)–(f) as (a)–(c) but for the overall TE flux  
835  $\langle [v'm']_{TE} \rangle$ . The grey solid line represents a best estimate of a linear fit and dashed grey lines the corresponding confidence band. Correlation ( $\rho$ ) and explained variance of the linear fit ( $R^2$ ) are indicated on the panels.

<sup>6</sup>In both cases, the slope of the linear fit is significantly different from zero as indicated by the p-values on the panels (using a two-tailed test, Fig. 10a,f).

## 5.2 On-method dependency

Given the large fraction of flux attributed to the cyclone sets of moderate intensity (or intensification, Fig. 9), it is not surprising to find low correlations with the number of intense (or strongly intensifying) cyclones. ~~Previously, the main conclusions drawn in Sects. 3 and 4 based on large cyclone sample sizes were not sensitive to the flux decomposition method. Yet, as pointed out in Sect. ??~~ ~~the fluxes attributed to individual cyclones can strongly differ from one method to the other. The high correlation between the number of intense cyclones and high-pass filtered eddy MSE flux —  $\rho(\langle [v^*m^*]_{HP} \rangle, n_{\text{intense}})$  — relative to the weaker correlation between number of intense cyclone and MSE fluxes defined from zonal anomalies —  $\rho(\langle [v^*m^*]_{ZA} \rangle, n_{\text{intense}})$  — is likely related to the contribution of stationary signals (in space or time) to the MSE flux and how these are treated in the MSE flux attribution method .~~ ~~In the frameworks tested in this study, a wave-like signal with a frequency  $\sim (11)^{-1}$  is filtered out in the HP framework while it is partly attributed to cyclones in the ZA framework. While the choice of the cut-off frequency (or likewise the spatial wavenumber) can be motivated dynamically (e.g. Eady, 1949), some spectral power of a warm conveyor belt, for instance, is contained in the flow that is filtered out. Arguably, this is overestimated in the ZA framework which does not filter out *any* low-frequency waves. Yet, in a situation where a cyclone locally constructively interferes with a planetary wave it is only a subjective choice whether to attribute the entire or filtered energy flux to the cyclone, and the choice depends on the research question.  $\rho(\langle [v^*m^*]_{HP} \rangle, n_{\text{intense}}) > \rho(\langle [v^*m^*]_{ZA} \rangle, n_{\text{intense}})$  suggests that while the intensity of a cyclone has a footprint in the high-frequency flux component, the low-frequency waves that are attributed to it within the ZA framework convolve its energy footprint in the seasonal integral.~~ ~~The TE framework is a special case with the amount of background flows attributed to cyclones lying somewhere between the other two methods. Recall that in the TE framework, transient eddies are derived from monthly means whereas the monthly means give rise to stationary eddies (SE). All cyclones during the duration of a full month therefore may influence how much fluxes are attributed to an individual cyclone.~~ 6.2

## 5.2 Cyclone numbers and total AHTheat transport

On the six-hourly timescale, the transient eddy and overturning circulations are temporally anti-correlated in the midlatitudes (Cox et al., 2024b). <sup>7</sup> One could argue that the splitting into transient eddy and mean ~~circulation of the flow~~ overturning circulation is therefore not strictly related to circulation features (e.g., surface (anti-)cyclones, troughs, and ridges), which naturally contain signals from eddy and mean components because the mean was computed including the eddies in the first place. Thus, ~~one would have to~~ we also investigate the total AHTheat transport,  $\langle [vm] \rangle$  (the left-hand side of Eq. 2), instead of the transient eddy MSE flux. ~~Recall, however, that the latitudinal extent of a cyclone and thereby the cyclone number were determined~~ We continue to count cyclones as above using the latitudinal extent of ~~the eddy~~ fluxes (Fig. ??). ~~How can one obtain a cyclone number when addressing the total fluxes, which have not been locally attributed to cyclones so far, instead? One pragmatic way forward is to assume that the eddy MSE fluxes provide a good approximation of the latitudinal extent of the~~

<sup>7</sup>In the TE framework, monthly mean TE fluxes are anti-correlated with SE+MOC fluxes

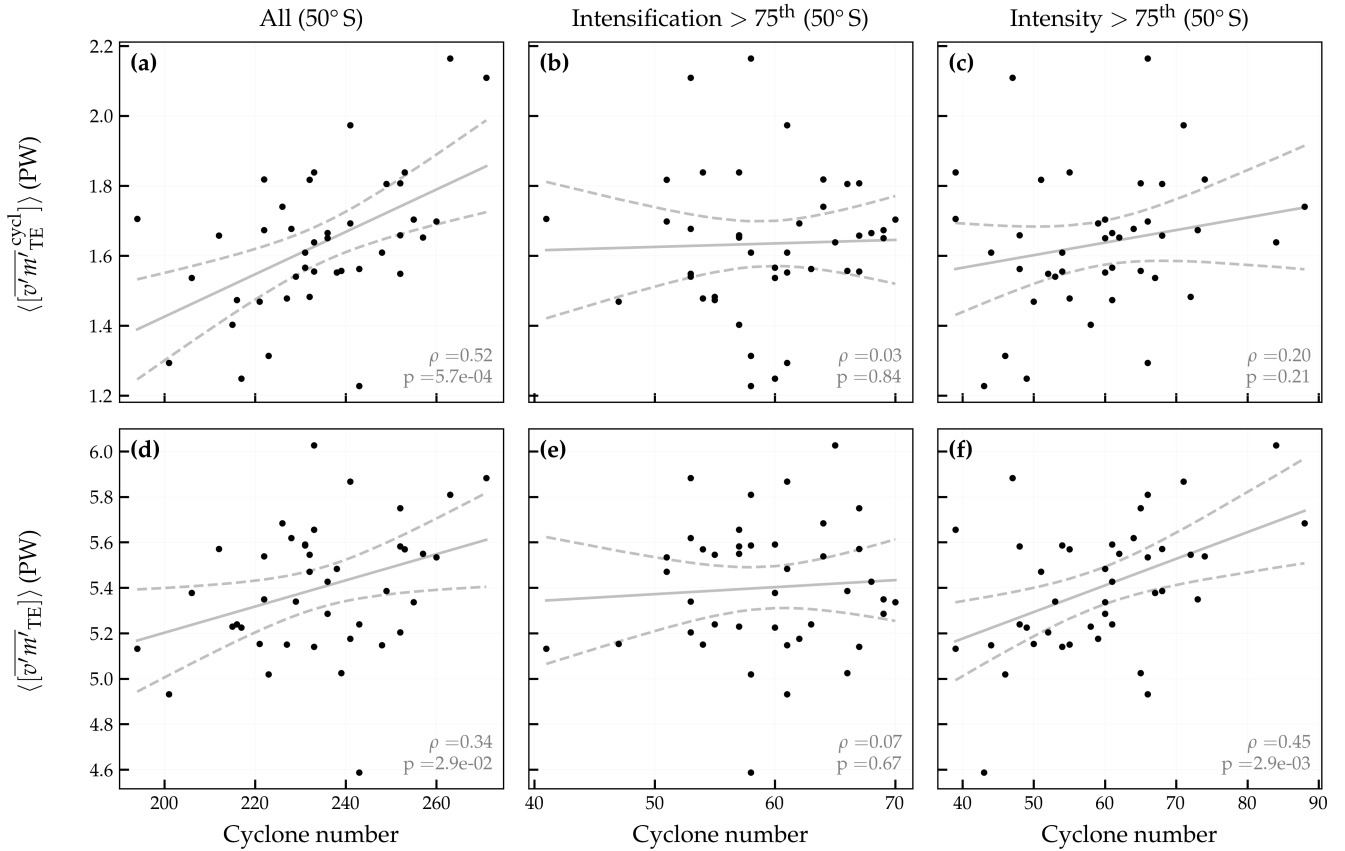


**Figure 10.** Relationship between seasonally averaged transient MSE flux and cyclone numbers for SH JJA at 50° S. (a) The cyclone-attributed transient MSE flux  $\langle [v'm'_{TE}]^{cycl} \rangle$  (units of PW) and the number of all cyclones with  $\langle [v'm'_{MA}]^{cycl} \rangle \neq 0$  at that latitude. (b, c) as (a) but for the number of strongly intensifying cyclones and intense cyclones, respectively. (d)–(f) as (a)–(c) but for the overall transient flux  $\langle [v'm'_{MA}] \rangle$ . The grey solid line represents a best estimate of a linear fit and dashed grey lines the corresponding confidence band. Correlation ( $\rho$ ) and p-value of the slope of the linear fit ( $p$ ) are indicated in each panel.

cyclone — i.e. continuing to count cyclones as above. Doing so yields a correlation between total AHT and cyclone number of  $\rho(\langle [v'm] \rangle, n_{all})$  of 0.63 — their attributed transient MSE fluxes.

870 For the total heat transport at 50° S for TE fluxes attributed with an attribution percentile rank of 90. Note that this correlation remains dependent on the flux decomposition method and attribution percentile because those influence the latitudinal extent of the attributed fluxes and thereby the cyclone count (Fig. ??). Nevertheless, the dependency on the flux decomposition method (correlation between 0.40–0.64, Fig. E1j) is comparably low. The correlation with the total cyclone number of cyclones passing through this latitude is 0.63. Of the latitude bands tested, however, 50° S is the latitude where this relationship correlation is largest (Fig. E2j). The decrease towards the pole is not fully understood but in-line with the relative potentially is

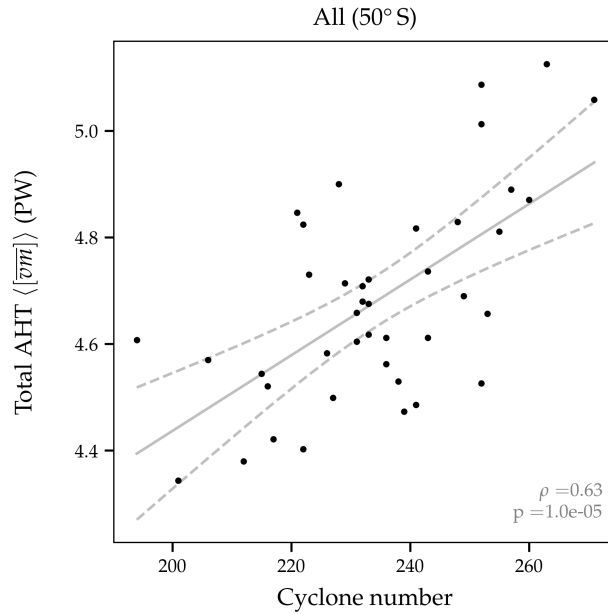


**Figure 11.** Relationship between seasonally averaged, zonally integrated total AHT heat transport,  $\langle [\overline{v\overline{m}}] \rangle$ , in at 50° S (PW) and number of cyclones with a non-zero TE-transient MSE flux attributed to them ( $\langle [\overline{v'm'}_{TE}^{cycl}] \rangle \neq 0$  ( $\langle [\overline{v'm'}_{MA}^{cycl}] \rangle \neq 0$ ) at the same latitude. Grey solid and dashed lines as in Fig. 10. Correlation  $\rho$  and explained variance  $R^2$  and the p-value of the slope of the linear fit ( $p$ ) are indicated on the panel.

875 connected to the increasing importance of planetary-scale fluxes increasing relative to synoptic-scale related MSE fluxes that increases towards the pole (Stoll et al., 2023). Notably, the correlations with  $n_{intense}$  and  $n_{intensif}$  are around zero throughout the SH (Fig. E1k,l). Note that Note that when simply taking the number of all cyclones in the entire SH,  $n_{all,SH}$  (instead of the number of cyclones only at 50° S,  $n_{all}$ ), the correlation reduces which. This suggests that capturing the latitudinal extent of cyclones is important ( $\rho(\langle [\overline{v\overline{m}}] \rangle, n_{all}) > \rho(\langle [\overline{v\overline{m}}] \rangle, n_{all,SH})$ ), as shown in Fig. E1j)2 is important.

880 To sum up, no robust relationship between the seasonal number of intense or strongly intensifying cyclones and the seasonal eddy-transient MSE flux is identified. Conversely, total AHT In contrast to the transient flux, the seasonal mean of the total zonally integrated MSE flux at 50° S exhibits a correlation of 0.40–0.64 more robust correlation of 0.40–0.64 with the number of eyelone all cyclones passing that latitude during that season. The correlation range results from the degrees of freedom in the counting method (cf. Fig. 2).

## 885 6 Summary and conclusions

### 6.1 Key findings

~~In this study we investigated~~ This study examines the relationship between ~~extratropical surface cyclones and AHT zonally integrated heat transport and life cycle characteristics of extratropical cyclones~~ during SH winter (JJA) ~~based on using~~ the ERA5 reanalysis. We ~~connected these using (vertically and zonally integrated)~~ have developed a novel method that combines ~~the vertically integrated transient~~ eddy MSE flux ~~and objectively identified cyclone tracks. The~~ with a feature-based cyclone tracking scheme. Specifically, the three central objectives of this study ~~were to unveil the evolution of local meridional eddy MSE fluxes along are:~~ (i) to reveal the temporal evolution of the local meridional transient MSE fluxes during the cyclone life cycles, ~~to assess the footprint of a cyclone in;~~ (ii) to quantify the contributions of cyclones to the zonally integrated eddy MSE flux depending on its transient MSE flux and assess how the contributions of individual cyclones vary depending on life cycle characteristics, ~~and such as lifetime and intensification rate, and;~~ (iii) to explore the relationship between cyclone number and (eddy) AHT numbers and heat transport on the seasonal scale. In the following, the key findings are ~~presented for each related research question in Sect. 1. summarized.~~

- ~~– Locally, meridional eddy MSE fluxes in the vicinity of cyclones peak~~ the meridional transient MSE fluxes peaks during the intensification phase and ~~before reaching declines before the cyclone reaches its~~ mature stage (Fig. 3). ~~Spatial,~~ which is in agreement with the theory of baroclinic growth (as is the vertical structure of the fluxes). Cyclone-centered composites reveal large ~~fluxes poleward MSE fluxes located~~ in the warm sector confined ~~by~~ between the warm and cold fronts ~~with a smaller signal and a smaller peak~~ in the cold sector (Fig. 4). ~~Fluxes are enhanced for strongly intensifying and intense~~ Furthermore, there is a clear positive (although nonlinear) relationship between the strength of the transient MSE flux and the growth rate and maximum intensity of cyclones (Fig. 5). Crucially, a non-negligible fraction of warm-sector and cold-sector fluxes are located outside of the cyclone masks defined by closed SLP contours. ~~Investigating the energy footprint of cyclones therefore requires attributing these fluxes to the cyclones as well.~~ Typically, warm-sector fluxes extend further equatorward and are spatially bound by the frontal zones. The poleward flux of latent heat is, as expected, confined to the warm sector which leads to an increasing contrast between warm-sector and cold-sector MSE fluxes towards the equator (Fig. 6). ~~Doing so in our study increases the fraction of poleward eddy MSE flux attributed to cyclones and reduces the meridional offset between the maxima in cyclone mask frequency (and the fluxes therein) and the overall eddy flux.~~
- ~~– In the zonal integral, the novel attribution method based on feature overlap attributes 30% of the transient MSE flux to cyclones. This method places the latitudinal maximum in cyclone attributed MSE flux closer to the overall transient MSE flux relative to only counting the MSE flux within cyclone masks~~ (Fig. 7). This supports the notion that MSE fluxes ~~within associated with warm conveyor belts are,~~ which are located typically along the boundaries and outside of the cyclone masks, are important contributors to zonally integrated (eddy) heat MSE transport proposed in Messori and Czaja (2015). ~~With our approach, around 30% of the overall (high-frequency or transient) eddy MSE fluxes are attributed to cyclones in midlatitudes.~~
- ~~– Considering the zonal integral, it was found that the life cycle characteristics influence the magnitude of cyclone-attributed eddy MSE fluxes. In particular, cyclone intensity is the life cycle characteristic for which the fluxes attributed to the~~

~~strongest cyclones is largest~~ The most intense cyclones have the largest fluxes attributed to them (Fig. ??). Like intensity, the intensification rate also shows a large ratio of fluxes attributed to strong vs. weak cyclones. Poleward propagation speed, which is not discussed in detail, features a comparably large ratio at some latitudes but does not stand out over intensity (Sinclair and Dacre, 2019). ~~The~~ 8. The attributed fluxes also increase with cyclone intensification rate. As expected, the accumulated fluxes increase with cyclone lifetime ~~—naturally— but when normalizing by the number of time steps this characteristic~~ but cyclone lifetime is a much weaker indicator for the attributed flux ~~—than intensity or intensification rate.~~ Previous research has found that the poleward propagation speed (and not necessarily intensity) is the characteristic for which the poleward moisture fluxes within a fixed radius around the center are the largest (Sinclair and Dacre, 2019). For MSE fluxes in this study, the cyclones with fastest poleward propagation speed show comparable lifetime-averaged fluxes to those of the most intense cyclones at some latitudes but not consistently larger ones (not shown).

925

930

- The ~~previously~~ identified link between cyclone intensity and attributed ~~eddy MSE fluxes on the scale of individual cyclones also extends~~ transient MSE fluxes also applies to the seasonal scale. Storms that have an intensity larger than the 75<sup>th</sup> climatological percentile collectively contribute to around 45 % of the seasonally integrated cyclone-attributed AHT heat transport (Fig. 9). ~~This contribution is almost matched by the cyclones intensifying most strongly. For those two characteristics, the ‘strong’ cyclones~~ The intense cyclones thereby transport roughly as much ~~eddy transient~~ MSE flux as the ~~‘moderate’~~ moderately intense cyclones despite the latter being, on average, twice as numerous. However, the ~~fractions~~ fraction of the MSE flux associated with the intense cyclones are not disproportionate enough ~~for the number of these cyclones to be robustly linked to the seasonal eddy MSE so that their number alone does not shape the seasonal mean transient~~ flux (Fig. 10). This also holds true for cyclone intensification and is further discussed below. For the total heat transport at 50° S, the correlation with the number of all cyclones at that latitude lies between 0.40–0.64 (Figs. 11 and E1j). However, the correlation is reduced at other latitudes (Fig. E2j) such that further research is needed to better understand whether changes in cyclone numbers can be related to atmospheric heat transport changes constrained by the Earth’s energy imbalance.

935

940

945

950

The ~~approximate~~ determined contributions of extratropical cyclones to the total AHT heat transport are summarized in Fig. 12: Cyclones contribute to the high-frequency (or ~~transient~~ eddy AHT ‘transient’) eddy heat transport which, depending on the flux decomposition, is accompanied by low-frequency (or ~~stationary~~ ‘stationary’) background fluxes and the mean overturning circulation. The high-frequency eddy MSE fluxes attributed to cyclones can be linked to different subsets of cyclones based on their intensity or intensification rate. Other high-frequency eddy MSE fluxes not attributed to cyclones may occur far from the cyclone center (possibly along fronts), be linked to high pressure systems, or be unrelated to weather features with closed contours such as meandering zonal flows.

## 6.2 ~~The interplay~~ On the choice and influence of scales ~~eddy-mean decompositions~~

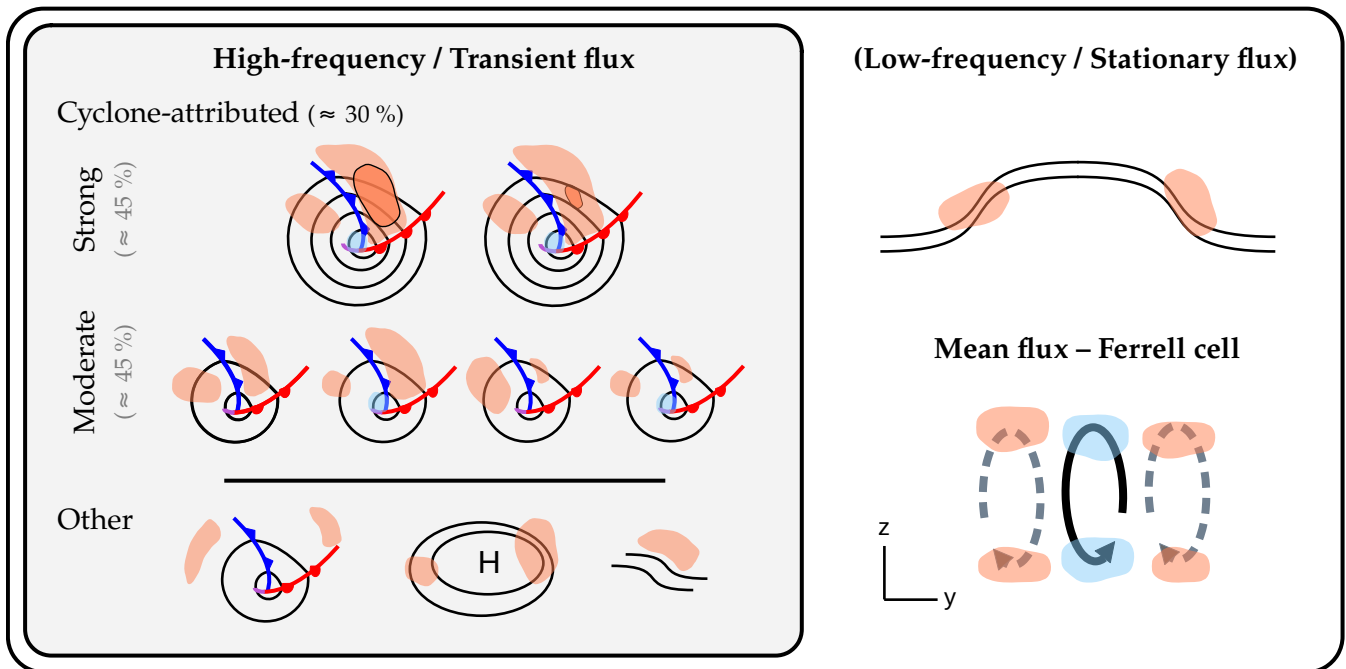


**Figure 12.** Schematic of the decomposition of total [AHT-atmospheric heat transport](#) into different flux components and contributions by extratropical cyclones: When adopting an eddy-mean decomposition, the [AHT-heat transport](#) is the sum of a high-frequency, transient eddy flux component, potentially a separate low-frequency or stationary eddy component, and the [zonal-mean-flux](#) related to [the mean](#) overturning [circulation](#). Orange and blue shading denotes poleward and equatorward meridional MSE fluxes, respectively. The high-frequency, transient eddy fluxes are further split into cyclone-attributed ( $\approx 30\%$  of the high-frequency eddy fluxes) and other fluxes. Surface cyclones in the left box are illustrated by SLP contours that are accompanied by warm fronts (red lines), cold fronts (blue), and occlusions (purple). ‘Strong’ and ‘moderate’ refer to the intensity or intensification rate of cyclones with ‘weak’ cyclones omitted. Grey percentage indications refer to the approximate contribution of those cyclones to the cyclone-attributed eddy MSE flux (and not the overall high-frequency eddy flux). Low-frequency or stationary flow is sketched by wave-like black lines in the top right. In the bottom right, the zonal mean flux is drawn in a latitudinal and vertical  $y$ - $z$  cross-section with the overturning circulation illustrated with solid black (Ferrell cell) and dashed grey (Hadley and polar cells) arrows.

~~Note that we broadly refer to high-frequency ‘eddy’ MSE fluxes in [In](#) the above summary (instead of ‘transient eddy’ MSE fluxes specifically as in Sects. 3–5) since these conclusions overall do not depend on [the conclusions are overall independent](#)~~  
 955 [of](#) the choice of eddy-mean decomposition method. A consequential method dependence [in our study](#) was only found for the correlation between the seasonal cyclone number and the [eddy-transient](#) MSE flux ([FigSect. E15 and Appendix E](#)). This points to a non-negligible influence of planetary, low-frequency waves to the local [eddy-transient](#) MSE flux attributed to individual systems ([Messori and Czaja, 2014; Stoll et al., 2023](#)). ~~In other words, our results suggest that the influence of a cyclone characteristic on its energy footprint in the zonal integral as discussed below ([Messori and Czaja, 2014; Stoll et al., 2023](#)).~~  
 960 [Because some fraction of this background flux is attributed to an individual extratropical cyclone, the effect of its life cycle](#)

characteristics on the zonally integrated flux is partly masked by a background signal of which a fraction is attributed to the cyclone. While for large enough sample sizes, this method-dependency averages out ( $N \gtrsim 200$  as in Sects. 3 and 4), this effect is thought to influence the picture but the effect influences the result when considering a seasonal set of intense cyclones, for instance ( $N \approx 60$ , Sect. 5). Recall that the most intense cyclones account for approximately half the cyclone-attributed eddy MSE flux. Therefore, under the somewhat naive assumption that cyclone-attributed eddy MSE fluxes were unrelated to background signals, one might have expected a correlation between

When high-pass filtering, a wave-like signal with a frequency  $\sim (11 \text{ d})^{-1}$  is filtered out whereas in the zonal anomaly framework the corresponding flux is partly attributed to cyclones. It is found that the number of intense cyclones and the cyclone-attributed eddy MSE flux modulates the high-pass filtered transient flux, while it does not determine the transient flux computed from zonal anomalies (Fig. 10f). Of the methods tested, high-pass filtering is most effective at separating synoptic signals and background flows (E1d,h). We argue that the lower correlation for the zonal anomaly method arises because part of the background flux is attributed to each cyclone — correspondingly, the correlation between eddy MSE independently of cyclone intensification rate or intensity. Conversely, the addition of this background signal leads to a higher correlation between the seasonal fluxes and the number of intense cyclones is largest for this method. With more and more background fluxes being attributed to the cyclones when defining eddies from anomalies of monthly means, or instantaneously as anomalies from zonal means, the correlation decreases towards zero. At the same time, high-pass filtering is the method with the smallest fraction of total AHT explained by high-frequency eddies overall cyclone number (Fig. E1b,f). The monthly anomaly framework is a special case with the amount of background flows attributed to cyclones lying somewhere between the other two methods. As a result, the correlations broadly fall within the two other methods (Fig. D1E1).

The lack of a robust relationship between seasonal cyclone numbers and seasonal mean eddy MSE flux suggests that the former is not directly constrained by planetary energetics. One can argue that this should not have been expected, however, because any energetic constraint would relate to the total AHT instead of the eddy AHT. Given an anti-correlation between eddy and zonal mean fluxes (Cox et al., 2024b), cyclones may be related to an arbitrarily large eddy flux which — compensated by the mean overturning — still fulfills the Earth's energy imbalance (Eq. 1). In addition to high-frequency (or transient) eddies, low-frequency (or stationary) eddies add further complexity depending on the decomposition method (Fig. 12).

Our results may suggest that high-pass filtering is the most suitable decomposition method to investigate the energy transport footprint of extratropical cyclones. While the choice of the cut-off frequency (or likewise the spatial wavenumber) can be motivated dynamically (e.g. Eady, 1949), some spectral power of a warm conveyor belt, for instance, is contained in the flow that is filtered out. As the spectrum of total AHT heat transport is predominantly continuous (see for instance supplementary of Stoll et al., 2023), choosing a scale separation in time or space is a balance between how much low wavenumber flux is attributed to a background component — which poses a degree of freedom in AHT variability — and how and how much it imprints in the transient eddy component, eventually near individual cyclones. Conversely, abandoning a flow decomposition would require the definition of an atmospheric reference state such that cold air moving equatorward is identified as counteracting the equator-to-pole energy imbalance. Thus far, when inspecting the total AHT at 50 S we find that its correlation with the number of cyclones (counting those that contribute to the eddy AHT at that latitude) lies between

0.40–0.64 (Figs. Note that high-pass filtering is the method with the smallest fraction of total heat transport explained by cyclone-attributed transient MSE flux (Fig. 11 and E1j). The comparably high correlation is reduced at other latitudes (Fig. D1). Closing the atmospheric heat budget (Eq. E2j), however, such that further research is needed to better understand whether changes in cyclone numbers can be related to AHT changes constrained by the Earth’s energy imbalance<sup>1</sup>) using such an approach can require computing many cross-terms (Franzke and Harnik, 2023). Thus, the choice of eddy-mean decomposition method depends on the research question.

### 6.3 Further remarks

Note that the contribution of low-frequency and planetary-scale waves to the zonally integrated AHT heat transport likely increases with height (Stoll et al. (as suggested by the dry and latent heat flux decomposition in 2023) Stoll et al. (2023)). Focusing on surface cyclones, one possible extension of this work is a repetition of the above analyses using only low-level fluxes. In addition to reducing the above sensitivity with respect to the definition of what is background flux, this would also segregate stratospheric contributions unrelated to surface weather. In the SH, we do not expect a strong influence of stratospheric fluxes on our results; at 65° S, stratospheric fluxes account for only 11 % of the column-integrated fluxes explaining 10 % of its variance (Cardinale et al., 2021).

While our analysis focused on SH winter, technically, the methods can readily be applied to the NH and other seasons as well. Yet, in the NH the stationary signal is much larger, which increases the sensitivity with respect to the flux decomposition method (not shown) and weakens the connection between AHT heat transport by cyclones and hemispheric scale radiative budget constraints. Furthermore, one has to reflect on whether and how to disentangle the signals arising from the Atlantic and Pacific basins due to different changes in cyclone characteristics. The response of the cyclone number to warming and storm track latitude, for instance, is different in these two basins (e.g. Seiler and Zwiers, 2016; Chang, 2018). Moreover, stratospheric contributions to the vertical integral are larger in the NH (Cardinale et al., 2021) such that one should consider a sensitivity analysis with respect to the vertical integration bound. ~~Lastly, by neglecting zonal heat fluxes we implicitly assumed that the energy imbalance is counteracted by heat being transported into a zonally symmetric polar cap. The larger zonal asymmetries in the NH (and horizontal tilting of storm tracks, Fig. 1a) question the applicability of this assumption as meridional heat fluxes alone might not accurately describe the circulation that underlies a possible energetic constraint.~~

More sophisticated methods for attributing different kinds of fluxes to cyclones (e.g., Fearon et al., 2021; Lopez-Martí et al., 2025) are conceivable. Warm and cold sector MSE fluxes could be identified using atmospheric river (Shields et al., 2018) or warm conveyor belt masks (Heitmann et al., 2024) and cold sector masks (Zolina and Gulev, 2003; Kolstad and Bracegirdle, 2008; Vannièrè et al., 2016), respectively. Note that depending on the identification method, WCB warm conveyor belt masks might require computing Lagrangian air parcel trajectories (Heitmann et al., 2024). ~~Attributing fluxes via surface fronts is another possibility (Papritz et al., 2014)~~ A different approach to capture the heat transport along the fronts could be to attribute fluxes via identified surface fronts (e.g., as in Papritz et al., 2014), although it is unclear how well these capture fluxes throughout the sectors (Messori et al., 2017). Instead of attributing fluxes to cyclones, one could directly study the influence of warm conveyor belt and cold sector numbers on the zonal energy budget. Since fluxes do not peak near the center of weather

**Table A1.** List of abbreviations used in this study.

Abbreviation	Meaning
<del>AHT Atmospheric heat transport</del> DJF	December, January, February
EQ	Equator
HP	High-pass (filtering method, framework)
JJA	June, July, August
(r)lat	(rotated) latitude
(r)lon	(rotated) longitude
<del>MOC MA</del>	<del>Meridional overturning circulation</del> <del>Monthly anomaly (framework)</del>
MSE	Moist static energy
NH	Northern Hemisphere
<del>SE Stationary eddy</del> SFA	Standardized flux anomalies
SH	Southern Hemisphere
SLP	Sea level pressure
SP	South Pole
<del>TE Transient eddy (framework)</del> TOA	Top of atmosphere
<del>WCB Warm conveyor belt</del> ZA	Zonal anomaly (framework)

1030 systems but rather between cyclones and anticyclones, that would make the question "~~What about the anticyclones?~~" — ~~which we have dismissed so far~~ — about the contribution of anticyclones obsolete (Ruggieri et al., 2020).

This study has not addressed trends in either MSE fluxes or cyclone numbers. The ~~introduced~~ decrease of SH winter cyclones in a warmer climate, however, motivates further research on the relationship between extratropical cyclones and zonal mean energetics. A follow-up study is planned applying ~~our diagnostics to aquaplanet simulations and future climate projections~~ there

1035 here developed diagnostics to idealized and fully-coupled climate simulations.

*Code and data availability.* The underlying ERA5 reanalysis data can be downloaded from <https://doi.org/10.24381/cds.bd0915c6> (Hersbach et al., 2020). A code repository to reproduce the data and the figures and a data archive are in preparation and will be made accessible upon publication.

## Appendix A: Abbreviations and terminology

1040 To facilitate the lecture of this study, a list of abbreviations (Table A1) and frequently used mathematical terms (Table A2) is provided.

**Table A2.** Description of selected terms used in this study. Subscripts of eddy fluxes change in accordance with dashes and asterisks.

Term	Description
$v'm'_{TE} - v'm'_{MA}$	Meridional <a href="#">eddy-transient</a> MSE fluxes derived from monthly anomalies
$v'Lq'_{TE} - v'Lq'_{MA}$	Meridional <a href="#">eddy-transient</a> moisture fluxes derived from monthly anomalies
$v'm'_{HP}$	Meridional <a href="#">eddy-transient</a> MSE fluxes derived from high-pass filtering
$v^*m^*_{ZA}$	Meridional <a href="#">eddy-transient</a> MSE fluxes derived from instantaneous anomalies from the zonal mean
$\langle v'm'_{TE} \rangle - \langle v'm'_{MA} \rangle$	Zonal mean (or zonally integrated) <a href="#">TE-transient</a> MSE fluxes
$\overline{v'm'_{TE}} - \overline{v'm'_{MA}}$	Monthly or seasonal mean <a href="#">TE-transient</a> MSE fluxes
$\langle v'm'_{TE} \rangle - \langle v'm'_{MA} \rangle$	Vertically integrated <a href="#">TE-transient</a> MSE fluxes
$\langle \langle v'm'_{TE} \rangle \rangle - \langle \langle v'm'_{MA} \rangle \rangle$	Vertically integrated zonal mean (or zonally integrated) <a href="#">TE-transient</a> MSE fluxes
$\langle \langle \overline{v'm'_{TE}} \rangle \rangle - \langle \langle \overline{v'm'_{MA}} \rangle \rangle$	Seasonal mean zonally and vertically integrated ('overall') <a href="#">TE-transient</a> MSE fluxes
$\langle v'm'^{cycl}_{TE} \rangle - \langle v'm'^{cycl}_{MA} \rangle$	Vertically integrated <a href="#">TE-transient</a> MSE fluxes attributed to cyclones
$\langle \langle v'm'^{cycl}_{TE} \rangle \rangle - \langle \langle v'm'^{cycl}_{MA} \rangle \rangle$	Zonal integral of vertically integrated <a href="#">TE-transient</a> MSE fluxes attributed to cyclones
$\langle \langle \overline{v'm'^{cycl}_{TE}} \rangle \rangle - \langle \langle \overline{v'm'^{cycl}_{MA}} \rangle \rangle$	Seasonal mean zonal integral of vertically integrated <a href="#">TE-transient</a> MSE fluxes attributed to cyclones
$\langle \overline{vm} \rangle$	Seasonal mean ('total') <a href="#">AHT-heat transport</a>
$v'm'^{clim}_{TE} - v'm'^{clim}_{MA}$	Climatology of meridional <a href="#">TE-transient</a> MSE fluxes
$\langle \langle v'^{*}m'^{*}_{TE} \rangle \rangle$	Seasonal mean zonal and vertical integral of 'overall' <a href="#">eddy-transient, cyclone-attributed</a> MSE fluxes
$\langle \langle \overline{v'^{*}m'^{*}_{TE}} \rangle \rangle$	Seasonal mean zonal integral of vertically integrated <a href="#">eddy-MSE fluxes attributed to cyclones</a>
$n_{all}$	Seasonal number of cyclones <a href="#">with that were attributed</a> non-zero <a href="#">cyclone-attributed eddy MSE fluxes</a>
$n_{all,SH}$	<del>Seasonal number of cyclones within the entire SH height</del>

## Appendix B: [Further details on the MSE flux attribution to cyclones and cyclone counting](#)

In our study, we identify events of large eddy MSE fluxes based on a seasonally and latitudinally varying flux threshold. This threshold is computed by aggregating all values of a latitude band of the same time of every year and computing a percentile based on that distribution. This is illustrated in Fig. B1. The identified features are then attributed to surface cyclones using SLP-derived masks as shown in Fig. 2. [The transient MSE fluxes differ for each flux decomposition method \(Fig. B2a–c\) and so do the identified flux features \(Fig. B2–d–f\). As a result, at a single instance a cyclone may be attributed some equatorward flux of positive MSE \(dark blue patches at 60° E in Fig. B2g,h\) or not \(Fig. B2i\).](#) Note that not all flux features overlap with cyclone masks (yellow patches in Fig. B2g–i).

## 1050 Appendix C: Sensitivity and variability of near-cyclone eddy MSE fluxes

To further strengthen the conclusions drawn from the cyclone composites, a significance test is performed for the [TE-monthly anomaly](#) framework. For this we address the standardized flux anomalies (SFA) from the climatological seasonal mean,

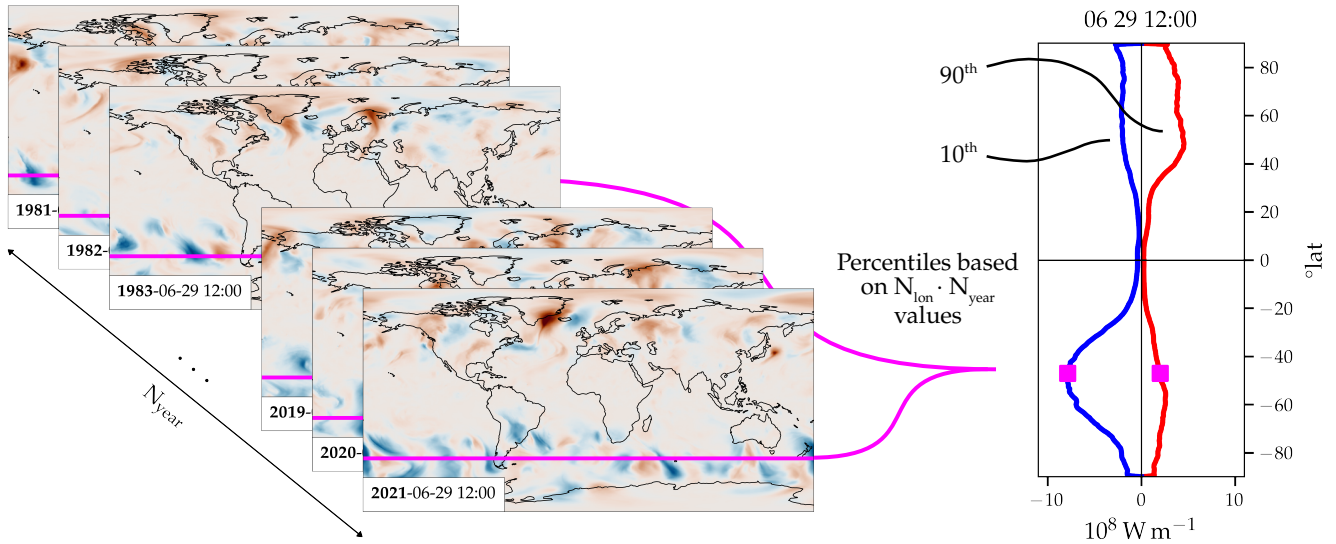


**Figure B1.** Illustration of the determination of the percentile threshold for eddy MSE flux events [based on the monthly anomaly framework](#): For every six-hourly time step of a year — 29 June, 12:00 UTC, for instance — eddy MSE flux thresholds for poleward and equatorward fluxes are calculated at each latitude. These are based on the values of that latitude band and every corresponding time of year during the analysis period. Thus, the sample size which the percentile is computed from is the number of years ( $N_{\text{lon}}$ ) times the number of grid-cells at a latitude circle ( $N_{\text{year}}$ ). The 10<sup>th</sup> and 90<sup>th</sup> percentiles of the vertically integrated eddy MSE fluxes (color shading on the left panel) for 29 June, 12:00 UTC are shown on the right in blue and red, respectively. The latitude of 47° S is highlighted in magenta.

$v'm'_{\text{TE}}^{\text{clim}} - v'm'_{\text{MA}}^{\text{clim}}$ , defined as

$$\text{SFA}(\text{lon}, \text{lat}, \text{time}, \text{pressure}) = \frac{v'm'_{\text{TE}}(\text{lon}, \text{lat}, \text{time}, \text{pressure}) - v'm'_{\text{TE}}^{\text{clim}}(\text{lon}, \text{lat}, \text{pressure})}{\sigma(v'm'_{\text{TE}})(\text{lon}, \text{lat}, \text{pressure})} - \frac{v'm'_{\text{MA}}(\text{lon}, \text{lat}, \text{time}, \text{pressure}) - v'm'_{\text{MA}}^{\text{clim}}(\text{lon}, \text{lat}, \text{pressure})}{\sigma(v'm'_{\text{MA}})(\text{lon}, \text{lat}, \text{pressure})} \quad (\text{C1})$$

1055 with  $\sigma$  the standard deviation over the climatological period. Locations in the composite where  $\text{mean}(\text{SFA}) = 0$ , we regard  
the  $v'm'_{\text{TE}} - v'm'_{\text{MA}}$  of the individual events that we used for compositing as not significantly different from climatological  
 $v'm'_{\text{TE}} - v'm'_{\text{MA}}$  fluxes. In other words, the null hypothesis,  $\text{mean}(\text{SFA}) = 0$ , is rejected if within the composite, fluxes are  
sampled that are on average different from climatology. We perform a two-sided, one sample  $t$ -test at each composite grid-cell  
(Fig. C1). Overall, the dynamical features that were identified in the composites are based on flux anomalies that on average  
1060 are significantly different from zero. Note that low  $v'm'_{\text{TE}} - v'm'_{\text{MA}}$  can be significant in the composite as it is lower than  
climatology.

Compared to the [TE framework](#) (see Sect. 2.3 for a description of the different frameworks), [monthly anomaly \(MA\) framework](#), it is also the intensification phase (and not the mature stage) during which fluxes are largest when adopting the  
[HP and ZA high-pass \(HP\) and zonal anomaly \(ZA\)](#) decompositions (not shown). A comparison of the fluxes at peak cyclone

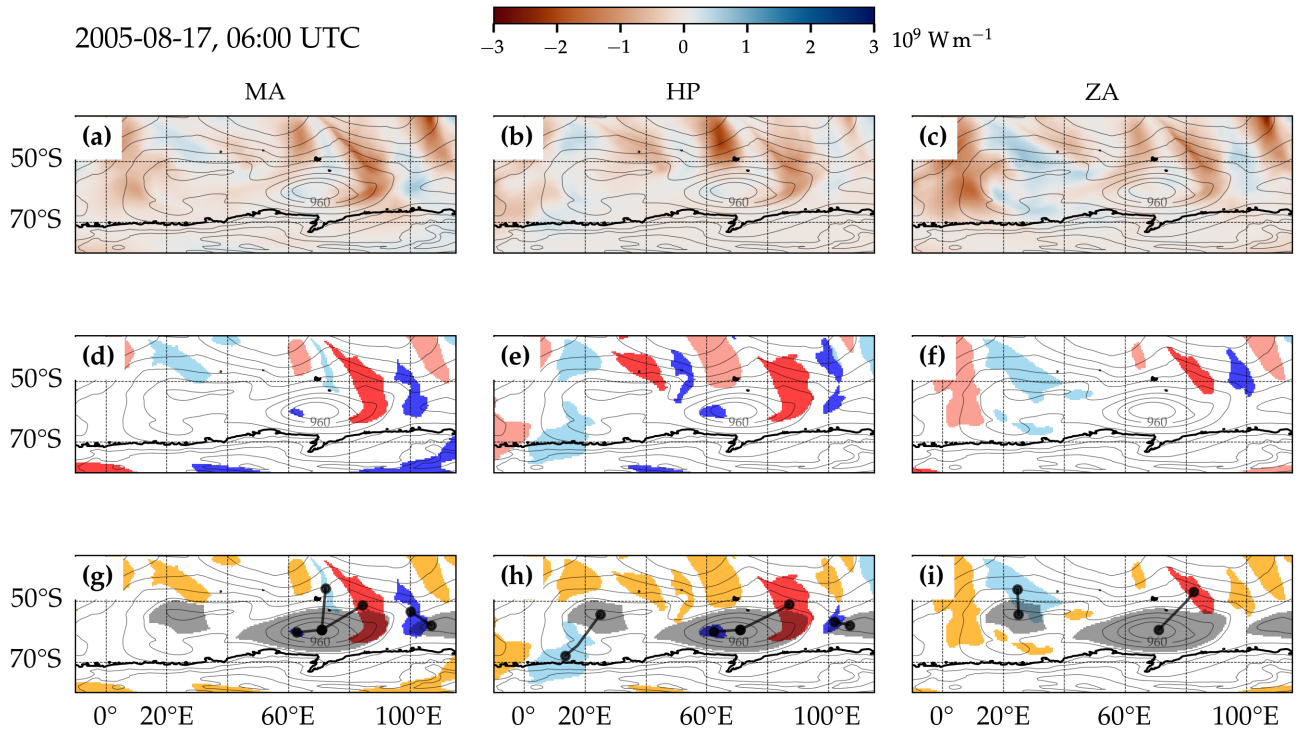


**Figure B2.** Snapshot of vertically integrated eddy MSE fluxes and their attribution to surface cyclones. (a) Vertically integrated eddy MSE fluxes calculated using the [TE-monthly anomaly](#) framework (shading in  $\text{W m}^{-2}$ ) and SLP (black contours in steps of 10 hPa). (b) and (c) (b) and (c) as in (a) but for the HP and ZA frameworks, respectively. (d)–(f) The binary masks corresponding to the identified flux features are shaded in reddish and bluish colors if MSE fluxes are poleward or equatorward, respectively, and in dark and light tones if fluxes correspond to positive and negative MSE anomalies, respectively. (g)–(i) [An-In](#) addition to above, surface cyclone masks are shown with grey patches. If flux features are not overlapping with cyclones, the features are colored yellow. Otherwise, black straight lines and dots indicate to which cyclones [the features are each feature is](#) attributed to. Coastlines are depicted with black lines.

1065 intensification reveals that at 850 hPa, high-pass filtered fluxes are marginally lower than [TE-MA](#) fluxes (Fig. C2a,b). Moreover, the contrast between warm and cold sectors is reduced in the ZA framework (Fig. C2c), which could be explained by strong warm sector anomalies raising the instantaneous zonal mean MSE such that cold sector anomalies become larger compared to the other methods. Note that for the NH, the differences between [TE-MA](#) and ZA are more pronounced (not shown) due to the time-stationary signal being declared as SE flux (Eq. 2). These descriptions are also valid for vertically integrated fluxes  
 1070 (Fig. C2d–f).

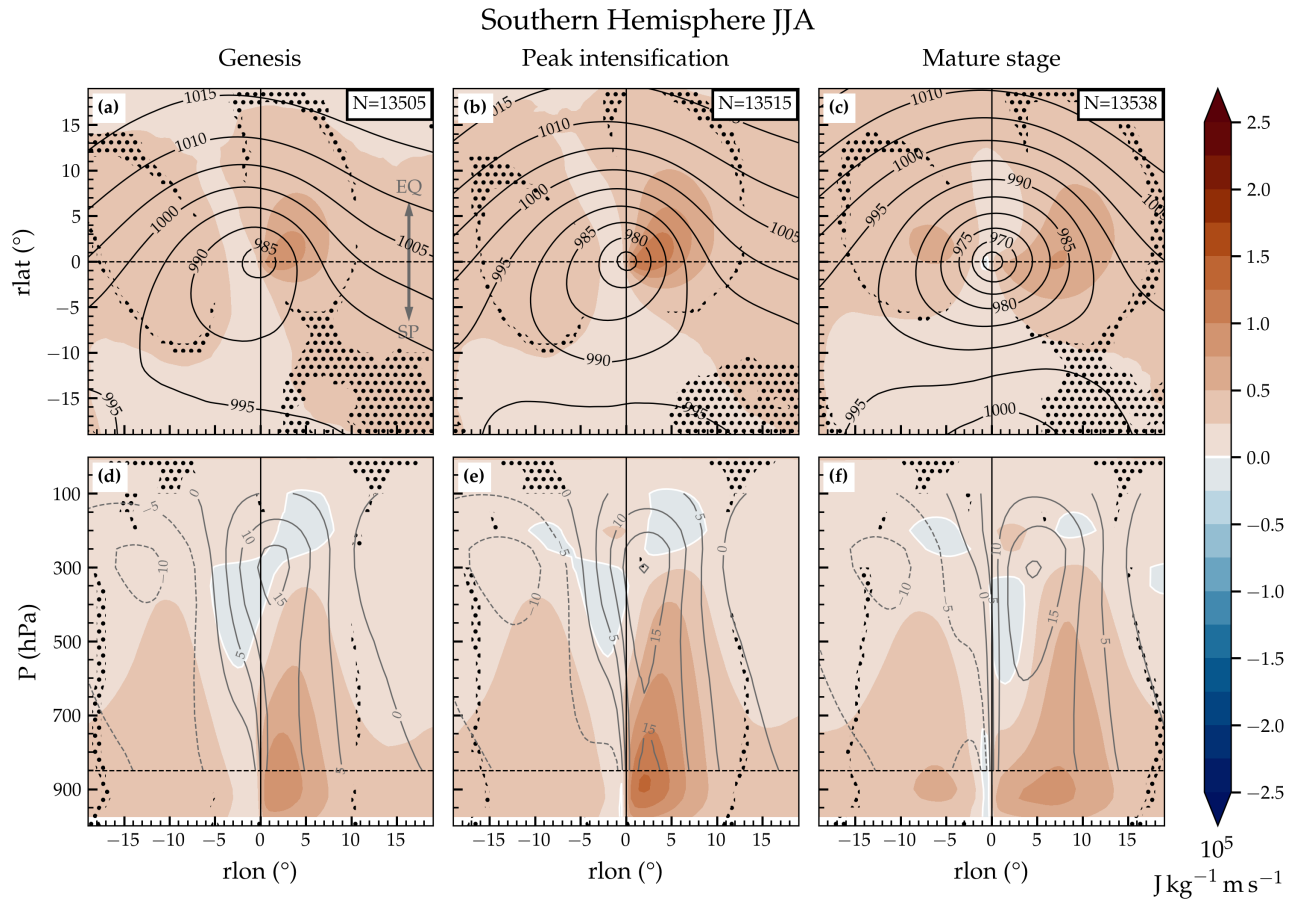


**Figure C1.** Statistical significance of composited **TE-transient** MSE flux anomalies as in Fig. 4. Dotted areas indicate where the null hypothesis mean(SFA) = 0 (see Eq. C1) is not rejected at the 95 % confidence level. In (d)–(f), grey contours indicate the (vertically sub-sampled) full meridional wind,  $v$ , as opposed to  $v'$  in Fig. 4d–f.

#### Appendix D: Method dependence of **cyclone-attributed** zonally integrated **eddy cyclone-attributed** MSE flux

As-

1075 The method sensitivity of the seasonal contributions to transient eddy MSE flux by cyclones, which was discussed in Sect. ??, a method sensitivity of the results in Sect 4.1, is shown in Fig. D1. Choosing lower percentiles moves the peak of the attributed fluxes towards the equator because larger masks (warm sectors extending further equatorward than the cyclone mask) are more often attached (Fig. D1a,d,g,j). Higher percentiles reduce the absolute fractions, yet percentages at 50° S remain close to 20 % for  $p = 0.95$  (yellow lines in Fig. D1b,e,h,k). The cause of the relatively reduced correlation around 60° S for the ZA framework (Fig. D1i) is not clear but might be related to the presence of planetary waves. A repetition with an upper integral bound of 500 hPa (Fig. D1l) suggests this signal arises from lower levels (and not stratospheric dynamics).

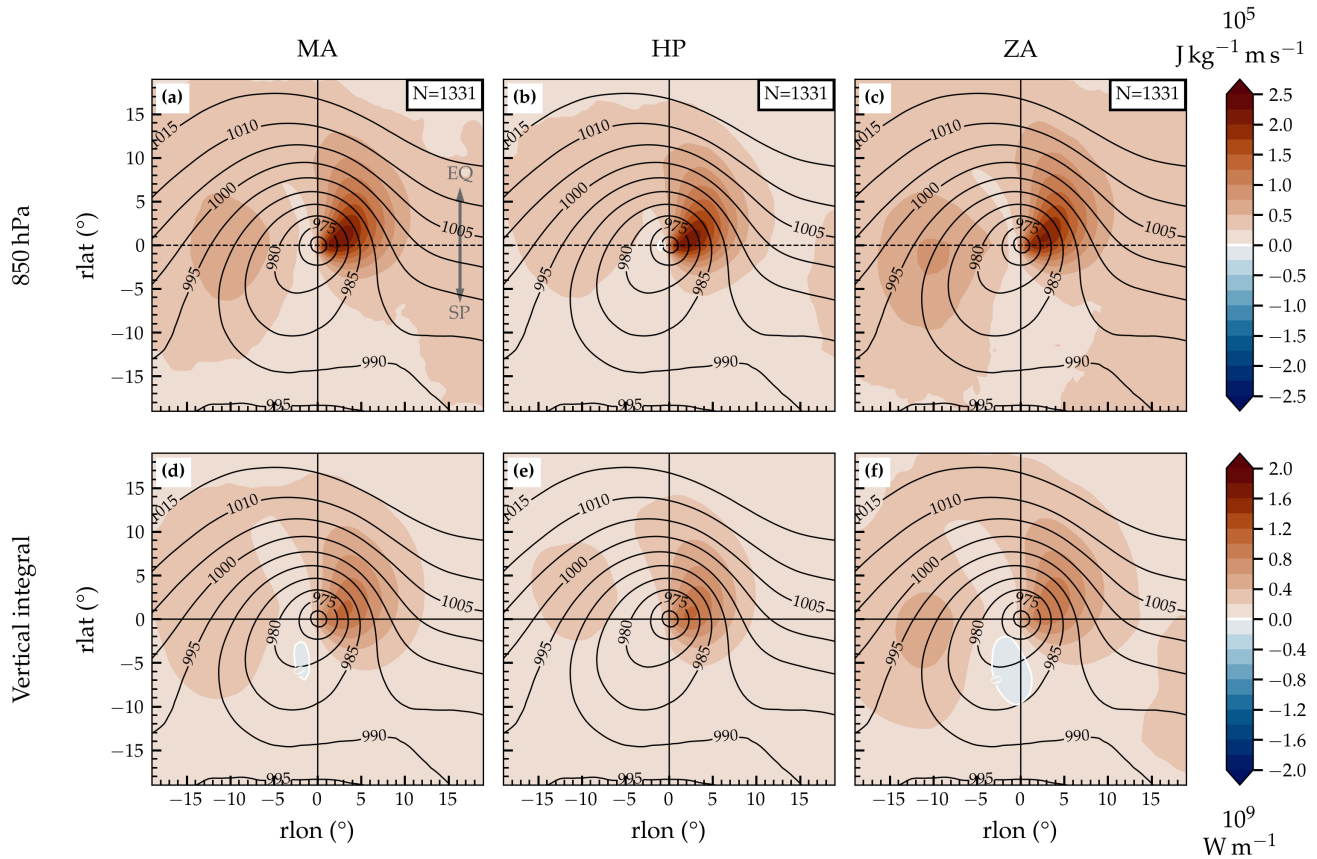


**Figure C2.** (a)–(c) Cyclone-centered eddy MSE flux at 850 hPa during time of maximum intensification for the 10 % most strongly intensifying SH cyclones during JJA for three different definitions of eddy flux (see method abbreviations in Sect. 1) in  $\text{J m}^{-1} \text{kg s}^{-1}$ . (d)–(f) Vertically integrated fluxes analogously to (a)–(c) but in units of  $\text{W m}^{-1}$ . Black contours indicate composite mean SLP in hPa. The number of cyclones in the composites are included in the upper right in panels (a)–(c). A grey arrow is included for better orientation indicating directions of equator (EQ) and South Pole (SP).

1080 The averages depicted in Fig. 4 based on attributing eddy MSE fluxes to cyclones is performed. Cyclone-attributed eddy MSE fluxes are shown for individual cyclones in Fig. 8 conceal the variability of the MSE fluxes attributed to individual cyclones. These are shown in Fig. D2 for the TE-MA framework, in particular the cyclones that intensify least and most rapidly across the SH. Zonally-integrated TE-MSE flux attributed to individual extratropical cyclones. (a) The lifetime-integrated flux (–) of the 200 most strongly intensifying cyclones (blue thin lines) is compared to the flux of the 200 cyclones that intensify least rapidly (red). Thick lines denote the arithmetic means shown in Fig. 8a. (b) As in (a) but for the lifetime-averaged flux in . The flux attribution percentile rank corresponds to 90%.

1085

The seasonal contributions to eddy MSE flux by cyclones are shown in Fig. 8. While the means (solid lines) amount to around 20 DJF. For the ZA framework, the sensitivity is performed for vertical integrals from  $\bar{p}_S$  to the TOA (Fig. 8j-l). Individual cyclones can be attributed more than 150 DJF-i) and  $\bar{p}_S$  to 500 PW across a latitude band of more than  $10^\circ$  (Fig. 8j-l). D2a).

1090 Regarding the method dependency of the zonally integrated eddy MSE fluxes attributed to cyclones of different life cycle characteristics, the lifetime-averaged fluxes of panels Figs 8e and 8f are repeated in Figs. 8g and 8h, respectively. The corresponding ratios b,d are shown for lifetime-accumulated and lifetime-averaged fluxes in Figs Fig. D3 and 8i. Sensitivity of cyclone-attributed averaged flux for all SH cyclones as in Fig. 8. Lines are equal to the ones in Fig. 8e for the different flux decomposition methods (see Sect. 2.3) and different flux percentile thresholds for attributing flux to cyclones 1095 (80, 90, and 95, see Sect. 2.4). The black dashed line represents the the average of all SH cyclones.

Cyclone-attributed TE MSE flux for cyclones that reach peak intensification between 50–60 S and have a minimum lifetime of 3 days as in Fig. 8f but repeated for different flux decomposition methods (columns, see Sect. 2.3) and different percentile thresholds for attributing flux to cyclones (80, 90, and 95). The black dashed line indicates the the arithmetic mean of all cyclones of that subset.

1100 Ratio of the flux related to the 200 cyclones of largest vs. lowest life cycle characteristic (indicated by the line style) based on the cyclones that pass 50–60 S: Fig. 8b,d are reproduced for different flux decomposition methods (columns, see Sect. 2.3) and different percentile thresholds for attributing flux to cyclones (rows, see Sect. 2.4). Purple lines correspond to lifetime-accumulated fluxes and yellow lines to lifetime-averaged fluxes.

## Appendix E: Sensitivity of the number–flux relationship to choice of flux decomposition method

1105 While the relationships between different seasonal TE-MA MSE fluxes and cyclone numbers are shown by scatter-plots (Fig. 10), for conciseness we only show the correlations—correlation values for the different flux decompositions and attribution percentiles. In addition to the relationships discussed in Fig. 10, we show correlations with the number of cyclones in the entire SH ( $n_{\text{all,SH}}$ ) and with total AHT heat transport ( $\langle [vm] \rangle$ ) —for  $50^\circ$  S in the left column of Fig. E1 and different latitudes in Fig. E2. Note that measuring intensification rate in Bergeron and intensity based on SLP anomalies from a climatology 1110 instead does not yield a qualitatively different picture (not shown).

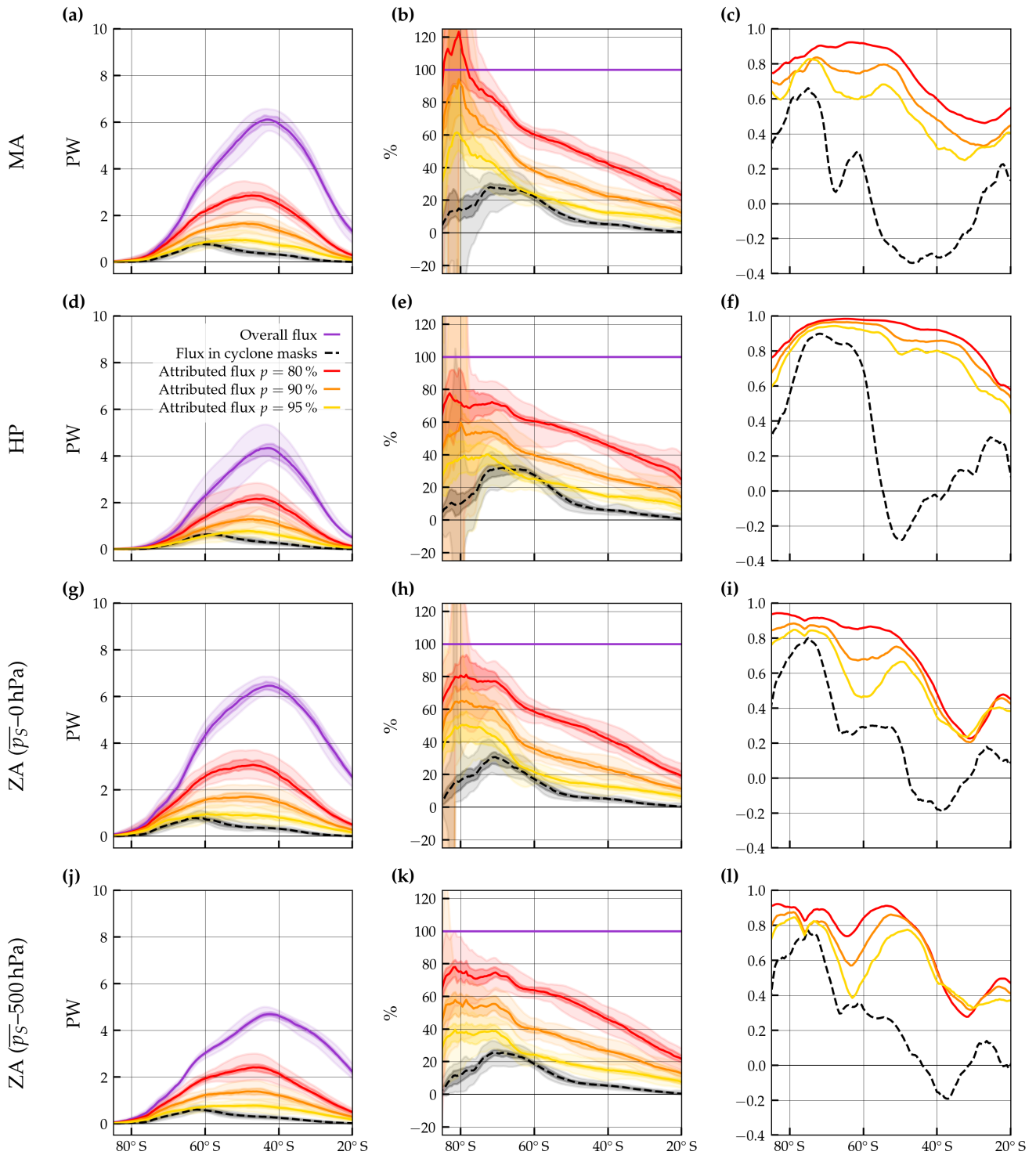


**Figure D1.** Same as Fig. 7 but repeated for different flux decomposition methods (see Sect. 2.3) and different percentile thresholds for attributing flux to cyclones (yellow, orange, and red distributions and lines corresponding to percentile ranks of 0.8, 0.9, and 0.95).

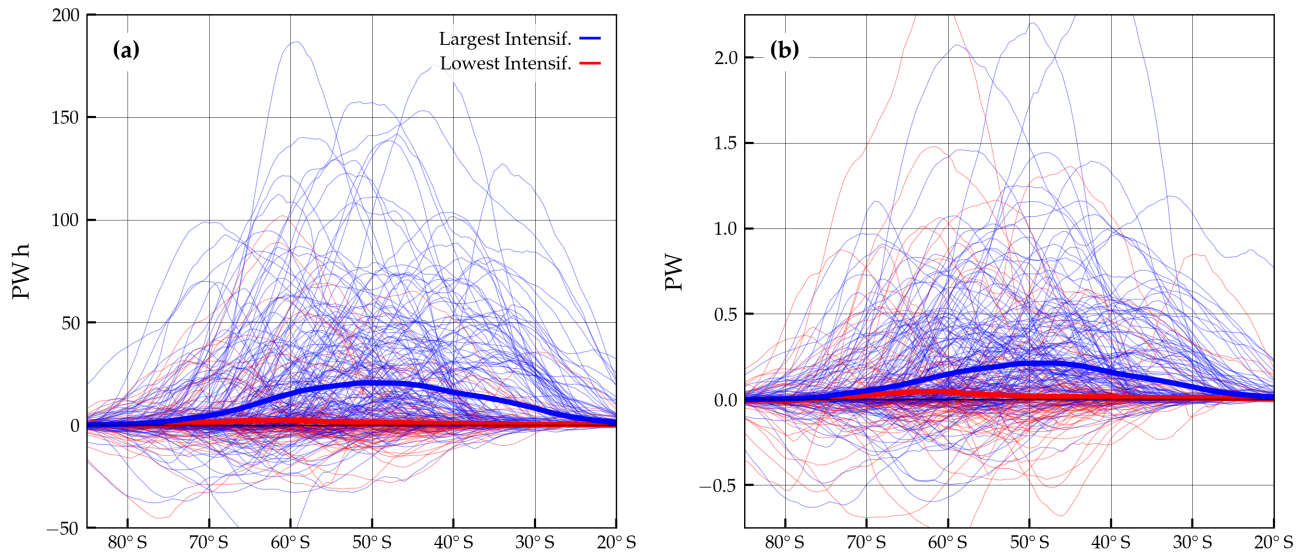


**Figure D2.** Same as Fig. 7 but repeated for different (a) The lifetime-integrated flux decomposition methods (see Sect. 2.3) and different percentile thresholds for attributing flux to of the 200 most strongly intensifying cyclones (yellow, dark orange, and red distributions and blue thin lines corresponding) is compared to percentile ranks the flux of 80, 90, and 95 the 200 cyclones that intensify least rapidly (red). Thick lines denote the arithmetic means shown in Fig. 8a. (b) As in (a) but for the lifetime-averaged flux in PW. The flux attribution percentile rank corresponds to  $p = 0.9$ .

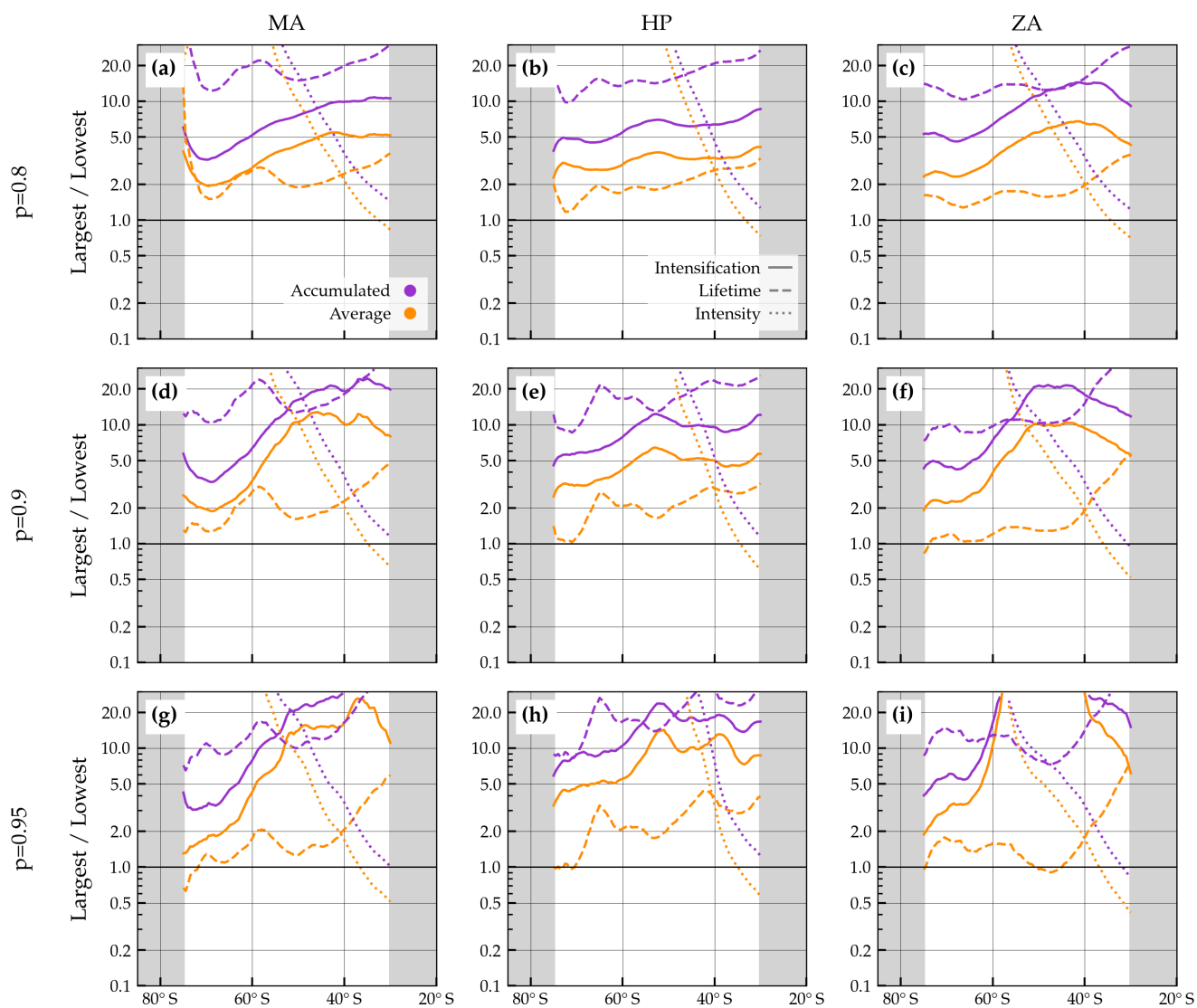


**Figure D3.** Ratio of the flux related to the 200 cyclones of largest vs. lowest characteristic based on all SH cyclones: Fig. 8b,d are combined and repeated for different flux decomposition methods (columns, see Sect. 2.3) and different percentile thresholds for attributing flux to cyclones (80-0.8, 90-0.9, and 95-0.95, see Sect. 2.4). Purple lines correspond to lifetime-accumulated fluxes, yellow lines to lifetime-averaged fluxes, and the linestyle signifies the cyclone life cycle characteristic.

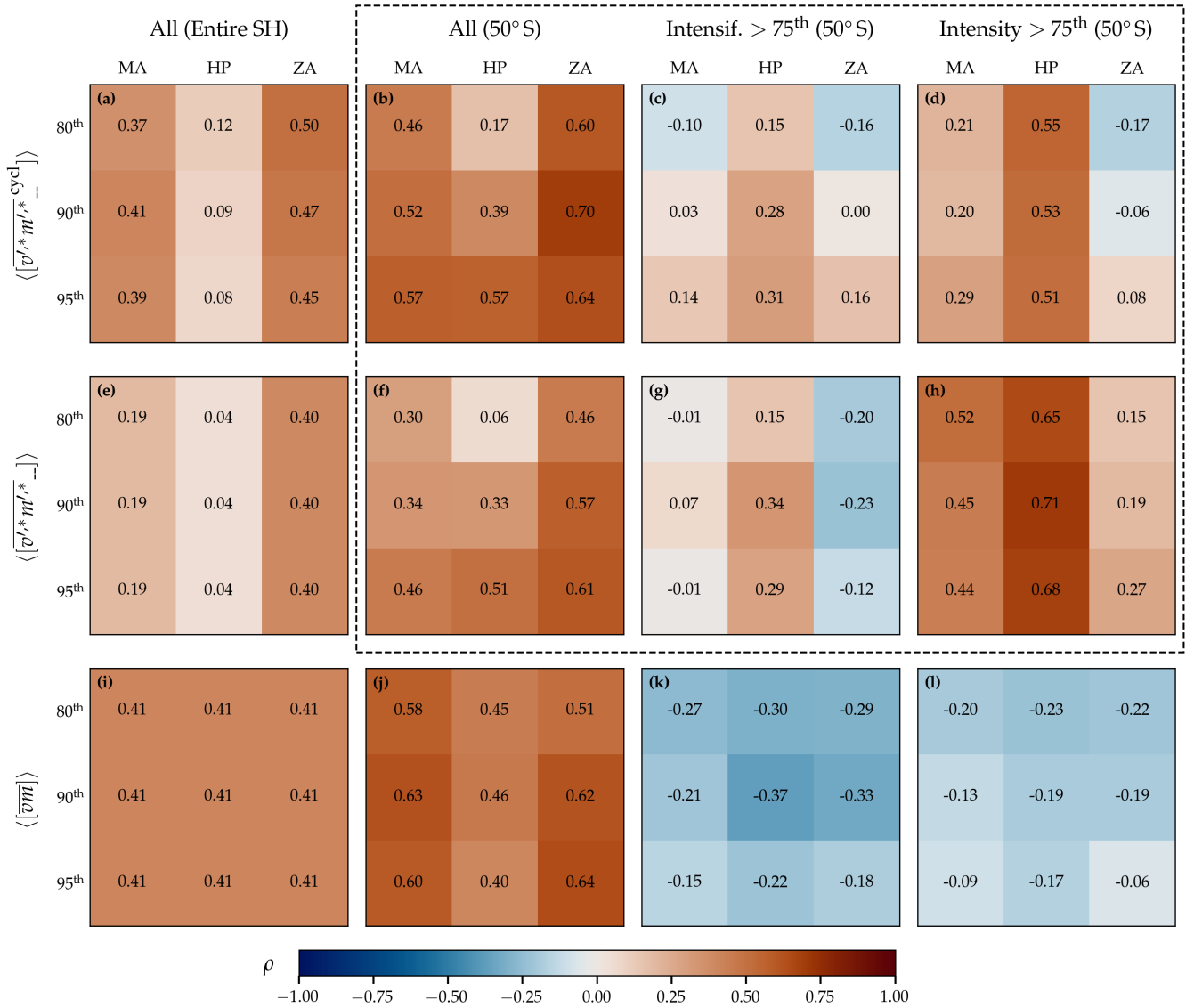


**Figure E1.** Sensitivity of the correlation ( $\rho$ ) between seasonally averaged MSE fluxes and seasonal cyclone number to flux decomposition method and flux attribution percentile for different MSE fluxes and groups of cyclones. **(a)** The correlation of the number of all SH cyclones with cyclone-attributed eddy MSE flux,  $\langle [v'^*m'^*_{-}{}^{\text{cycl}}] \rangle$ , at 50° S is shown for each percentile and flux decomposition method. Depending on the decomposition method, these fluxes correspond to temporal anomalies (' for **TE-MA** and HP) or zonal anomalies (\* for ZA). Numerical values are accentuated with colors. Data correspond to SH JJA. This is repeated for **(b)** all cyclones with  $\langle [v'^*m'^*_{-}{}^{\text{cycl}}] \rangle \neq 0$  at 50° S, **(c)** the cyclones with  $\langle [v'^*m'^*_{-}{}^{\text{cycl}}] \rangle \neq 0$  at 50° S that have an intensification rate above the 75<sup>th</sup> climatological percentile, and **(d)** as **(c)** but for intensity instead of intensification rate. **(e–h)** as **(a–d)** but for the overall eddy MSE flux  $\langle [v'^*m'^*_{-}] \rangle$ . **(i–l)** as **(a–d)** but for the total atmospheric MSE transport  $\langle [\overline{vm}] \rangle$ . The arrangement of the panels outlined by the black dashed line corresponds to the arrangement of the panels in Fig. 10.

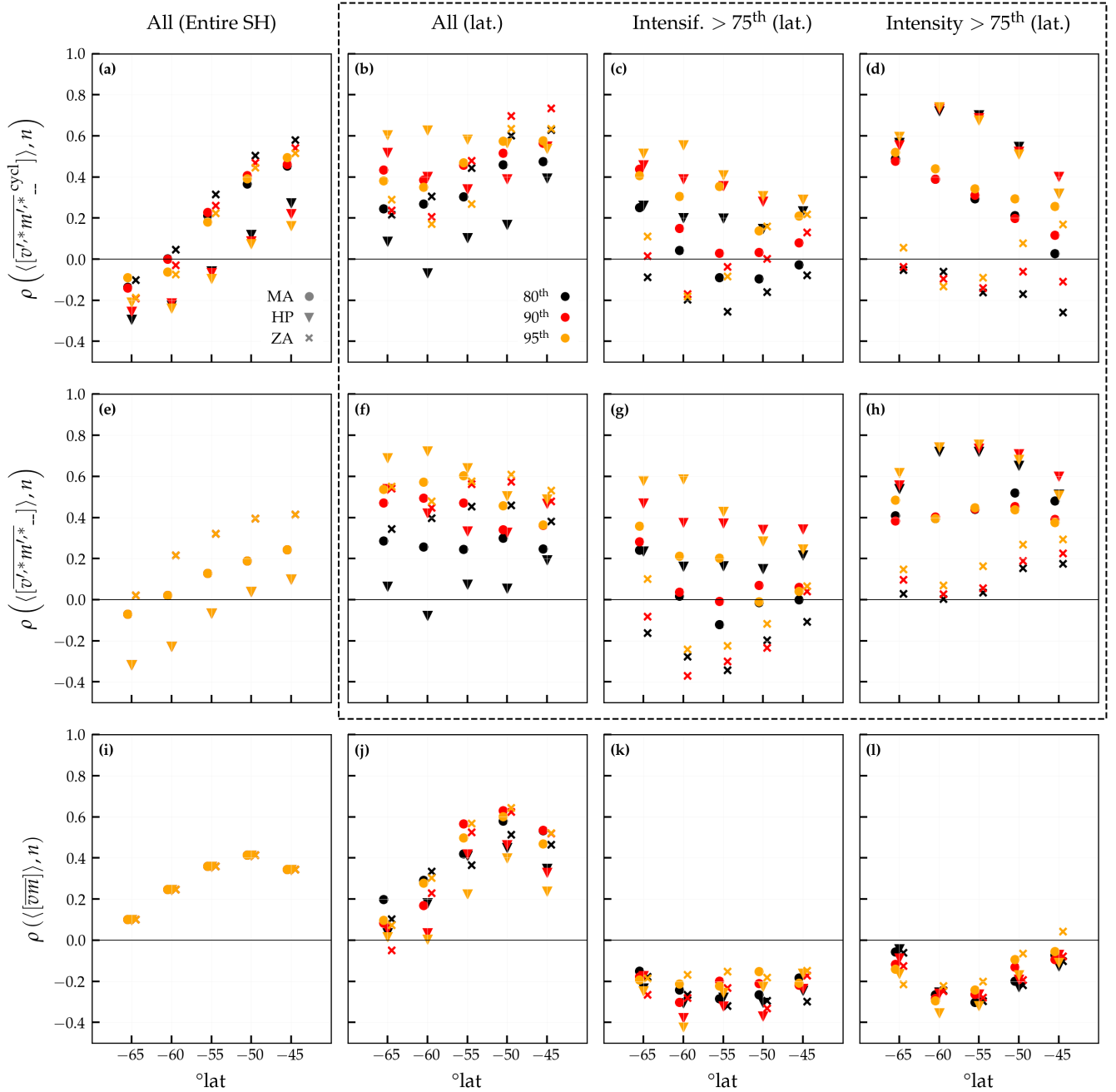


**Figure E2.** Sensitivity of the correlation ( $\rho$ ) between seasonally averaged MSE fluxes and seasonal cyclone number to flux decomposition method and flux attribution percentile as in Fig. E1 for different latitudes. (a) As in Fig. E1a, the correlation of the number of all SH cyclones with cyclone-attributed eddy MSE flux,  $\langle [\overline{v'_{*}m'_{*}}]_{\text{cycl}} \rangle, n$ , is shown here in steps of  $5^{\circ}$  latitude. Colors of the markers indicate the percentile and shapes the decomposition method. Markers for the different flux decomposition methods are slightly offset on the x-axis for better clarity. (b–l) as in (a) but for the different fluxes and groups of cyclones, arranged as in Fig. E1. The arrangement of the panels outlined by the black dashed line is consistent with Fig. 10.

*Author contributions.* SS conceived the project and acquired the funding. All authors contributed to the conceptualization of the study. JZ developed and implemented the methods, performed the data analysis, visualized the results, and prepared the original draft. AH supported assembling and maintaining ERA5 data. AH, AD, and SS contributed to the interpretation and discussion of the results and reviewed and edited the manuscript.

1115 *Competing interests.* At least one of the (co-)authors is a member of the editorial board of Weather and Climate Dynamics. The peer-review process was guided by an independent editor, and the authors have no other competing interests to declare.

*Acknowledgements.* We would like to acknowledge the Applied Physics Laboratory at the University of Washington for supporting a visit which greatly fostered scientific discussions regarding the results and outline of this work. We thank colleagues at the Institute for Atmospheric and Climate Science at ETH Zurich for constructive feedback. Furthermore, we would like to thank Heini Wernli for helpful discussions and feedback on the manuscript. [Moreover, we would like to thank three anonymous reviewers for their detailed feedback and helpful suggestions, which enabled us to improve the quality of this paper.](#) The `cd` library was used for data processing (Schulzweida, 2018). An AI-powered search engine was used for parts of code development (phind.com). J.Z., A.H., and S.S. were supported by the Swiss National Science Foundation through project grant Nr. 204181. A.D. was supported by the National Science Foundation Award AGS-2311154.

1120

## References

- 1125 Armour, K. C., Siler, N., Donohoe, A., and Roe, G. H.: Meridional Atmospheric Heat Transport Constrained by Energetics and Mediated by Large-Scale Diffusion, *J. Climate*, 32, 3655–3680, <https://doi.org/10.1175/JCLI-D-18-0563.1>, 2019.
- Attinger, R., Spreitzer, E., Boettcher, M., Forbes, R., Wernli, H., and Joos, H.: Quantifying the role of individual diabatic processes for the formation of PV anomalies in a North Pacific cyclone, *Quarterly Journal of the Royal Meteorological Society*, 145, 2454–2476, <https://doi.org/10.1002/QJ.3573>, 2019.
- 1130 Barnes, E. A. and Hartmann, D. L.: The Global Distribution of Atmospheric Eddy Length Scales, *J. Climate*, 25, 3409–3416, <https://doi.org/10.1175/JCLI-D-11-00331.1>, 2012.
- Barpanda, P. and Shaw, T.: Using the Moist Static Energy Budget to Understand Storm-Track Shifts across a Range of Time Scales, *J. Atmos. Sci.*, 74, 2427–2446, <https://doi.org/10.1175/JAS-D-17-0022.1>, 2017.
- Blanchard-Wrigglesworth, E., Cox, T., Espinosa, Z. I., and Donohoe, A.: The Largest Ever Recorded Heatwave—Characteristics and At-  
1135 tribution of the Antarctic Heatwave of March 2022, *Geophys. Res. Lett.*, 50, e2023GL104910, <https://doi.org/10.1029/2023GL104910>, 2023.
- Boer, G.: Some dynamical consequences of Greenhouse gas warming, *Atmosphere-Ocean*, 33, 731–751, <https://doi.org/10.1080/07055900.1995.9649551>, 1995.
- Boer, G. J. and Sargent, N. E.: Vertically Integrated Budgets of Mass and Energy for the Globe, *J. Atmos. Sci.*, 42, 1592–1613,  
1140 [https://doi.org/10.1175/1520-0469\(1985\)042<1592:VIBOMA>2.0.CO;2](https://doi.org/10.1175/1520-0469(1985)042<1592:VIBOMA>2.0.CO;2), 1985.
- Booth, J. F., Wang, S., and Polvani, L.: Midlatitude storms in a moister world: lessons from idealized baroclinic life cycle experiments, *Clim. Dynam.*, 41, 787–802, <https://doi.org/10.1007/s00382-012-1472-3>, 2013.
- Büeler, D. and Pfahl, S.: Potential Vorticity Diagnostics to Quantify Effects of Latent Heating in Extratropical Cyclones. Part I: Methodology, *J. Atmos. Sci.*, 74, 3567–3590, <https://doi.org/10.1175/JAS-D-17-0041.1>, 2017.
- 1145 Callaghan, J. and Power, S. B.: Major coastal flooding in southeastern Australia 1860-2012, associated deaths and weather systems, *Aust. Meteorol. Ocean*, 64, 183–213, <https://doi.org/10.22499/2.6403.002>, 2014.
- Cardinale, C. J., Rose, B. E. J., Lang, A. L., and Donohoe, A.: Stratospheric and Tropospheric Flux Contributions to the Polar Cap Energy Budgets, *J. Climate*, 34, 4261–4278, <https://doi.org/10.1175/JCLI-D-20-0722.1>, 2021.
- Catto, J. L., Shaffrey, L. C., and Hodges, K. I.: Can Climate Models Capture the Structure of Extratropical Cyclones?, *J. Climate*, 23,  
1150 1621–1635, <https://doi.org/10.1175/2009JCLI3318.1>, 2010.
- Chang, E. K.: Projected Significant Increase in the Number of Extreme Extratropical Cyclones in the Southern Hemisphere, *J. Climate*, 30, 4915–4935, <https://doi.org/10.1175/JCLI-D-16-0553.1>, 2017.
- Chang, E. K., Guo, Y., and Xia, X.: CMIP5 multimodel ensemble projection of storm track change under global warming, *J. Geophys. Res.-Atmos.*, 117, 23 118, <https://doi.org/10.1029/2012JD018578>, 2012.
- 1155 Chang, E. K. M.: CMIP5 Projected Change in Northern Hemisphere Winter Cyclones with Associated Extreme Winds, *J. Climate*, 31, 6527–6542, <https://doi.org/10.1175/JCLI-D-17-0899.1>, 2018.
- Chikoore, H., Mbokodo, I. L., Singo, M. V., Mohomi, T., Munyai, R. B., Havenga, H., Mahlobo, D. D., Engelbrecht, F. A., Bopape, M. J. M., and Ndarana, T.: Dynamics of an extreme low temperature event over South Africa amid a warming climate, *Weather and Climate Extremes*, 44, 100 668, <https://doi.org/10.1016/J.WACE.2024.100668>, 2024.

- 1160 Clark, J. P., Feldstein, S. B., and Lee, S.: Moist Static Energy Transport Trends in Four Global Reanalyses: Are They Downgradient?, *Geophys. Res. Lett.*, 49, <https://doi.org/10.1029/2022GL098822>, 2022.
- Cornér, J., Bouvier, C., Doiteau, B., Pantillon, F., and Sinclair, V. A.: Classification of North Atlantic and European extratropical cyclones using multiple measures of intensity, *Natural Hazards and Earth System Sciences*, 25, 207–229, <https://doi.org/10.5194/NHESS-25-207-2025>, 2025.
- 1165 Cox, T., Donohoe, A., Armour, K. C., Frierson, D. M., and Roe, G. H.: Comment on “Moist Static Energy Transport Trends in Four Global Reanalyses: Are They Downgradient?” by Clark et al. (2022), *Geophysical Research Letters*, 50, <https://doi.org/10.1029/2023GL102804>, 2023.
- Cox, T., Donohoe, A., Armour, K. C., Frierson, D. M., and Roe, G. H.: Trends in Atmospheric Heat Transport Since 1980, *J. Climate*, 37, 1539–1550, <https://doi.org/10.1175/JCLI-D-23-0385.1>, 2024a.
- 1170 Cox, T., Donohoe, A., Armour, K. C., Roe, G. H., and Frierson, D. M. W.: A New Method for Calculating Instantaneous Atmospheric Heat Transport, *J. Climate*, 37, 4337–4346, <https://doi.org/10.1175/JCLI-D-23-0521.1>, 2024b.
- Dacre, H. F., Martinez-Alvarado, O., and Hodges, K. I.: Precipitation Efficiencies in a Climatology of Southern Ocean Extratropical Cyclones, *J. Geophys. Res.-Atmos.*, 128, e2023JD039239, <https://doi.org/10.1029/2023JD039239>, 2023.
- Dai, P. and Nie, J.: Robust Expansion of Extreme Midlatitude Storms Under Global Warming, *Geophysical Research Letters*, 49, e2022GL099007, <https://doi.org/10.1029/2022GL099007>, 2022.
- 1175 Donohoe, A., Armour, K. C., Roe, G. H., Battisti, D. S., and Hahn, L.: The Partitioning of Meridional Heat Transport from the Last Glacial Maximum to CO<sub>2</sub> Quadrupling in Coupled Climate Models, *J. Climate*, 33, 4141–4165, <https://doi.org/10.1175/JCLI-D-19-0797.1>, 2020.
- Eady, E. T.: Long Waves and Cyclone Waves, *Tellus*, 1, 33–52, <https://doi.org/10.3402/tellusa.v1i3.8507>, 1949.
- Fearon, M. G., Doyle, J. D., Ryglicki, D. R., Finocchio, P. M., and Sprenger, M.: The Role of Cyclones in Moisture Transport into the Arctic, *Geophys. Res. Lett.*, 48, e2020GL090353, <https://doi.org/10.1029/2020GL090353>, 2021.
- 1180 Franzke, C. L. E. and Harnik, N.: Long-Term Trends of the Atmospheric Circulation and Moist Static Energy Budget in the JRA-55 Reanalysis, *J. Climate*, pp. 1–49, <https://doi.org/10.1175/jcli-d-21-0724.1>, 2023.
- Fritsch, F. N. and Carlson, R. E.: Monotone Piecewise Cubic Interpolation, *SIAM J. Numer. Anal.*, 17, 238–246, <https://doi.org/10.1137/0717021>, 1980.
- 1185 Geen, R., Czaja, A., and Haigh, J. D.: The effects of increasing humidity on heat transport by extratropical waves, *Geophys. Res. Lett.*, 43, 8314–8321, <https://doi.org/10.1002/2016GL070214>, 2016.
- Geng, Q. and Sugi, M.: Possible Change of Extratropical Cyclone Activity due to Enhanced Greenhouse Gases and Sulfate Aerosols—Study with a High-Resolution AGCM, *J. Climate*, 16, 2262–2274, [https://doi.org/10.1175/1520-0442\(2003\)16<2262:PCOECA>2.0.CO;2](https://doi.org/10.1175/1520-0442(2003)16<2262:PCOECA>2.0.CO;2), 2003.
- Gill, A. E.: *Atmosphere—ocean dynamics*, Academic Press, New York, 1982.
- 1190 Grams, C. M., Wernli, H., Böttcher, M., Čampa, J., Corsmeier, U., Jones, S. C., Keller, J. H., Lenz, C. J., and Wiegand, L.: The key role of diabatic processes in modifying the upper-tropospheric wave guide: a North Atlantic case-study, *Q.J. Roy. Meteor. Soc.*, 137, 2174–2193, <https://doi.org/10.1002/QJ.891>, 2011.
- Grieger, J., Leckebusch, G. C., Donat, M. G., Schuster, M., and Ulbrich, U.: Southern Hemisphere winter cyclone activity under recent and future climate conditions in multi-model AOGCM simulations, *Int. J. Climatol.*, 34, 3400–3416, <https://doi.org/10.1002/JOC.3917>, 2014.
- 1195 Heitmann, K., Sprenger, M., Binder, H., Wernli, H., and Joos, H.: Warm conveyor belt characteristics and impacts along the life cycle of extratropical cyclones: case studies and climatological analysis based on ERA5, *Weather Clim. Dynam.*, 5, 537–557, <https://doi.org/10.5194/wcd-5-537-2024>, 2024.

- Hersbach, H., Bell, B., Berrisford, P., Hirahara, S., Horányi, A., Muñoz-Sabater, J., Nicolas, J., Peubey, C., Radu, R., Schepers, D., Simmons, A., Soci, C., Abdalla, S., Abellan, X., Balsamo, G., Bechtold, P., Biavati, G., Bidlot, J., Bonavita, M., Chiara, G., Dahlgren, P., Dee, D., Diamantakis, M., Dragani, R., Flemming, J., Forbes, R., Fuentes, M., Geer, A., Haimberger, L., Healy, S., Hogan, R. J., Hólm, E., Janisková, M., Keeley, S., Laloyaux, P., Lopez, P., Lupu, C., Radnoti, G., Rosnay, P., Rozum, I., Vamborg, F., Villaume, S., and Thépaut, J.: The ERA5 global reanalysis, *Q.J. Roy. Meteor. Soc.*, 146, 1999–2049, <https://doi.org/10.1002/qj.3803>, 2020.
- Hoskins, B. J., James, I. N., and White, G. H.: The Shape, Propagation and Mean-Flow Interaction of Large-Scale Weather Systems, *J. Atmos. Sci.*, 40, 1595–1612, [https://doi.org/10.1175/1520-0469\(1983\)040<1595:TSPAMF>2.0.CO;2](https://doi.org/10.1175/1520-0469(1983)040<1595:TSPAMF>2.0.CO;2), 1983.
- 1200 Kang, J. M., Shaw, T. A., Kang, S. M., Simpson, I. R., and Yu, Y.: Revisiting the reanalysis-model discrepancy in Southern Hemisphere winter storm track trends, *npj Clim. Atmos. Sci.*, 7, 1–10, <https://doi.org/10.1038/s41612-024-00801-3>, 2024.
- Kaspi, Y. and Schneider, T.: The Role of Stationary Eddies in Shaping Midlatitude Storm Tracks, *J. Atmos. Sci.*, 70, 2596–2613, <https://doi.org/10.1175/JAS-D-12-082.1>, 2013.
- Kolstad, E. W. and Bracegirdle, T. J.: Marine cold-air outbreaks in the future: An assessment of IPCC AR4 model results for the Northern Hemisphere, *Clim. Dynam.*, 30, 871–885, <https://doi.org/10.1007/S00382-007-0331-0/FIGURES/10>, 2008.
- 1210 König, W., Sausen, R., and Sielmann, F.: Objective Identification of Cyclones in GCM Simulations, *J. Climate*, 6, 2217–2231, [https://doi.org/10.1175/1520-0442\(1993\)006<2217:OIOCIG>2.0.CO;2](https://doi.org/10.1175/1520-0442(1993)006<2217:OIOCIG>2.0.CO;2), 1993.
- Lambert, S. J. and Fyfe, J. C.: Changes in winter cyclone frequencies and strengths simulated in enhanced greenhouse warming experiments: Results from the models participating in the IPCC diagnostic exercise, *Climate Dynamics*, 26, 713–728, <https://doi.org/10.1007/S00382-006-0110-3/TABLES/4>, 2006.
- 1215 Lembo, V., Fabiano, F., Galfi, V. M., Graverson, R. G., Lucarini, V., and Messori, G.: Meridional-energy-transport extremes and the general circulation of Northern Hemisphere mid-latitudes: dominant weather regimes and preferred zonal wavenumbers, *Weather Clim. Dynam.*, 3, 1037–1062, <https://doi.org/10.5194/wcd-3-1037-2022>, 2022.
- Lindzen, R. S. and Farrell, B.: A Simple Approximate Result for the Maximum Growth Rate of Baroclinic Instabilities, *Journal of the Atmospheric Sciences*, 37, 1648–1654, [https://doi.org/10.1175/1520-0469\(1980\)037<1648:ASARFT>2.0.CO;2](https://doi.org/10.1175/1520-0469(1980)037<1648:ASARFT>2.0.CO;2), 1980.
- 1220 Lopez-Marti, F., Ginesta, M., Faranda, D., Rutgersson, A., Yiou, P., Wu, L., and Messori, G.: Future changes in compound explosive cyclones and atmospheric rivers in the North Atlantic, *Earth Sys. Dynam.*, 16, 169–187, <https://doi.org/10.5194/ESD-16-169-2025>, 2025.
- Marshall, J., Donohoe, A., Ferreira, D., and McGee, D.: The ocean’s role in setting the mean position of the Inter-Tropical Convergence Zone, *Clim. Dynam.*, 42, 1967–1979, <https://doi.org/10.1007/s00382-013-1767-z>, 2014.
- 1225 Mayer, J., Mayer, M., and Haimberger, L.: Consistency and Homogeneity of Atmospheric Energy, Moisture, and Mass Budgets in ERA5, *Journal of Climate*, 34, 3955–3974, <https://doi.org/10.1175/JCLI-D-20-0676.1>, 2021.
- Mayer, M., Kato, S., Bosilovich, M., Bechtold, P., Mayer, J., Schröder, M., Behrangi, A., Wild, M., Kobayashi, S., Li, Z., and L’Ecuyer, T.: Assessment of Atmospheric and Surface Energy Budgets Using Observation-Based Data Products, *Surv. Geophys.*, pp. 1–28, <https://doi.org/10.1007/S10712-024-09827-X/TABLES/5>, 2024.
- 1230 Messori, G. and Czaja, A.: On the sporadic nature of meridional heat transport by transient eddies, *Q.J. Roy. Meteor. Soc.*, 139, 999–1008, <https://doi.org/10.1002/qj.2011>, 2013.
- Messori, G. and Czaja, A.: Some considerations on the spectral features of meridional heat transport by transient eddies, *Q.J. Roy. Meteor. Soc.*, 140, 1377–1386, <https://doi.org/10.1002/QJ.2224>, 2014.
- Messori, G. and Czaja, A.: On local and zonal pulses of atmospheric heat transport in reanalysis data, *Q.J. Roy. Meteor. Soc.*, 141, 2376–2389, <https://doi.org/10.1002/qj.2529>, 2015.
- 1235

- Messori, G., Geen, R., and Czaja, A.: On the spatial and temporal variability of atmospheric heat transport in a hierarchy of models, *J. Atmos. Sci.*, 74, 2163–2189, <https://doi.org/10.1175/JAS-D-16-0360.1>, 2017.
- Neelin, J. D. and Held, I. M.: Modeling Tropical Convergence Based on the Moist Static Energy Budget, *Mon. Weather Rev.*, 115, 3–12, [https://doi.org/10.1175/1520-0493\(1987\)115<0003:MTCBOT>2.0.CO;2](https://doi.org/10.1175/1520-0493(1987)115<0003:MTCBOT>2.0.CO;2), 1987.
- 1240 Novak, L., Ambaum, M. H. P., and Tailleux, R.: The Life Cycle of the North Atlantic Storm Track, *J. Atmos. Sci.*, 72, 821–833, <https://doi.org/10.1175/JAS-D-14-0082.1>, 2015.
- Papritz, L., Pfahl, S., Rudeva, I., Simmonds, I., Sodemann, H., and Wernli, H.: The Role of Extratropical Cyclones and Fronts for Southern Ocean Freshwater Fluxes, *J. Climate*, 27, 6205–6224, <https://doi.org/10.1175/JCLI-D-13-00409.1>, 2014.
- Peixoto, J. P. and Oort, A. H.: *Physics of climate*, American Institute of Physics, Melville, New York, 1992.
- 1245 Pfahl, S. and Wernli, H.: Quantifying the Relevance of Cyclones for Precipitation Extremes, *J. Climate*, 25, 6770–6780, <https://doi.org/10.1175/JCLI-D-11-00705.1>, 2012.
- Pfahl, S., Schwierz, C., Croci-Maspoli, M., Grams, C. M., and Wernli, H.: Importance of latent heat release in ascending air streams for atmospheric blocking, *Nat. Geosci.*, 8, 610–614, <https://doi.org/10.1038/ngeo2487>, 2015.
- Pomroy, H. R. and Thorpe, A. J.: The Evolution and Dynamical Role of Reduced Upper-Tropospheric Potential Vorticity in Intensive Observing Period One of FASTEX, *Mon. Weather Rev.*, 128, 1817–1834, [https://doi.org/10.1175/1520-0493\(2000\)128<1817:TEADRO>2.0.CO;2](https://doi.org/10.1175/1520-0493(2000)128<1817:TEADRO>2.0.CO;2), 2000.
- 1250 Priestley, C. H.: Heat transport and zonal stress between latitudes, *Q.J. Roy. Meteor. Soc.*, 75, 28–40, <https://doi.org/10.1002/qj.49707532307>, 1949.
- Priestley, M. D. K. and Catto, J. L.: Future changes in the extratropical storm tracks and cyclone intensity, wind speed, and structure, *Weather Clim. Dynam.*, 3, 337–360, <https://doi.org/10.5194/wcd-3-337-2022>, 2022.
- 1255 Rudeva, I. and Gulev, S. K.: Climatology of Cyclone Size Characteristics and Their Changes during the Cyclone Life Cycle, *Mon. Weather Rev.*, 135, 2568–2587, <https://doi.org/10.1175/MWR3420.1>, 2007.
- Rudeva, I., Simmonds, I., Crock, D., and Boschat, G.: Midlatitude Fronts and Variability in the Southern Hemisphere Tropical Width, *Journal of Climate*, 32, 8243–8260, <https://doi.org/10.1175/JCLI-D-18-0782.1>, 2019.
- 1260 Rüdüsühli, S., Sprenger, M., Leutwyler, D., Schär, C., and Wernli, H.: Attribution of precipitation to cyclones and fronts over Europe in a kilometer-scale regional climate simulation, *Weather and Climate Dynamics*, 1, 675–699, <https://doi.org/10.5194/wcd-1-675-2020>, 2020.
- Ruggieri, P., Alvarez-Castro, M. C., Athanasiadis, P., Bellucci, A., Materia, S., and Gualdi, S.: North Atlantic Circulation Regimes and Heat Transport by Synoptic Eddies, *J. Climate*, 33, 4769–4785, <https://doi.org/10.1175/JCLI-D-19-0498.1>, 2020.
- Rydsaa, J. H., Graversen, R. G., Heiskanen, T. I., and Stoll, P. J.: Changes in atmospheric latent energy transport into the Arctic: Planetary versus synoptic scales, *Q.J. Roy. Meteor. Soc.*, 147, 2281–2292, <https://doi.org/10.1002/QJ.4022>, 2021.
- 1265 Sanders, F. and Gyakum, J. R.: Synoptic-Dynamic Climatology of the “Bomb”, *Mon. Weather Rev.*, 108, 1589–1606, [https://doi.org/10.1175/1520-0493\(1980\)108<1589:SDCOT>2.0.CO;2](https://doi.org/10.1175/1520-0493(1980)108<1589:SDCOT>2.0.CO;2), 1980.
- Schemm, S. and Rivière, G.: On the Efficiency of Baroclinic Eddy Growth and How It Reduces the North Pacific Storm-Track Intensity in Midwinter, *J. Climate*, 32, 8373–8398, <https://doi.org/10.1175/JCLI-D-19-0115.1>, 2019.
- 1270 Schemm, S. and Sprenger, M.: Frontal-wave cyclogenesis in the North Atlantic – a climatological characterisation, *Quarterly Journal of the Royal Meteorological Society*, 141, 2989–3005, <https://doi.org/10.1002/qj.2584>, 2015.
- Schemm, S., Wernli, H., and Papritz, L.: Warm Conveyor Belts in Idealized Moist Baroclinic Wave Simulations, *J. Atmos. Sci.*, 70, 627–652, <https://doi.org/10.1175/JAS-D-12-0147.1>, 2013.

- Schemm, S., Rudeva, I., and Simmonds, I.: Extratropical fronts in the lower troposphere—global perspectives obtained from two automated methods, *Quarterly Journal of the Royal Meteorological Society*, 141, 1686–1698, <https://doi.org/10.1002/QJ.2471>, 2015.
- 1275 Schemm, S., Sprenger, M., and Wernli, H.: When during Their Life Cycle Are Extratropical Cyclones Attended by Fronts?, *B. Am. Meteorol. Soc.*, 99, 149–165, <https://doi.org/10.1175/BAMS-D-16-0261.1>, 2018.
- Schemm, S., Papritz, L., and Rivière, G.: Storm track response to uniform global warming downstream of an idealized sea surface temperature front, *Weather Clim. Dynam.*, 3, 601–623, <https://doi.org/10.5194/wcd-3-601-2022>, 2022.
- 1280 Schulzweida, U.: CDO User Guide, <https://doi.org/10.5281/ZENODO.1435455>, 2018.
- Seiler, C. and Zwiers, F. W.: How will climate change affect explosive cyclones in the extratropics of the Northern Hemisphere?, *Clim. Dynam.*, 46, 3633–3644, <https://doi.org/10.1007/S00382-015-2791-Y/FIGURES/6>, 2016.
- Shapiro, M. A. and Keyser, D.: Fronts, Jet Streams and the Tropopause, in: *Extratropical Cyclones: The Erik Palmén Memorial Volume*, edited by W., N. C. and Holopainen, E. O., pp. 167–191, American Meteorological Society, Boston, MA, ISBN 978-1-944970-33-8, [https://doi.org/10.1007/978-1-944970-33-8\\_10](https://doi.org/10.1007/978-1-944970-33-8_10), 1990.
- 1285 Shaw, T. A., Baldwin, M., Barnes, E. A., Caballero, R., Garfinkel, C. I., Hwang, Y. T., Li, C., O’Gorman, P. A., Rivière, G., Simpson, I. R., and Voigt, A.: Storm track processes and the opposing influences of climate change, *Nature Geoscience*, 9, 656–664, <https://doi.org/10.1038/ngeo2783>, 2016.
- Shaw, T. A., Barpanda, P., and Donohoe, A.: A Moist Static Energy Framework for Zonal-Mean Storm-Track Intensity, *J. Atmos. Sci.*, 75, 1979–1994, <https://doi.org/10.1175/JAS-D-17-0183.1>, 2018.
- 1290 Shields, C. A., Rutz, J. J., Leung, L. Y., Martin Ralph, F., Wehner, M., Kawzenuk, B., Lora, J. M., McClenny, E., Osborne, T., Payne, A. E., Ullrich, P., Gershunov, A., Goldenson, N., Guan, B., Qian, Y., Ramos, A. M., Sarangi, C., Sellars, S., Gorodetskaya, I., Kashinath, K., Kurlin, V., Mahoney, K., Muszynski, G., Pierce, R., Subramanian, A. C., Tome, R., Waliser, D., Walton, D., Wick, G., Wilson, A., Lavers, D., Prabhat, Collow, A., Krishnan, H., Magnusdottir, G., and Nguyen, P.: Atmospheric River Tracking Method Intercomparison Project (ARTMIP): Project goals and experimental design, *Geosci. Model Dev.*, 11, 2455–2474, <https://doi.org/10.5194/GMD-11-2455-2018>, 2018.
- 1295 Simmons, A. J.: Trends in the tropospheric general circulation from 1979 to 2022, *Weather Clim. Dynam.*, 3, 777–809, <https://doi.org/10.5194/wcd-3-777-2022>, 2022.
- Sinclair, M. R.: An Objective Cyclone Climatology for the Southern Hemisphere, *Mon. Weather Rev.*, 122, 2239–2256, [https://doi.org/10.1175/1520-0493\(1994\)122<2239:AOCFT>2.0.CO;2](https://doi.org/10.1175/1520-0493(1994)122<2239:AOCFT>2.0.CO;2), 1994.
- 1300 Sinclair, V. A. and Catto, J. L.: The relationship between extra-tropical cyclone intensity and precipitation in idealised current and future climates, *Weather and Climate Dynamics Discussions*, <https://doi.org/doi.org/10.5194/wcd-2022-62>, 2022.
- Sinclair, V. A. and Dacre, H. F.: Which Extratropical Cyclones Contribute Most to the Transport of Moisture in the Southern Hemisphere?, *J. Geophys. Res.-Atmos.*, 124, 2525–2545, <https://doi.org/10.1029/2018JD028766>, 2019.
- 1305 Sinclair, V. A., Rantanen, M., Haapanala, P., Räisänen, J., and Järvinen, H.: The characteristics and structure of extra-tropical cyclones in a warmer climate, *Weather Clim. Dynam.*, 1, 1–25, <https://doi.org/10.5194/wcd-1-1-2020>, 2020.
- Sprenger, M., Fragkoulidis, G., Binder, H., Croci-Maspoli, M., Graf, P., Grams, C. M., Knippertz, P., Madonna, E., Schemm, S., Škerlak, B., and Wernli, H.: Global Climatologies of Eulerian and Lagrangian Flow Features based on ERA-Interim, *B. Am. Meteorol. Soc.*, 98, 1739–1748, <https://doi.org/10.1175/BAMS-D-15-00299.1>, 2017.
- 1310 Steinfeld, D., Boettcher, M., Forbes, R., and Pfahl, S.: The sensitivity of atmospheric blocking to upstream latent heating-numerical experiments, *Weather Clim. Dynam.*, 1, 405–426, <https://doi.org/10.5194/WCD-1-405-2020>, 2020.

- Stoll, P. J., Graverson, R. G., and Messori, G.: The global atmospheric energy transport analysed by a wavelength-based scale separation, *Weather Clim. Dynam.*, 4, 1–17, <https://doi.org/10.5194/WCD-4-1-2023>, 2023.
- 1315 Thorncroft, C. D., Hoskins, B. J., and McIntyre, M. E.: Two paradigms of baroclinic-wave life-cycle behaviour, *Quarterly Journal of the Royal Meteorological Society*, 119, 17–55, <https://doi.org/10.1002/qj.49711950903>, 1993.
- Trenberth, K. E.: Climate Diagnostics from Global Analyses: Conservation of Mass in ECMWF Analyses, *Journal of Climate*, 4, 707–722, [https://doi.org/10.1175/1520-0442\(1991\)004<0707:CDGAC>2.0.CO;2](https://doi.org/10.1175/1520-0442(1991)004<0707:CDGAC>2.0.CO;2), 1991.
- Troup, A. J. and Streten, N. A.: Satellite-Observed Southern Hemisphere Cloud Vortices in Relation to Conventional Observations, *J. Appl. Meteor.*, 11, 909–917, [https://doi.org/10.1175/1520-0450\(1972\)011<0909:SOSHCV>2.0.CO;2](https://doi.org/10.1175/1520-0450(1972)011<0909:SOSHCV>2.0.CO;2), 1972.
- 1320 Tsukernik, M. and Lynch, A. H.: Atmospheric Meridional Moisture Flux over the Southern Ocean: A Story of the Amundsen Sea, *J. Climate*, 26, 8055–8064, <https://doi.org/10.1175/JCLI-D-12-00381.1>, 2013.
- Ullrich, P. A., Zarzycki, C. M., McClenny, E. E., Pinheiro, M. C., Stansfield, A. M., and Reed, K. A.: TempestExtremes v2.1: A community framework for feature detection, tracking, and analysis in large datasets, *Geosci. Model Dev.*, 14, 5023–5048, <https://doi.org/10.5194/GMD-14-5023-2021>, 2021.
- 1325 Vanni re, B., Czaja, A., Dacre, H., Woollings, T., and Parfitt, R.: A potential vorticity signature for the cold sector of winter extratropical cyclones, *Q.J. Roy. Meteor. Soc.*, 142, 432–442, <https://doi.org/10.1002/QJ.2662>, 2016.
- Wernli, H. and Gray, S. L.: The importance of diabatic processes for the dynamics of synoptic-scale extratropical weather systems-a review, *Weather Clim. Dynam.*, 5, 1299–1408, <https://doi.org/10.5194/wcd-5-1299-2024>, 2024.
- Wernli, H. and Schwierz, C.: Surface Cyclones in the ERA-40 Dataset (1958–2001). Part I: Novel Identification Method and Global Climatology, *J. Atmos. Sci.*, 63, <https://doi.org/10.1175/JAS3766.1>, 2006.
- 1330 Wille, J. D., Alexander, S. P., Amory, C., Baiman, R., Barth lemy, L., Bergstrom, D. M., Berne, A., Binder, H., Blanchet, J., Bozkurt, D., Bracegirdle, T. J., Casado, M., Choi, T., Clem, K. R., Codron, F., Datta, R., Di Battista, S., Favier, V., Francis, D., Fraser, A. D., Fourr , E., Garreaud, R. D., Genthon, C., Gorodetskaya, I. V., Gonz lez-Herrero, S., Heinrich, V. J., Hubert, G., Joos, H., Kim, S. J., King, J. C., Kittel, C., Landais, A., Lazzara, M., Leonard, G. H., Lieser, J. L., Maclennan, M., Mikolajczyk, D., Neff, P., Ollivier, I., Picard, G., Pohl, B., Ralph, F. M., Rowe, P., Schlosser, E., Shields, C. A., Smith, I. J., Sprenger, M., Trusel, L., Udy, D., Vance, T., Vignon,  ., Walker, C., Wever, N., and Zou, X.: The Extraordinary March 2022 East Antarctica “Heat” Wave. Part I: Observations and Meteorological Drivers, *J. Climate*, 37, 757–778, <https://doi.org/10.1175/JCLI-D-23-0175.1>, 2024.
- Zhang, Y. and Wang, W.-C.: Model-Simulated Northern Winter Cyclone and Anticyclone Activity under a Greenhouse Warming Scenario, *J. Climate*, 10, 1616–1634, [https://doi.org/10.1175/1520-0442\(1997\)010<1616:MSNWCA>2.0.CO;2](https://doi.org/10.1175/1520-0442(1997)010<1616:MSNWCA>2.0.CO;2), 1997.
- 1340 Zolina, O. and Gulev, S. K.: Synoptic Variability of Ocean–Atmosphere Turbulent Fluxes Associated with Atmospheric Cyclones, *J. Climate*, 16, 2717–2734, [https://doi.org/10.1175/1520-0442\(2003\)016<2717:SVOOTF>2.0.CO;2](https://doi.org/10.1175/1520-0442(2003)016<2717:SVOOTF>2.0.CO;2), 2003.